This is to certify that the

dissertation entitled

Spectroscopic Studies of Solution Phase Self-Assembly Phenomena Using "Tailor-Made Impurity" Probe Molecules

presented by

Jeffrey Paul Rasimas

has been accepted towards fulfillment
of the requirements for

Ph.D. degree in Chemistry

Major professor

Date 7/15/96

SPEC
PHEN

SPECTROSCOPIC STUDIES OF SOLUTION PHASE SELF-ASSEMBLY PHENOMENA USING "TAILOR-MADE IMPURITY" PROBE MOLECULES

By

Jeffrey Paul Rasimas

A DISSERTATION

Submitted to
Michigan State University
in partial fulfillment of the requirements
for the degree of

DOCTOR OF PHILOSOPHY

Department of Chemistry

1996

SPECTR
PHENOME

Despit

processes, ou

to this phase

occur frequen

distances. A

processes ha

information a

methods allo

$(10^{-12} - 10^{-9}$ s

The majority

focused on n

limited in the

long-range or

binary system

ABSTRACT

SPECTROSCOPIC STUDIES OF SOLUTION PHASE SELF-ASSEMBLY PHENOMENA USING "TAILOR-MADE IMPURITY" PROBE MOLECULES

By

Jeffrey Paul Rasimas

Despite the fact that solutions are the medium of choice for many chemical processes, our fundamental understanding of the intermolecular interactions that give rise to this phase of matter are limited. Interactions between individual molecules in solution occur frequently, and are characterized by short persistence times and short interaction distances. A useful approach to understanding fundamental solvation and solution phase processes has involved using a spectroscopically active probe molecule to infer information about the surrounding medium from its transient optical response. Such methods allow accessing the dynamical behavior of the probe molecules on short time (10^{-12} - 10^{-9} s) and length scales (1-30 Å) that are chemically relevant in these systems. The majority of studies using probe molecules to understand solvation effects have focused on neat solvents. Such studies have provided much useful information but are limited in their ability to discern organization by the absence of any driving force for long-range order within the system. The focus of this dissertation is on more complex binary systems, selected for their ability to self-assemble under appropriate conditions.

Aqueo

phase microst

during the cr

understood t

mesoscopic s

This

possess a gl

impurity" m

aggregation

solutions Th

"tailor-made

crystalline ag

the foundat

crystallizati

Aqueous β-D-glucose solutions are used to develop an understanding of solution phase microstructure. This model system is useful for elucidating the processes involved during the crystallization of compounds from solution, a phenomenon that remains understood to a limited extent. The relationships between molecular aggregation, mesoscopic solution organization and macroscopic crystal growth remain to be made.

This dissertation reports on the use of dual-function probe molecules which possess a glycoside moiety attached to selected fluorophores. These "tailor-made impurity" molecules ensure participation of the optically active specie in molecular aggregation that occurs in subsaturated, saturated and supersaturated aqueous glucose solutions. The data facilitate fundamental understandings of the optical responses of the "tailor-made impurities" and provide information on the existence and lifetime(s) of pre-crystalline aggregates in concentrated aqueous glucose solutions. This dissertation sets the foundation for a widely applicable, "lock-and-key" approach to the study of crystallization from a molecular, rather than bulk, perspective.

To Elizabeth and Peter

I wou

Professors G

encouragemc

I would like

Baker and A

that I recog

Browning fo

Furthermore,

analyzing the

happening

supporting m

ACKNOWLEDGMENTS

I would like to thank several people who assisted me in completion of this work. Professors Gary Blanchard and Kris Berglund have provided guidance, assistance, and encouragement throughout this project, for which I am extremely grateful. Additionally, I would like to thank the other members of my guidance committee, Professors Greg Baker and Alec Scranton, for their assistance in this work. In addition, it is imperative that I recognize the Marine Division of the Cadillac Motor Company and John M. Browning for providing me with an outlet for the frustrations of graduate school. Furthermore, I also thank the Blanchard Group for assistance in performing the work, analyzing the data, and listening to endless theories about what might or might not be happening. Ultimately, I would like to thank the National Science Foundation for supporting me and this research through grant CTS-94-07563.

TABLE OF CONTENTS

Table

LIST OF TABLES

Table 6

Table 6

Table 6

Figure

Figure 2 1

Figure 2 2

Figure 2 3

Figure 2 4

Figure 2 5

Figure 2 6

Figure 2 7

LIST OF FIGURES

Figure 2 8

Figure 2 9

Figure 2 10

Figure 2 11

Figure 2 12

Figure 2 13

Figure 2 14

Figure 3 1 T
b
b
n
f
t
n

Figure 3 2 P

Figure 3 3 T

Figure 3 4 S
re
g
N
gr
k
st
gr

Figure 3 5 Fl
w
en
at
fu
th

Figure 3 6 G
wa
wa
Na
wh
re
no

Figure 3 7 Kn
eq
pu
Ini
of

Figure 4 5

Figure 4 6

Figure 5 1

Figure 5 2

Figure 5 3

Figure 5 4

Figure 5 5

Figure 5 6

Figure 5 7

Figure 5 8

Figure 5 9

Figure 5 10

Figure 5 11

Figure 5 12

Figure 6 1

Figure 6 2.

Figure 6 3.

Figure 6.4 R
e
c

Figure 6.5 C
s
re
a
s

Figure 6.6 C
(C
th
re
S

Figure 6.7 R
an
D
(s
sa

Despit

processes, our

to this phase

liquid phase r

because they a

that occur h

characterized b

common appro

using a spect

surrounding m

methods to ac

10^{-9} s) and len

majority of the

where the chr

that, by using

system are sr

magnitude lo

Studies on sir

behavior, yet

Chapter 1

Introduction

Despite the fact that solutions are the medium of choice for many chemical processes, our fundamental understanding of the intermolecular interactions that give rise to this phase of matter remains limited. There has been significant research interest in liquid phase molecular interactions, and much of this work is focused on neat solvents because they are believed to be a simple starting point for these studies. The interactions that occur between individual molecules in solution occur frequently, and are characterized by short persistence times and short interaction distances. Therefore, a common approach to understanding solvation and solution phase processes has involved using a spectroscopically active probe molecule to infer information about the surrounding medium from its transient optical response.[1-43] These studies provide methods to access the dynamical behavior of the probe molecule on time scales (10^{-12} - 10^{-9} s) and length scales (1-30 Å) that are chemically relevant in liquids.[44] However, a majority of these studies have involved using a probe molecule in simple solvent systems, where the chromophore is present in low concentration in a neat solvent. It is assumed that, by using a low probe molecule concentration, the pertubations imposed on the system are small. For example, typical probe concentrations are 6 to 8 orders of magnitude lower than the surrounding medium, making this assumption reasonable. Studies on simple systems have been useful in developing an understanding of the probe behavior, yet there is not necessarily a direct correlation between these systems and more

complicated n

molecule is us

and, while le

probe molecu

content of suc

the present un

which one of t

concentration

The pr

poorly unders

relationship be

growth [51-66] T

drop in the

aggregates o

from other a

conclusion fr

be related t

formation o

molecular o

spontaneou

crystals. T

changes in

shown to p

complicated matrices. There have been a limited number of studies where a probe molecule is used to interrogate the properties of comparatively simple binary systems,[45-50] and, while leading, it is clear that without additional information on the location of the probe molecule with respect to local inhomogeneities within the system, the information content of such measurements is limited. It is the purpose of this dissertation to advance the present understanding of more complex liquid systems, with special focus on those in which one of the constituents self-assembles into a crystalline solid at sufficiently high concentration.

The processes involved during the crystallization of compounds from solution are poorly understood. There have been some previous efforts to understand the relationship between the structure of supersaturated solutions and crystal nucleation and growth.[51-60] These studies were based largely on diffusion in aqueous solutions where a drop in the constituent diffusion coefficient was associated with the formation of aggregates of unknown composition. Other studies demonstrated that crystallization from other aqueous systems formed glass-like solids at high supersaturations.[61-64] A conclusion from that work was that the ability or inability of a solution to nucleate must be related to the "structure" associated with the supersaturated solution, with the formation of nuclei being solvent-mediated. Despite this indication of cooperative molecular organization, there remains a significant regime of uncertainty between the spontaneous formation of molecular aggregates and the precipitation of macroscopic crystals. There have been attempts to correlate macroscopic solution properties to changes in solution microstructure,[65-67] however, no macroscopic property has been shown to predict the microscopic changes of interest accurately. There remains the need

to develop te

binary liquid

solution organ

Probe

understand mo

several ambig

systematic ma

probe molecul

dyes or polycy

functionality

eliminating th

solution is to

functionality

on the struc

interest, wh

assembly ph

sufficiently

In

covalently

allows pro

saturated

spectrosco

studied in

to develop techniques which provide direct information about local organization in binary liquid systems. The relationships between molecular aggregation, mesoscopic solution organization and macroscopic crystal growth remain to be made.

Probe molecules have been used in the work described in this dissertation to understand molecular-scale organization in complex binary liquid systems. There are several ambiguities inherent in such an approach, and these can be addressed in a systematic manner. Most notable is the uncertainty associated with the location of the probe molecule in the solution. The probes used are typically fluororphores (e.g. laser dyes or polycyclic aromatic hydrocarbons) which do not, in general, possess the chemical functionality required to associate with the crystallizing species. One approach to eliminating the uncertainty of the location of the spectroscopic probe as is "reads" the solution is to modify the chemical identity of the probe molecule to include a pendant functionality able to interact directly with the species of interest.[68] This approach relies on the structural similarity of an "impurity" molecule with respect to the solute of interest, which provides a "lock-and-key" methodology to study liquid phase self-assembly phenomena. It is important to note that the concentration of the probe be sufficiently small that its presence does not perturb the properties of the solution.

In this dissertation, the use of "tailor-made impurity" probes possessing a covalently bonded glycoside moiety is explored. The pendant glycoside functionality allows probe participation in molecular aggregation or clustering that may occur in saturated and supersaturated aqueous β-D-glucose solutions. The fundamental spectroscopic and dynamical behavior of glycoside based chromophores have not been studied in detail.[69-71] The work contained in this dissertation describes efforts aimed at

developing t

The experim

and glycosyl

There are se

the utility of

1. W

es

2. If

ass

3. Wh

sim

4. Doe

"loc

mea

5. Doe

chr

6. Can

Each of these qu

Chapter

chromophores

developing the "lock-and-key" methodology of studying solution phase self-assembly. The experiments focus on understanding three chromophores; carminic acid, resorufin, and glycosyl-resorufin. Each probe molecule accesses different properties of the matrix. There are several families of fundamental questions addressed in this work to evaluate the utility of the "lock-and-key" strategy:

1. What are the electronic properties of these glycosylated chromophores, especially relative to their non-glycosylated analogs?
2. If the chromophore has acid/base or ionic character, what role do equilibria associated with the chromophore play in the spectroscopic behavior?
3. What is the dynamical behavior of the "tailor-made impurity" molecule in simple systems, where aggregation is precluded?
4. Does the "tailor-made impurity" incorporate into β-D-glucose crystals as a "lock-and-key" probe, without affecting the overall crystal structure measurably?
5. Does the structure and functionality of the "tailor-made impurity" chromophore affect formation of aggregates?
6. Can aggregation be observed spectroscopically using this approach?

Each of these questions is addressed in this dissertation.

Chapter 2 describes a semi-empirical computational study of glycosylated chromophores. This work predicts the spectroscopic properties of the molecules

carminic acid,

phenoxazone

affect its linea

glycoside abou

isomeric forms

Chapter

using the sodiu

species form r

associative co

chromophores

Chapter 7

Chapter

acid in a series

understood usi

provided a basc

behavior of this

was found to be

Chapter

formation of pr

describes the pH

The data indicate

microstructure

supersaturated g

carminic acid, glycosyl-oxazine, glycosyl-phenoxazine, glycosyl-oxazone, and glycosyl-phenoxazone. It was found that addition of a glycoside to a chromophore does not affect its linear response substantially, and that the rotational isomerization of the glycoside about its tethering bond to the chromophore can result in formation of isomeric forms of the "lock-and-key" molecule.

Chapter 3 describes a study of solution phase ionic association and dissociation using the sodium/resorufin complex. It was found that solvent mediated charge-transfer species form rapidly (<50 ps). This work demonstrates the important role of pre-associative complex formation and its effects on the overall dynamics of ionic chromophores. The dynamics of resorufin in aqueous glucose will be described in Chapter 7.

Chapter 4 details a study of the "tailor-made impurity" chromophore carminic acid in a series of *n*-alcohols. It was found that the fluorescence lifetime behavior can be understood using the calculated properties detailed in Chapter 2. This work also provided a baseline understanding of the previously unstudied and complex dynamical behavior of this pH-sensitive chromophore. This dynamical behavior of carminic acid was found to be useful as a microscopic probe of local polarity.

Chapter 5 is a study of carminic acid and its use as a "lock-and-key" probe of the formation of pre-crystalline aggregates in aqueous glucose solutions. This chapter describes the pH-dependence of its linear response, as well as its picosecond dynamics. The data indicated that the "lock-and-key" methodology is viable for studying solution microstructure. It was found that there is significant short-range structure in supersaturated glucose solutions. Pre-crystalline aggregate lifetimes were short (<1 ns),

and this sugg

dominant rol

Chapt

resorufin and

indicated a n

with glucose

aggregates

underscore th

aggregates

which aggreg

Chapt

spectroscopic

future directi

microstructur

and this suggested that the kinetic contributions to crystallization are expected to play a dominant role in solution.

Chapter 6 describes a comparison between the spectroscopic behavior of resorufin and glycosyl-resorufin in aqueous glucose solutions. The response of resorufin indicated a non-specific interaction with glucose, however glycosyl-resorufin interacted with glucose in a "lock-and-key" fashion to show inclusion into pre-crystalline aggregates. These results, when compared to analogous data for carminic acid, underscore the important role of protons in determining the stability of pre-crystalline aggregates. In addition, this comparison implicates glycosyl-resorufin as a site about which aggregation occurs in solution.

Chapter 7 summarizes the use of "tailor-made impurity" probe molecules as spectroscopic probes of glucose pre-crystalline aggregate formation and describes the future directions and generality of the "lock-and-key" approach to studying solution microstructure.

1.1. Litera

1 Morris, D

2 Butler, R

3 Weaver, V
8956

4 Hambir, S

5 Jiang, Y

6 Aicart, E

7 Snyder, R

8 Snyder, R

9 Marcus, Y

10 Ohtaki, I

11 Snyder,

12 Battacha

13 Stengle,

14 Porter, C

15 Spears, I

16 Biancha

17 Philips, I

18 Biancha

19 Millar, D

20 Waldeck
1981,

1.1. Literature Cited

1. Morris, D. L. Jr.; Gustafson, T. L. *J. Phys. Chem.*, **1994**, *98*, 6725.

2. Butler, R. M.; Lynn, M. A.; Gustafson, T. L. *J. Phys. Chem.*, **1993**, *97*, 2609.

3. Weaver, W. L.; Huston, L. A.; Iwata, K.; Gustafson, T. L. *J. Phys. Chem.*, **1992**, *96*, 8956.

4. Hambir, S. A.; Jiang, Y.; Blanchard, G. J. *J. Chem. Phys.*, **1993**, *98*, 6075.

5. Jiang, Y.; Blanchard, G. J. *J. Phys. Chem.*, **1994**, *98*, 6436.

6. Aicart, E.; Tardagos, G.; Costas, M. *J. Sol. Chem.*, **1989**, *18*, 369.

7. Snyder, R. G.; Aljibury, A. L.; Strauss, H. L. *J. Chem. Phys.*, **1984**, *81*, 5352.

8. Snyder, R. G.; Schachtschneider, J. H. *Spectrochimica Acta*, **1963**, *19*, 85.

9. Marcus, Y. *J. Sol. Chem.*, **1992**, *21*, 1217.

10. Ohtaki, H. *J. Sol. Chem.*, **1992**, *21*, 39.

11. Snyder, R. G. *J. Chem. Phys.*, **1967**, *47*, 1316.

12. Battacharyya, S. N.; Patterson, D. *J. Sol. Chem.*, **1980**, *9*, 753.

13. Stengle, T. R.; Hosseini, S. M.; Williamson, K. L. *J. Sol. Chem.*, **1986**, *15*, 777.

14. Porter, G.; Sadkowski, P. J.; Tredwell, C. J. *Chem. Phys. Lett.*, **1977**, *49*, 416.

15. Spears, K. G.; Cramer, L. E. *Chem. Phys.*, **1978**, *30*, 1.

16. Blanchard, G. J. *J. Phys. Chem.*, **1988**, *92*, 6303.

17. Philips, L. A.; Webb, S. P.; Clark, J. H. *J. Chem. Phys.*, **1985**, *83*, 5810.

18. Blanchard, G. J.; Wirth, M. J. *J. Phys. Chem.*, **1986**, *90*, 2521.

19. Millar, D. P.; Shah, R.; Zewail, A. H. *Chem. Phys. Lett.*, **1979**, *66*, 435.

20. Waldeck, D. H.; Cross, A. J.; Jr.; McDonald, D. B.; Fleming, G. R. *J. Chem. Phys.*, **1981**, *74*, 3381.

21 von Jena.

22 Spears, K.

23 Templeto
89, 3238

24 Mokhtari,

25 Wagener,

26 Declemy,

27 Castner, E

28 Nagarajan,
86, 3183

29 Maroncelli

30 Simon, J. [

31 Barbara, P

32 Maroncelli
95, 1012

33 Jarzeba, W
57

34 Elsaesser,

35 Lingle, R.
5667

36 Anfinrud,
1180

37 Heilweil, E
Chem., 19

38 Heilweil, E
181

21. von Jena, A.; Lessing, H. E. *Chem. Phys. Lett.*, **1981**, *78*, 187.

22. Spears, K. G.; Steinmetz, K. M. *J. Phys. Chem.*, **1985**, *89*, 3623.

23. Templeton, E. F. G.; Quitevis, E. L.; Kenney-Wallace, G. A. *J. Phys. Chem.*, **1985**, *89*, 3238.

24. Mokhtari, A.; Chesnoy, J.; Laubereau, A. *Chem. Phys. Lett.*, **1989**, *155*, 593.

25. Wagener, A.; Richert, R. *Chem. Phys. Lett.*, **1991**, *176*, 329.

26. Declemy, A.; Rulliere, C.; Kottis, Ph. *Chem. Phys. Lett.*, **1987**, *133*, 448.

27. Castner, E. W.; Maroncelli, M.; Fleming, G. R. *J. Chem. Phys.*, **1987**, *86*, 1090.

28. Nagarajan, V.; Brearly, A. M.; Kang, T. J.; Barbara, P. F. *J. Chem. Phys.*, **1987**, *86*, 3183.

29. Maroncelli, M.; Fleming, G. R. *J. Chem. Phys.*, **1987**, *86*, 6221.

30. Simon, J. D. *Acc. Chem. Res.*, **1988**, *21*, 128.

31. Barbara, P. F.; Jarzeba, W. *Adv. Photochem.*, **1990**, *15*, 1.

32. Maroncelli, M.; Fee, R. S.; Chapman, C. F.; Fleming, G. R. *J. Phys. Chem.*, **1991**, *95*, 1012.

33. Jarzeba, W.; Walker, G. C.; Johnson, A. E.; Barbara, P. F. *Chem. Phys.*, **1991**, *152*, 57.

34. Elsaesser, T.; Kaiser, W. *Annu. Rev. Phys. Chem.*, **1991**, *42*, 83.

35. Lingle, R.; Jr.; Xu, X.; Yu, S. C.; Zhu, H.; Hopkins, J. B. *J. Chem. Phys.*, **1990**, *93*, 5667.

36. Anfinrud, P. A.; Han, C.; Lian, T.; Hochstrasser, R. M. *J. Phys. Chem.*, **1990**, *94*, 1180.

37. Heilweil, E. J.; Casassa, M. P.; Cavanagh, R. R.; Stephenson, J. C. *Ann. Rev. Phys. Chem.*, **1989**, *40*, 143.

38. Heilweil, E. J.; Cavanagh, R. R.; Stephenson, J. C. *Chem. Phys. Lett.*, **1987**, *134*, 181.

39. Heilwe

40. Heilwe
1986, 8

41. Jiang, Y

42. Jiang, Y

43. Jiang, Y

44. Israelac
1991

45. Blancha

46. Beddard

47. Christen

48. Gudgin-

49. Gudgin-

50. Dutt, G

51. Chatkrbo

52. Chakrabo

53. Pan, B.,

54. Myerson,

55. Chang, Y

56. Chang, Y

57. Chang, Y

58. Myerson,
E J., eds

39. Heilweil, E. J.; Cavanagh, R. R.; Stephenson, J. C. *J. Chem. Phys.*, **1989**, *89*, 230.

40. Heilweil, E. J.; Casassa, M. P.; Cavanagh, R. R.; Stephenson, J. C. *J. Chem. Phys.*, **1986**, *85*, 5004.

41. Jiang, Y.; Blanchard, G. J. *J. Phys. Chem.*, **1994**, *98*, 9411.

42. Jiang, Y.; Blanchard, G. J. *J. Phys. Chem.*, **1994**, *98*, 9417.

43. Jiang, Y.; Blanchard, G. J. *J. Phys. Chem.*, **1995**, *99*, 7904.

44. Israelachvili, J., ed. Intermolecular and Surface Forces, Academic Press, London, **1991**.

45. Blanchard, G. J. *Anal. Chem.*, **1989**, *61*, 2394.

46. Beddard, G. S.; Doust, T.; Hudales, J. *Nature*, **1981**, *294*, 145.

47. Christensen, R. L.; Drake, R. C.; Phillips, D. *J. Phys. Chem.*, **1986**, *90*, 5960.

48. Gudgin-Templeton, E. F.; Kenney-Wallace, G. A. *J. Phys. Chem.*, **1986**, *90*, 2896.

49. Gudgin-Templeton, E. F.; Kenney-Wallace, G. A. *J. Phys. Chem.*, **1986**, *90*, 5441.

50. Dutt, G. B.; Doriswamy, S.; *J. Chem. Phys.*, **1992**, *96*, 2475.

51. Chatkrborty, R.; Berglund, K. A. *AIChE Sym. Ser*, **1991**, *87*, 114.

52. Chakraborty, R.; Berglund, K. A. *J. Cryst. Growth.*, **1992**, *125*, 81.

53. Pan, B.; Chakraborty, R.; Berglund, K. A. *J. Cryst. Growth*, **1993**, *130*, 587.

54. Myerson, A. S.; Sorel, L. S. *AIChE J.*, **1982**, *28*, 778.

55. Chang, Y. C.; Myerson, A. S. *AIChE J.*, **1985**, *31*, 980.

56. Chang, Y. C.; Myerson, A. S. *AIChE J.*, **1986**, *32*, 1567.

57. Chang, Y. C.; Myerson, A. S. *AIChE J.*, **1986**, *32*, 1747.

58. Myerson, A. S.; Chang, Y. C. Industrial Crystallization '84, Jancic, S. J.; DeJong, E. J.; eds.: Elsevier, Amsterdam, **1984**, 27.

59. Sorrel.

60 Crystal
eds. A

61. Tamma
1925.

62. Mullin,

63. Mullin,

64. Mullin,

65. Larson,

66 Larson,

67. Narayar

68 Weissbu

69 Kirkbrig

70. Jorgens

71 Stapelfe

59. Sorrel, L. S.; Myerson, A. S. *AIChE J.*, **1982**, *28*, 772.

60. Crystal Growth of Organic Materials, Myerson, A. S.; Green, D. A.; Meenan, P.; eds.: ACS Conference Preeceedings, Washington, D. C., **1995.**

61. Tamman, G. States of Aggregation, Mehl, R. F. trans., van Nostrand, New York, **1925.**

62. Mullin, J. W.; Leci, C. *Philos. Mag.*, **1969**, *19*, 1075.

63. Mullin, J. W.; Leci, C. *J. Crystal Growth*, **1969**, *5*, 75.

64. Mullin, J. W.; Leci, C. *Chemy Ind.*, **1968**, 1517.

65. Larson, M. A.; Garside, J. *Chem. Eng. Sci.*, **1986**, *41*, 1285.

66. Larson, M. A.; Garside, J. *J. Cryst. Growth*, **1986**, *76*, 88.

67. Narayanan, H.; Youngquist, G. R. *AIChE Symposium Series*, **1987**, *253*, 1-7.

68. Weissbuch, I.; Addadi, L.; Lahav, M. ; Leiserowitz, L. *Science*, **1991**, *253*, 637.

69. Kirkbright, G. F.; West, T. S.; Woodward, C. *Talanta*, **1966**, *13*, 1637.

70. Jorgensen, K.; Skibsted, L. H. *Food Chemistry*, **1991**, *40*, 25.

71. Stapelfeldt, H.; Jun, H.; Skibsted, L. H. *Food Chemistry*, **1993**, *48*, 1.

2.1. Intro

Resea
provided a gr
phases A si
defined nature
achieving a f
solutions has
length scales
experiments t
liquid phase h
any organizat
examine neat
probe molec
molecules f
assumed tha
probe molec
specific inte
Both of the
cases they
classes of
limiting

2.1. Introduction

Research into understanding the interactions between dissimilar molecules has provided a great deal of information on structure and reactivity in both the solid and gas phases. A significant factor in achieving this progress has been the comparatively well defined nature of intermolecular interactions in these two phases. In sharp contrast, achieving a fundamental understanding of intermolecular interactions in liquids and solutions has proven to be extremely difficult, primarily because of the short time and length scales over which molecular organization persists in this phase. The majority of experiments that provide information on the nature of intermolecular interactions in the liquid phase have used optical spectroscopy because of the short time scale(s) on which any organization is present in such systems. For these experiments, it is possible to examine neat liquids using stimulated transient Raman techniques[1,2] or, more typically, a probe molecule is used to "read" information out of a solution.[3-7] The use of probe molecules for this purpose has found wide acceptance and, in many instances, it is assumed that the probe molecule is a passive monitor of the surrounding medium, *i.e.* probe molecule *intramolecular* processes are well understood and that there are no site-specific intermolecular interactions between the probe molecule and its surroundings. Both of these assumptions serve, of course, to simplify data interpretation and in many cases they have turned out to be valid, but there exist a variety of experiments and classes of probe molecules for which one or both of these assumptions have proven to be limiting.[8,9,28] Understanding the optical and chemical properties of the probe molecule

are therefore

spectroscopic

The v

optical respon

moment on e

and thus ob

Indeed, there

that intramole

molecules, and

probe molecul

straightforwar

demonstrates

semiempirical

dynamics mea

with a site-sp

that, on excit

its heterocyc

coumarins ha

single, unifo

predicted th

and those

experimenta

are therefore necessary prerequisites for the successful interpretation of transient spectroscopic data used in understanding molecular scale interactions in the liquid phase.

The very properties that make probe molecules useful, such as a prominent optical response at frequencies accessible to short pulse lasers or a large change in dipole moment on excitation, can also serve to complicate the optical response of the molecule and thus obviate straightforward data interpretation in terms of local organization. Indeed, there is a large body of information in the literature indicating the important role that intramolecular processes play in the transient optical response of certain probe molecules, and that the transient absorption and/or emission characteristics of a given probe molecule may not be related to the local environment of the probe molecule in a straightforward way.[3-5,8,28] Our previous work on several families of probe molecules demonstrates that there is an excellent correspondence between experimental data and semiempirical calculations.[8,10-14] For example, the state-dependent reorientation dynamics measured for oxazines and thiazines in polar protic solvents were consistent with a site-specific solvent-solute interaction, and semiempirical calculations indicated that, on excitation, the oxazine chromophore accumulated significant electron density at its heterocyclic nitrogen.[11-13,15] In addition, the transient optical response of the coumarins has been shown recently not to be accounted for simply by the presence of a single, uniform (shifting) electronic state.[8] In that work, semiempirical calculations predicted the existence of several excited electronic states in close energetic proximity, and those predictions provided an explanation consistent with a large body of experimental data. Thus, there is compelling experimental evidence that validates the

qualitative pr

organic molec

Most

systems, *i.e.* d

interest lies in

solvent and th

solvent. Spec

molecular org

In order to ex

moiety to facil

in the sugar

develop a d

questions th

semiempirica

glycosyloxaz

these molec

- Can a s

  intramo

  experim

- How d

  carmin

qualitative predictive power of semiempirical calculations for moderately large polar organic molecules.

Most examinations of solvent-solute interactions have been performed in binary systems, *i.e.* dilute solutions of a probe molecule in a single organic solvent. Our present interest lies in understanding local structure in ternary systems where, in addition to the solvent and the solute, there is a third constituent that exhibits limited solubility in the solvent. Specifically, this work will be used toward developing an understanding of molecular organization associated with the onset of crystallization in sugar solutions.[16,17] In order to examine these systems, a family of probe molecules containing a glycoside moiety to facilitate the incorporation of the probe molecule into local structure(s) formed in the sugar solutions will be utilized. The first step in this research program is to develop a detailed understanding of the probe molecules and address several basic questions that cannot be answered directly by experiment. This chapter reports a semiempirical computational study of three classes of molecules; carminic acid, glycosyloxazines and glycosyloxazones (Figure 2.1). The questions addressed regarding these molecules are:

- Can a simple linear optical response be expected from these molecules or might intramolecular relaxation effects be expected to play an important role in the experimental data?

- How does the pH of the solution affect the optical response and state ordering of carminic acid?

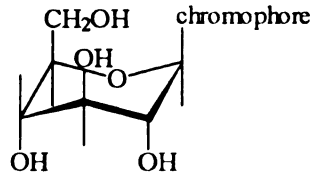

(a)

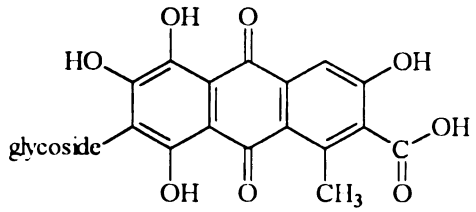

(b)

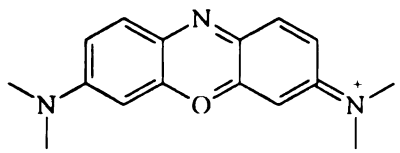

(c)

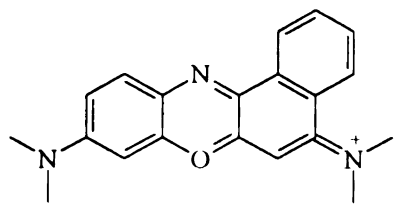

(d)

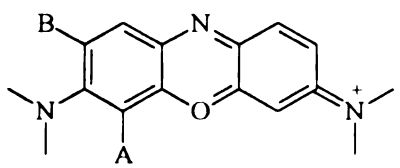

(e)

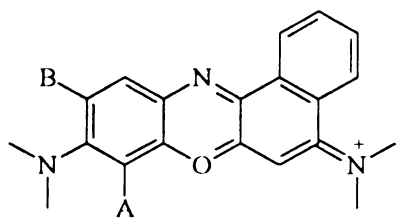

(f)

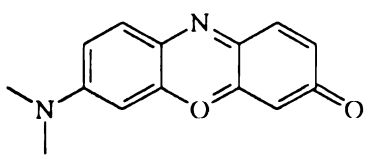

(g)

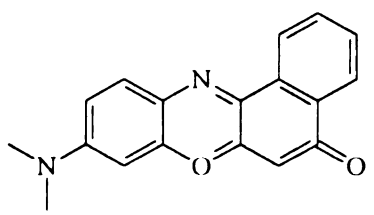

(h)

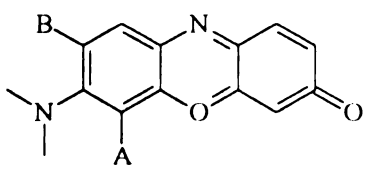

(i)

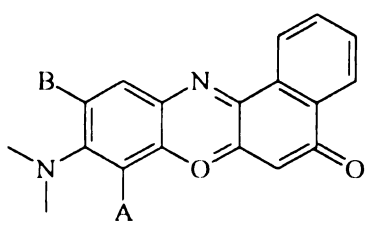

(j)

Figure 2.1. "Tailor-made impurity" molecules modeled using AM1 Semi-empirical computations.

- For oxaz
  optical re
- Will rotat
  optical re

These
reasonably st
crossing bein
calculated to
energetic prox
that the addi
chromophore
previously rep
formation of
arises from st
hindrance als
Importantly,
bond does no
to be concer
These calcula
these molecu
chromophore
attention.

- For oxazines and oxazones, how does the addition of a glycoside moiety affect the optical response of the chromophore?

- Will rotation of the chromophore about its bond to the glycoside moiety affect its optical response?

These calculations indicate that all of the chromophores selected will exhibit a reasonably straightforward linear optical response, with the potential for intersystem crossing being the most significant concern. The deprotonation of carminic acid is calculated to cause a spectral blue shift, and move the first triplet state into close energetic proximity to the first excited singlet state. For the oxazones, it is calculated that the addition of the glycoside moiety will affect the optical response of the chromophore to only a small extent, while for the oxazines it is noted, in addition to the previously reported accumulation of charge at the ring bound nitrogen on excitation, the formation of a stable twisted internal charge transfer conformation in the S_1 state that arises from steric hindrance due to the presence of the glycoside moiety. This steric hindrance also gives rise to a substantial (~10%) blue shift of the $S_0 \leftrightarrow S_1$ transition. Importantly, for all of the chromophores, rotation about the chromophore-glycoside bond does not affect the energy of the $S_0 \leftrightarrow S_1$ transition, and therefore there is no need to be concerned about any conformation-specific contributions to the linear response. These calculations serve to predict the qualitative features of the optical response(s) of these molecules and to answer fundamental questions about the effects of substitution on chromophores that, in their native forms, have received significant experimental attention. In addition to the uses for these probe molecules, similar glycosylated

chromophore

important flu

2.2. Expe

Semie

parameteriza

IBM compa

modification

molecules ar

Figure 2.1

mechanics r

level using a

protonated

formed by

Semiempiric

molecule w

geometricall

optimized g

single conf

calculations

approximati

will hold fo

assume the

chromophores have found application in fluorescent immunoassays and other biologically important fluorescence-based measurements.[18-21]

2.2. Experimental

Semiempirical calculations were performed using the Austin Model 1 (AM1) parameterization running on Hyperchem software (Release 3.0; Autodesk, Inc.) on an IBM compatible PC (Gateway 2000 486-66V). The AM1 parameterization [22-24] is a modification of the MNDO parameterization[25-26] that is more accurate for polar molecules and transition states. The calculation strategy for the molecules shown in Figure 2.1 was to perform an initial optimization of the structures using a molecular mechanics routine (MM+),[27] followed by geometry optimization at the semiempirical level using an SCF algorithm. Two structures for carminic acid were calculated, the fully protonated form (H_4CA), and the singly deprotonated form, (H_3CA^-). H_3CA^- was formed by removing the acidic proton from the carboxylic acid functionality. Semiempirical optimization was performed until the lowest energy conformation for each molecule was attained. Electronic energy calculations were performed on the geometrically SCF-optimized molecules. For these calculations, the ground state optimized geometry was used and RHF closed-shell calculations were performed for single configuration interaction (CI) with 100 microstates. Previously, similar calculations using a large number of CI states were believed to provide a fair approximation of correlation effects in coumarins,[28] and it is believed that this condition will hold for these calculations as well. It is important to recall that these calculations assume the molecules are isolated and in an absolute vacuum.

2.3. Resu

Carm

electronic pr

barriers for

Understandir

important be

Additionally,

5.43, pK_{a3} =

H_4CA and tl

reports a sur

the negative

show a trend

While it is t

possess a si

states, it is

permanent d

charge distri

H_3CA^- are

moments re

necessarily c

within the m

singly charge

2.3. Results and Discussion

Carminic Acid. Calculations on carminic acid were performed to understand the electronic properties of both H_4CA and H_3CA^- as well as to determine isomerization barriers for rotation of the glycosyl moiety about its bond to the chromophore. Understanding the pH dependence of the optical response of this fluorophore is important because pK_{a1} = 2.8 (deprotonation of the carboxylic acid) for carminic acid. Additionally, carminic acid possesses three other labile phenolic protons[29-32] with pK_{a2} = 5.43, pK_{a3} = 8.10 and $pK_{a4} \cong 13$. We discuss in this work only the protonated form, H_4CA and the monodeprotonated form, H_3CA^-, for reasons detailed below. Table 2.1 reports a summary of the electronic properties calculated for both the neutral H_4CA and the negatively charged H_3CA^- molecules. The dipole moments calculated for H_4CA show a trend of decreasing polarity as the molecule is excited to higher electronic states. While it is typically held that the ground electronic states of polar organic molecules possess a smaller permanent dipole moment than the first excited electronic singlet states, it is entirely possible that the excited states of certain molecules will have a permanent dipole moment smaller than that of the ground state, owing to the change in charge distribution caused by excitation. The permanent dipole moments calculated for H_3CA^- are physically unrealistic. It is believed that these large calculated dipole moments result from limitations inherent to the AM1 parameterization and to the necessarily discrete way in which such calculations account for the presence of charges within the molecule. Despite these limitations, the qualitative trends predicted for other singly charged species have been proven correct by experimental data, and therefore it is

Table 2.1. Calculated Properties of Carminic Acid

	energy relative to S_0 (cm^{-1})

Table 2.1. Calculated Properties of Carminic Acid

		energy relative to S_0 (cm^{-1})						
molecule	ΔH_f (kcal/mole)	T_2	S_1	T_3	S_2	$\mu(S_0)$ (D)	$\mu(T_1)$ (D)	$\mu(S_1)$ (D)
carminic acid (netural)	-516.14	22852	28355	29176	32931	3.45	1.92	1.56
carminic acid (-1 charge)	-551.10	33830	30140	34118	33971	24.36	15.94	8.87

believed th

sense

Fig

from AM

states is q

S_0) = 199

state (ΔE

($\Delta E(T_1$-S

($\Delta E(S_1$-S

two form

lower in e

the possi

species

H_2CA^-, a

for their

an aquec

neutral c

lower in

state nea

suggests

to the T

deprotor

believed that the data reported here for both H_4CA and H_3CA^- are useful in a qualitative sense.

Figure 2.2 shows the energy level diagrams for H_4CA and H_3CA^- determined from AM1 calculations using configuration interaction (CI). The ordering of the energy states is quite different for the two species, with H_4CA having two triplet states ($\Delta E(T_1\text{-}S_0)$ = 19951 cm^{-1}, $\Delta E(T_2\text{-}S_0)$ = 22852 cm^{-1}), between the ground and first excited singlet state ($\Delta E(S_1\text{-}S_0)$ = 28355 cm^{-1}). The monodeprotonated species has a triplet state ($\Delta E(T_1\text{-}S_0)$ = 29858 cm^{-1}) in close energetic proximity to the first excited singlet state ($\Delta E(S_1\text{-}S_0)$ = 30140 cm^{-1}). State ordering for higher excited states also differs for the two forms, with the most dramatic difference being that H_3CA^- has triplet states slightly lower in energy, but always in close proximity to higher excited singlet states, suggesting the possibility of efficient coupling between the singlet and triplet manifolds for this species. These calculations agree with observed spectroscopic properties of H_4CA and H_3CA^-, as studied by Stapelfeldt *et al.*[30-31] and serve to provide a mechanistic explanation for their observations. Their experimental data showed that the fluorescence intensity of an aqueous solution of carminic acid at basic pH is less than the emission intensity of neutral or acidic solutions. As shown in Figure 2.2, there is a triplet state (T_1) slightly lower in energy than the first excited singlet state (S_1) for H_3CA^-, with no analogous state near the S_1 for H_4CA. The lower fluorescence intensity observed for H_3CA^- suggests that depopulation of the S_1 state occurs through efficient intersystem crossing to the T_1 state. Stapelfeldt *et al.*[30] suggest that the main depopulation pathway for deprotonated forms involves an intersystem crossing to T_1, followed by photo-oxidation

Figure 2.2.

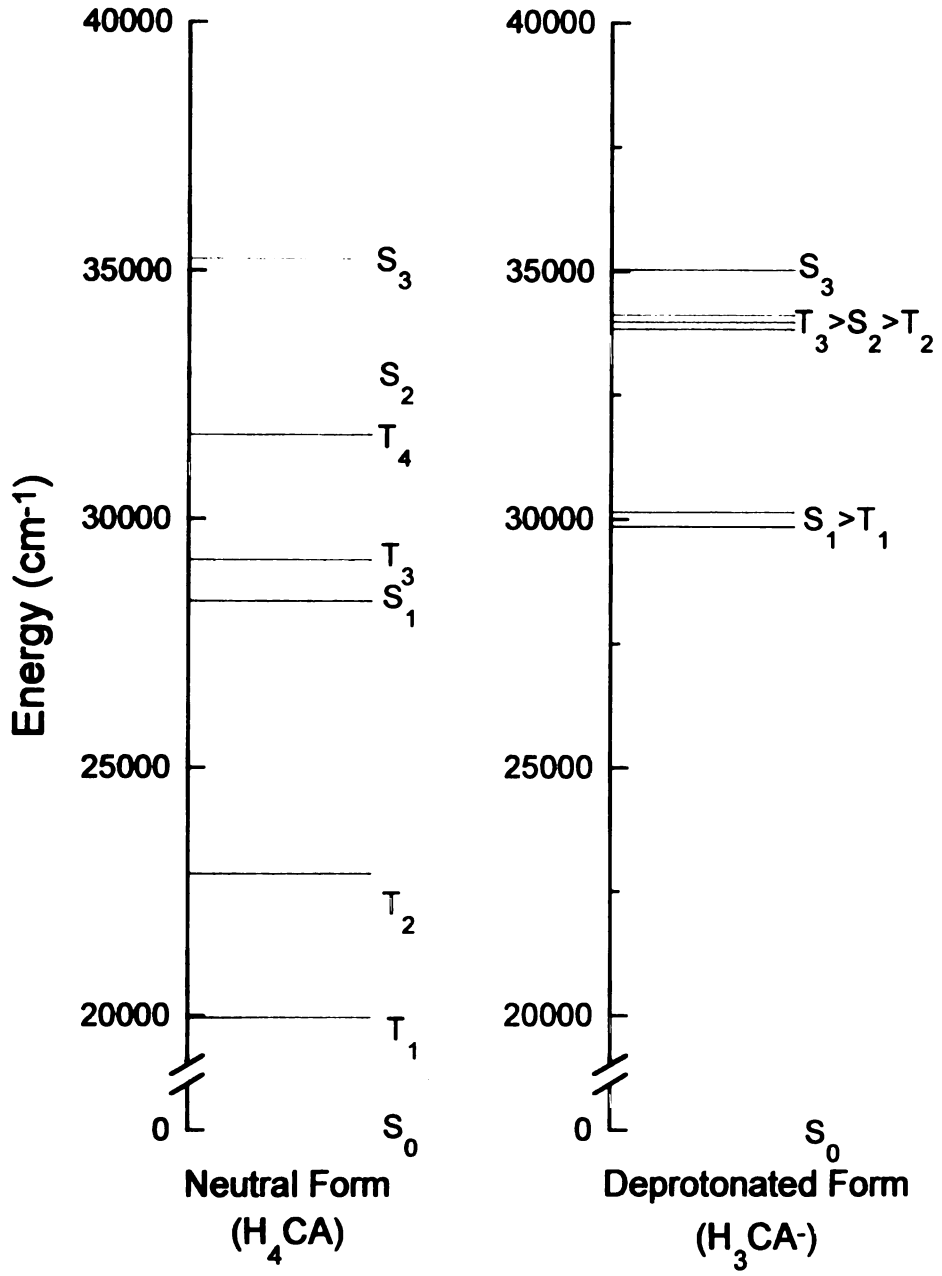

Figure 2.2. AM1/CI semi-empirical energies calculated for carminic acid in its fully protonated (H_4CA) and singly deprotonated (H_3CA^-) forms.

and subsequent

state ordering

speculation on

scope of this w

T_2 for H_4CA s

the fully proton

In unde

important to c

Figure 2.3 sho

states ($\Delta p_{sd} = p$

For H_4CA, t

anthraquinone

significant char

molecular orbit

the glycoside m

of H_4CA is

chromophore

conjugated with

produce steric

molecule

In an e

may produce in

and subsequent depopulation of triplet state $H_3CA^{\cdot}$. These calculations of electronic state ordering for $H_3CA^{\cdot}$ show that this singlet deactivation route is likely, although speculation on photo-oxidation subsequent to intersystem crossing is well outside the scope of this work. The larger energy separation between S_1 and the triplet states T_1 and T_2 for H_4CA suggests that depopulation of the S_1 state through intersystem crossing in the fully protonated species is less likely to be efficient.

In understanding how a probe molecule will interact with its surroundings, it is important to consider how the electron distribution differs among the electronic states. Figure 2.3 shows the calculated *change* in electron density (ρ_{cd}) between the S_1 and S_0 states ($\Delta\rho_{cd} = \rho_{cd}(S_1) - \rho_{cd}(S_0)$) at each atom for H_4CA (Fig. 2.3a) and $H_3CA^{\cdot}$ (Fig. 2.3b). For H_4CA, the changes in electron density upon excitation occur within the anthraquinone chromophore while the glycoside group does not experience any significant change in electron density. The primary implication of this result is that the molecular orbitals responsible for the optical response of H_4CA are not associated with the glycoside moiety, and this finding is intuitively reasonable. The absorption maximum of H_4CA is ~550 nm in polar organic solvents, indicating a highly conjugated chromophore. Because the glycoside group does not possess π orbitals that are conjugated with the π orbitals of the chromophore, it is expected the glycoside group to produce steric, rather than electronic, perturbations to the optical response of this molecule.

In an effort to understand any potential steric effects that the glycoside group may produce in the optical response of carminic acid, the isomerization barriers for

Figure 2.3 Ca
(S
car
pos
S
±0

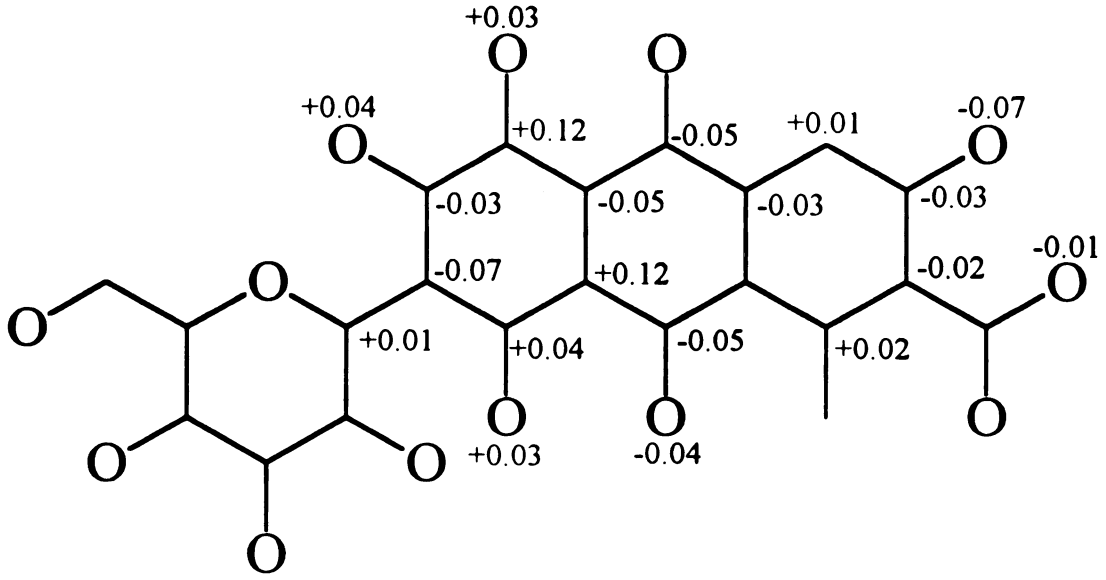

(a)

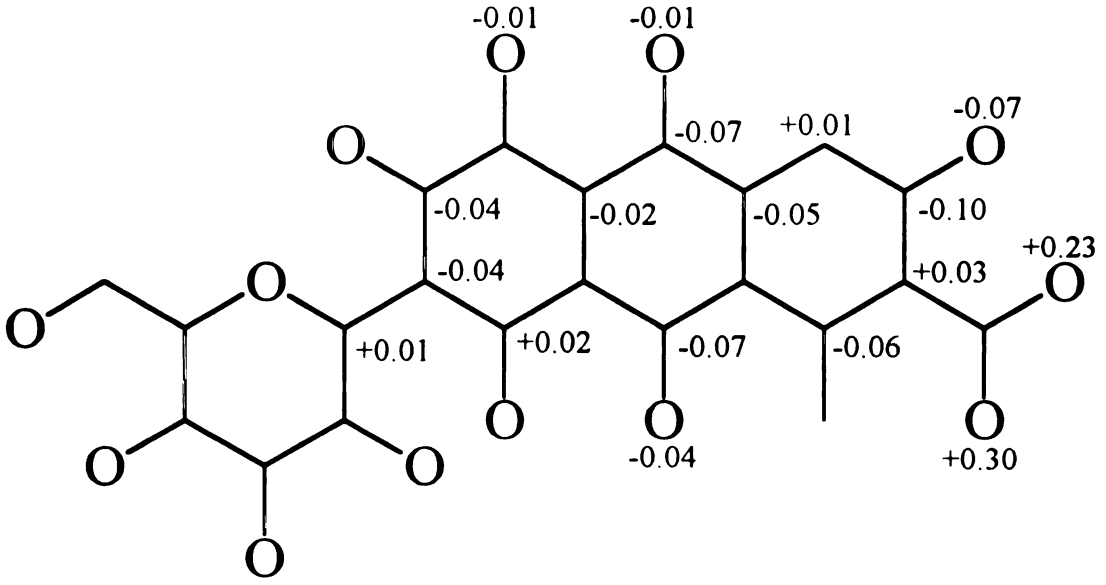

(b)

Figure 2.3. Calculated change in electron distribution between the singlet excited state (S_1) and the ground state (S_0) for carminic acid. Structure (a) is for neutral carminic acid, while (b) is for the singly deprotonated (-1 charge) form. A positive sign indicates a decrease in electron densty upon excitation from the S_0 to S_1 electronic states. Protons are not shown, nor are values less than ±0.01.

rotation of the

state. first trip

calculated. Th

for the two fo

at a glycoside-

a local maximu

310°, the barri

for H_2CA^-. Th

acid will be co

It is equally si

virtually identic

the linear optic

makes with the

isomerization p

are several po

converge. This

not calculate ch

form of the isom

for H_2CA^-, indi

rather than elec

performed using

angle without m

routines allow m

rotation of the glycoside moiety about its bond with the chromophore for the ground state, first triplet state, and first excited singlet state of both H_4CA and H_3CA^- have been calculated. These data are shown in Figure 2.4. The isomerization barriers are similar for the two forms of carminic acid, with the minimum energy of both species occurring at a glycoside-chromophore dihedral angle of 55°. The calculated barrier height reaches a local maximum of ~90 kcal/mole at 155° for H_4CA and ~68 kcal/mole for H_3CA^-. At 310°, the barrier height is calculated to be ~180kcal/mole for H_4CA and ~127 kcal/mole for H_3CA^-. The heights of these barriers indicate that the glycoside moiety of carminic acid will be constrained to a relatively narrow range of angles and will not rotate freely. It is equally significant that the angular dependence of the isomerization barriers are virtually identical for all the electronic states calculated. These calculations indicate that the linear optical response of the chromophore will not depend on the dihedral angle it makes with the glycoside group, and therefore there is little or no information about this isomerization process available from electronic absorption or emission spectra. There are several points in the calculation of H_3CA^- isomerization barrier that failed to converge. This failure serves as another indication that the AM1 parameterization does not calculate charged species as effectively as neutral species. Additionally, the overall form of the isomerization barrier calculated for H_4CA is similar to the barrier calculated for H_3CA^-, indicating that the isomerization coordinate(s) of this motion are sterically, rather than electronically, mediated. It should be noted that these calculations were performed using a calculation routine that determined the energy at a given dihedral angle without minimization of the complete structure. Recent advances in calculation routines allow minimization of the overall structure at each dihedral angle, and

-200
-250
-300
-350
-400
-450
-500
-550
0
ΔH_f (kcal/mole)
-200
-250
-300
-350
-400
-450
-500
-550
0

Figure 2.4.

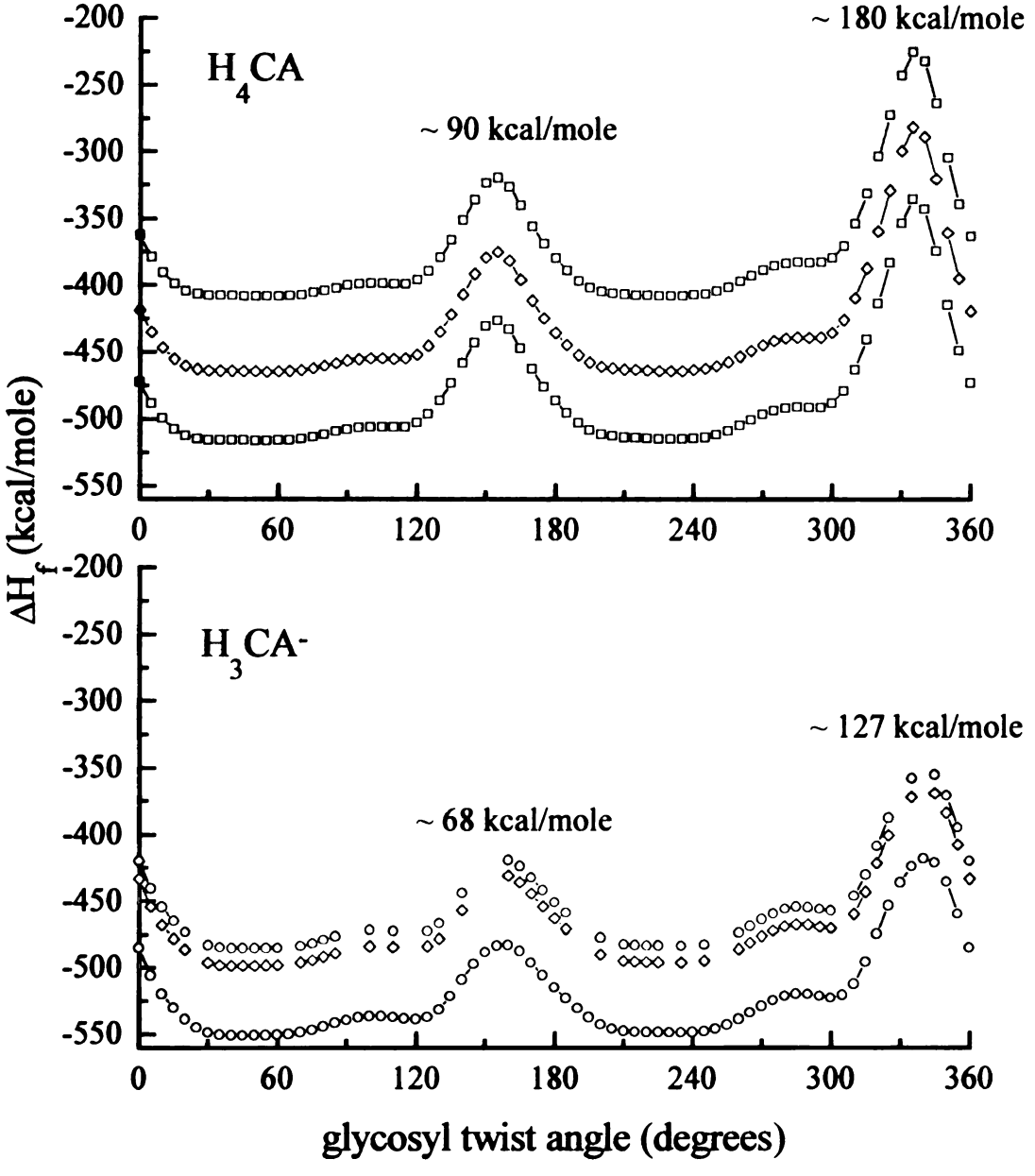

Figure 2.4. Calculated energy dependence of the glycosyl group rotation for the S_0 (O), T_1 (◊), and S_1 (□) states of carminic acid. The dihedral angle is the angle made by the glycosyl group with respect to the chromophore. Missing points indicate a failure of the calculation to converge at the given dihedral angle. Relative energies at a given dihedral angle were $S_1>T_1>S_0$.

recalculated da

discussed here

calculation rou

Oxazin

2-glycosyl ana

isomerization b

parameterizatio

the series so tha

could be unde

results for seve

presented here

complex polar c

and 203 kcal m

values are in qu

and 233 kcal m

parameterizatio

calculated for t

species (Figure

and phenoxaz

synthesized and

These synthetic

different subst

unsubstituted c

recalculated data (not shown) for carminic acid provide qualitatively similar data to that discussed here. None of the results discussed are affected by this change in the calculation routine.

Oxazines and Phenoxazines. The electronic properties of oxazine, phenoxazine, 2-glycosyl and 18-glycosyl oxazine and phenoxazine as well as the rotational isomerization barriers for the latter two compounds have been calculated using the AM1 parameterization. These calculations include unsubstituted oxazine and phenoxazine in the series so that effects of glycosylation on the electronic properties of the chromophore could be understood clearly. There have been reports of semiempirical calculation results for several of these molecules using the MNDO parameterization,[33] and the data presented here serve as a direct comparison of AM1 and MNDO parameterizations for complex polar organic molecules. In the previous work, heats of formation (ΔH_f) of 187 and 203 kcal/mole were calculated for oxazine and phenoxazine, respectively. These values are in qualitative agreement with the values presented in this work, (208 kcal/mol and 233 kcal/mol, respectively) with the small differences being due to the different parameterizations used. Table 2.2 contains a summary of the electronic properties calculated for the unsubstituted chromophores as well as the 2- and 18-glycosylated species (Figure 2.1 c-f). The electronic properties for two isomers of glycosyloxazines and phenoxazines were calculated because both of these compounds are being synthesized and will be used in future experimental studies of crystallization phenomena. These synthetic efforts may ultimately include several different species with slightly different substituents, and we have chosen to calculate the properties of the unsubstituted chromophores to maximize the utility of these results. Previous

Table 2.2. Calculated Properties of Oxazines and Glycosyloxazines

molecule	ΔH_f (kcal/mole)	energy relative to S_0 (cm^{-1})		
		T_1	S_1	T_2

Table 2.2. Calculated Properties of Oxazines and Glycosyloxazines

		energy relative to S_0 (cm^{-1})						
molecule	ΔH_f (kcal/mole)	T_2	S_1	T_3	S_2	$\mu(S_0)$ (D)	$\mu(T_1)$ (D)	$\mu(S_1)$ (D)
oxazine	208.43	20292	20292	25269	24212	2.52	3.78	3.64
2-glycosyloxazine	-6.97	23349	23381	26347	25153	10.89	10.30	13.92
18-glycosyloxazine	-7.52	23487	23520	28849	25579	19.50	19.16	14.75
phenoxazine	233.21	21277	19371	24931	25890	3.25	4.03	6.00
2-glycosylphenoxazine	14.35	25223	24235	26087	26307	10.77	9.46	4.10
18-glycosylphenoxazine	12.83	25907	24442	28277	26044	17.51	15.34	11.95

calculations ha

minimal effect

oxazine and ph

higher electron

molecules[11-15]

are found to be

is also observed

that the sensit

different than t

Figure

oxazine and gl

The most strik

of the $S_0 \leftrightarrow S$

This calculation

glycosylated sp

detecting the S

response of the

is due to steric

serves to twist

chromophore

and glycosylate

energies of the

calculations have shown that small modifications of oxazines and phenoxazines have minimal effect on their calculated properties. The dipole moments we have calculated for oxazine and phenoxazine show a trend of increasing polarity as the molecule is excited to higher electronic states, in agreement with previous experimental examinations of these molecules.[11-15] However, upon glycosylation , the dipole moments of the ground state are found to be, in general, larger than those calculated for excited states, a trend that it is also observed in carminic acid. This prediction is important in the sense that it implies that the sensitivity of the glycosylated chromophore(s) to polar environments will be different than that of the native chromophore.

Figure 2.5 illustrates the results of AM1/CI calculations of energy levels for oxazine and glycosyoxazine. Electronic state *ordering* is similar for the three molecules. The most striking difference between the oxazine and glycosyloxazine is that the energy of the $S_0 \leftrightarrow S_1$ transition in the native chromophore is lower than that of the glycosides. This calculation, which is consistent with the calculated results for isomerization of the glycosylated species (*vide infra*), implies that the glycosyl moiety plays little or no role in detecting the $S_0 \leftrightarrow S_1$ transition energy and that its dominant contribution to the optical response of the chromophore is sterically based. The blue shift calculated on substitution is due to steric interactions of the glycosyl moiety with the neighboring amino group that serves to twist the amino group away from the orientation it prefers in the native chromophore. The close energetic proximity of the S_1 and T_2 states in both the native and glycosylated oxazine suggests the possibility of efficient intersystem crossing. The energies of the T_2 and S_1 states are calculated to be the same ($E=S_0 + 20292\ cm^{-1}$), and

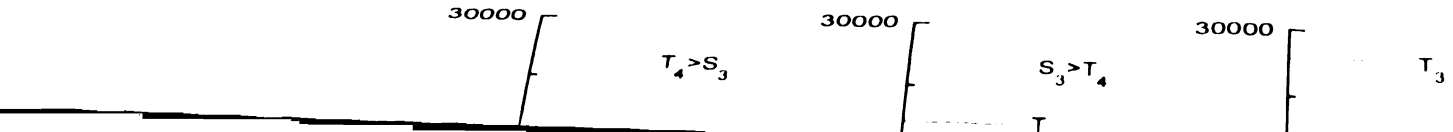
30000
$T_4 > S_3$
30000
$S_3 > T_4$
30000
T_3

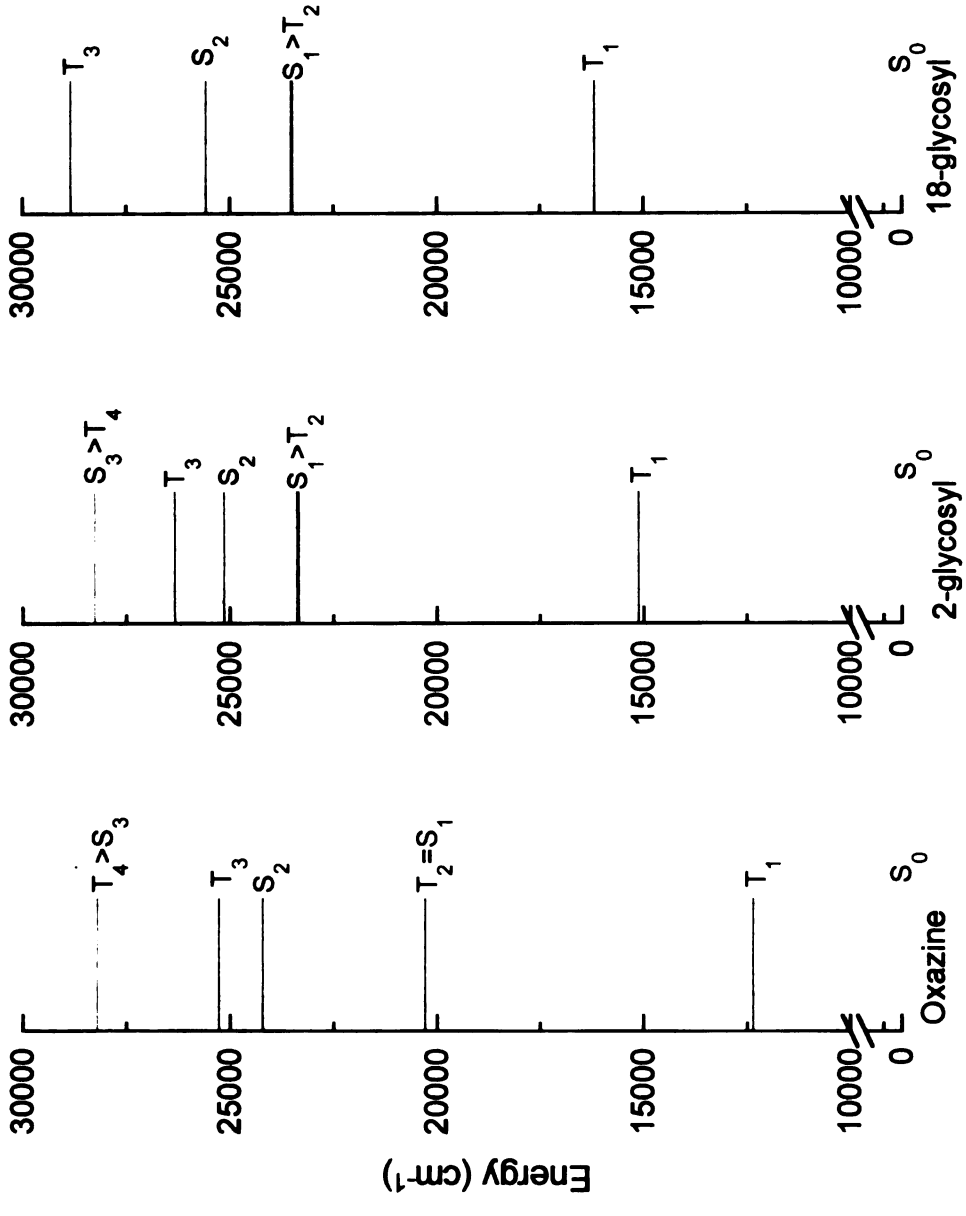

Figure 2.5. Oxazine and glycosyloxazine electronic state ordering determined from AM1 calculations using configuration interaction (CI).

in the glycosy

32 cm^{-1}). Wh

standpoint (kT

only to reinfo

these calculati

and thus the

uncertainty S

that the excite

is optimized

geometry on e

these calculati

are likely to

chromophore,

a functionality

compare indivi

the locations of

Figure

the first triple

glycosyloxazine

). These energ

the T_1 state will

phenoxazine and

in the glycosylated oxazines the calculated energy difference is negligible (ΔE (S_1-T_2) = 32 cm^{-1}). While this is obviously a negligible energy difference from an experimental standpoint (kT = 200 cm^{-1} at 300 K), two sources of uncertainty in the calculations serve only to reinforce the assertion that these two states are functionally degenerate. First, these calculations rely on parameterizations derived from ground state experimental data, and thus the estimation of excited state parameters necessarily involves significant uncertainty. Secondly, where transition energies are considered, it is important to realize that the excited state calculations are based on a molecule whose ground state geometry is optimized. There are many polar organic molecules that exhibit significant changes in geometry on excitation, as evidenced by their large steady-state Stokes shifts,[8,10,28] and these calculations do not account for such changes. Substituted polar organic molecules are likely to exhibit different excited state geometries than that of the native chromophore, especially when the substitution gives rise to significant steric hindrance of a functionality that is part of the conjugated chromophore. These calculations, in effect, compare individual points on two different surfaces, and cannot provide information on the locations of the minima of these two surfaces.

Figure 2.5 shows that the energy difference between the first excited state and the first triplet state for oxazine ($\Delta E(S_1\text{-}T_1)$ = 7932 cm^{-1}) is different from 2-glycosyloxazine ($\Delta E(S_1\text{-}T_1)$ = 8248 cm^{-1}) and 18-glycosyloxazine ($\Delta E(S_1\text{-}T_1)$ = 7333 cm^{-1}). These energy differences are all large enough so that energy transfer from the S_1 to the T_1 state will be inefficient. Figure 2.6 displays energy level diagrams calculated for phenoxazine and glycosylated phenoxazines. In all three species, the state ordering is

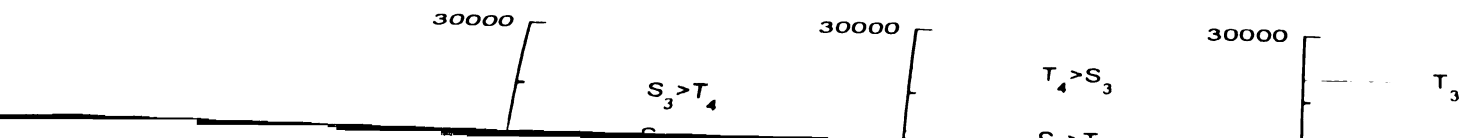
30000
$S_3>T_4$
30000
$T_4>S_3$
30000
T_3

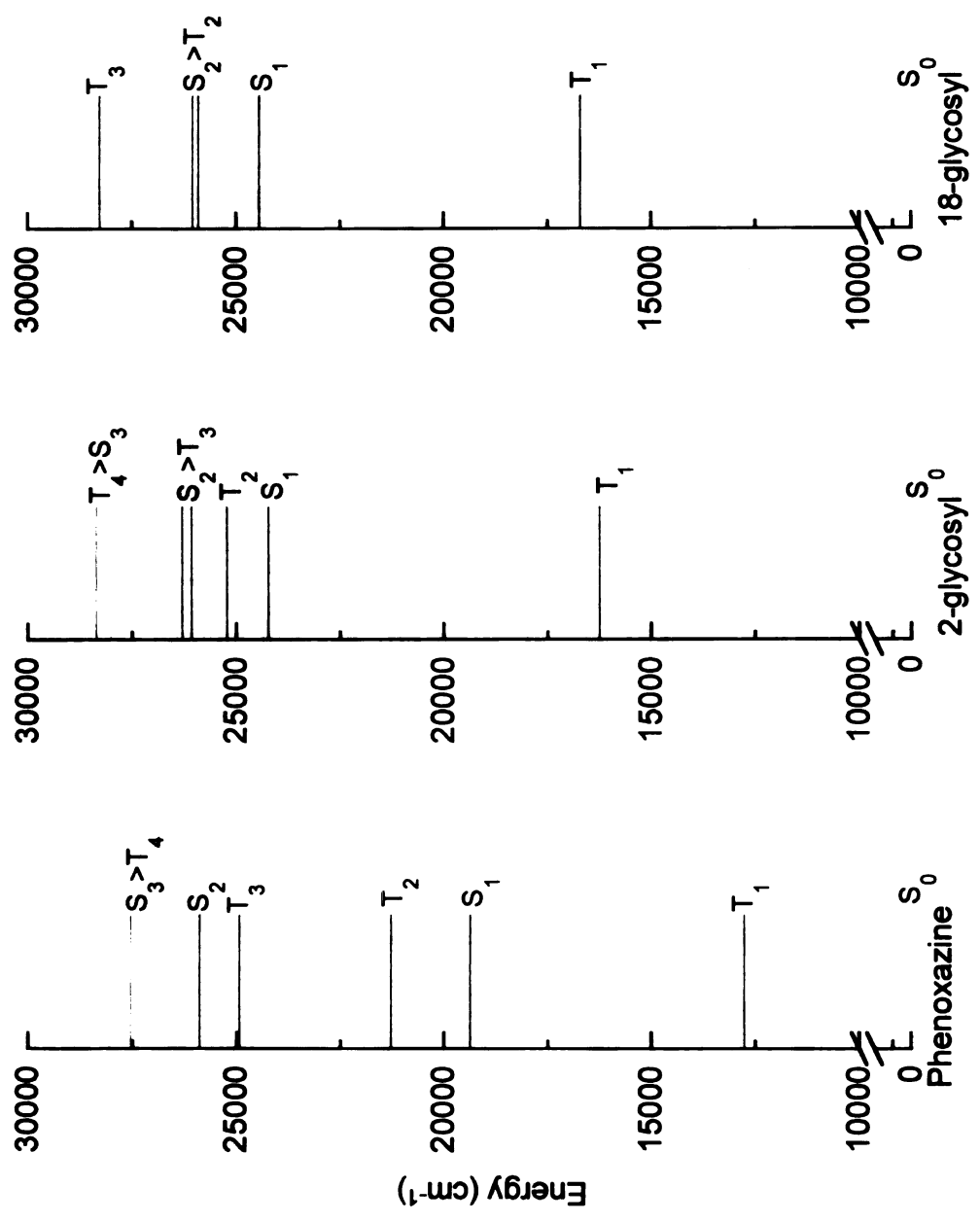

Figure 2.6. Phenoxazine and glycosylphenoxazine electronic state ordering determined from AM1 calculations using configuration interaction (CI).

similar, with a

S_1 state for a

difference betv

T_1) = 7979

glycosylpheno

The st

glycosylated sp

density upon e

excited and gr

electron densit

electron densit

neighboring car

similarly large

in oxazine be

accumulation o

polarity.[11-15] It

hydrogen bon

dependent cha

glycosyloxazine

glycoside moie

for both molec

was observed in

loses significan

similar, with a triplet state between the ground and first excited state. Additionally, the S_1 state for all species is well separated energetically from triplet states. The energy difference between the S_1 and T_1 states for the glycosyloxazines are also similar ($\Delta E(S_1\text{-}T_1)$ = 7979 cm^{-1} for 2-glycosylphenoxazine, $\Delta E(S_1\text{-}T_1)$ = 7727 cm^{-1} for 18-glycosylphenoxazine).

The state dependent electronic distributions for oxazine, phenoxazine, and the glycosylated species have also been calculated. Figure 2.7 shows the change in electron density upon excitation, where the changes are defined as the difference between the excited and ground electronic singlet states. A negative sign represents an increase in electron density upon excitation. Figure 2.7a represents the change in calculated electron density in oxazine. The heterocyclic nitrogen gains electron density and its neighboring carbons lose electron density upon excitation. The other atoms do not show similarly large changes. It has been previously determined that the nitrogen heteroatom in oxazine becomes negatively charged upon excitation, and this state dependent accumulation of electron density can be used as a probe of local solvent structure and polarity.[11-15] It is hoped to use glycosylated oxazine as a probe of local polarity and hydrogen bond formation in the crystallization of sugars. Calculated excitation-dependent changes in electron density distribution for 2-glycosyloxazine and 18-glycosyloxazine are shown in Figure 2.7b and 2.7c, respectively. The addition of the glycoside moiety to the oxazine chromophore affects the electron distribution similarly for both molecules. The heterocyclic nitrogen gains electron density upon excitation, as was observed in the "bare" oxazine. The amine nitrogen closest to the glycoside moiety loses significant electron density on excitation. This large change in electron density is

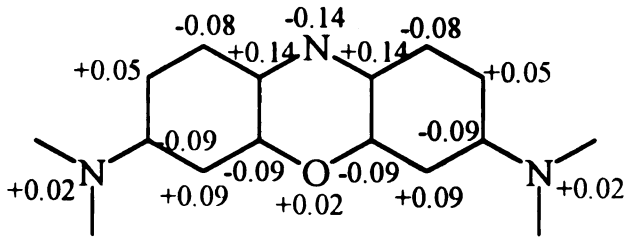

(a)

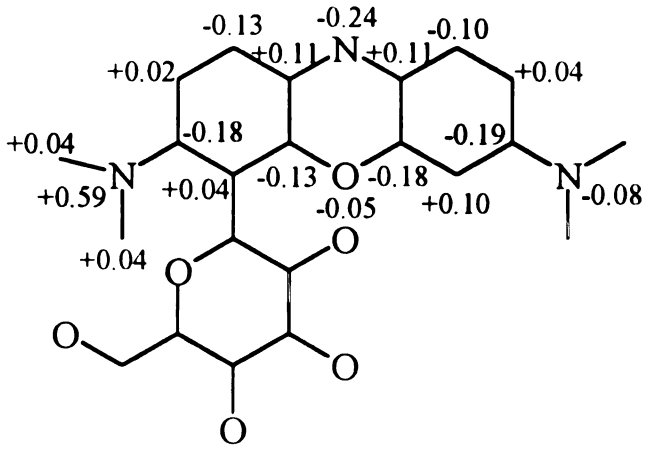

(b)

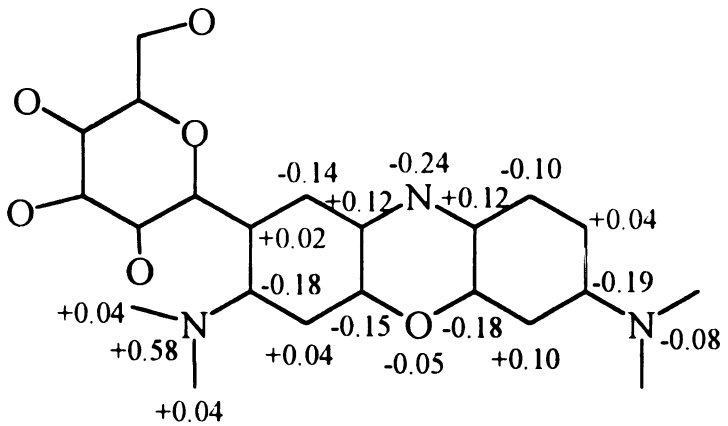

(c)

Figure 2.7. Calculated change in electon distribution between the singlet excited state (S_1) and the ground state (S_0) for oxazine and glycosyloxazines. Structure (a) is for oxazine, structure (b) is for 2-glycosyloxazine, and structure (c) is for 18-glycosyloxazine. A positive sign indicates a decrease in electron density upon excitation from the S_0 to S_1 electronic states. Protons are not shown, nor are values less than ±0.01.

likely due to

glycoside fu

group is ofte

prediction o

because the e

the chromoph

is consistent

energies of th

data for the p

28. Figure 2

the nitrogen he

was observed

consistent with

does not exhib

oxazine or phe

change in optic

as for carminic

As for

group about it

calculations we

isomerization b

phenoxazine 7

29a) and 18-gl

likely due to the steric constraints placed on this amino group by the presence of the glycoside functionality. The excited state accumulation of charge at a (twisted) amino group is often referred to as a twisted internal charge transfer (TICT) S_1 state.[34-39] The prediction of a TICT S_1 state for modified oxazines and phenoxazines is important because the existence of such a state could serve to influence the polarity dependence of the chromophore spectroscopic response substantially. The prediction of this TICT state is consistent with the data shown in Figures 2.5 and 2.6, where the $S_0 \leftrightarrow S_1$ transition energies of these molecules increase with modification. The electron density distribution data for the phenoxazine and glycoside modified phenoxazines are presented in Figure 2.8. Figure 2.8a is unsubstituted phenoxazine, and we calculate that, like the oxazine, the nitrogen heteroatom accumulates electron density on excitation. The TICT state that was observed for the glycosyloxazines is also seen for the glycosylphenoxazines, consistent with the similarity of the unsubstituted chromophores. The glycoside moiety does not exhibit any change in electron distribution on excitation for either the modified oxazine or phenoxazine. Thus steric rather than electronic factors will determine any change in optical response associated with the modification of these chromophores, just as for carminic acid.

As for carminic acid, the isomerization barriers for rotation of the glycoside group about its bond with the oxazine chromophore have been determined. These calculations were also performed for the modified oxazine. It is expected that the isomerization barriers observed for the oxazine will be similar to that for the modified phenoxazine. These calculations are presented in Figure 2.9 for 2-glycosyloxazine (Fig. 2.9a) and 18-glycosyloxazine (Fig. 2.9b). These data are qualitatively similar, with

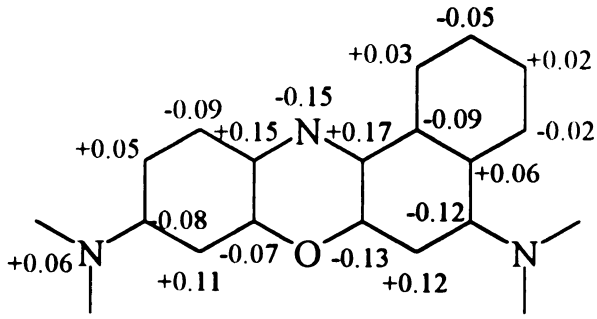

(a)

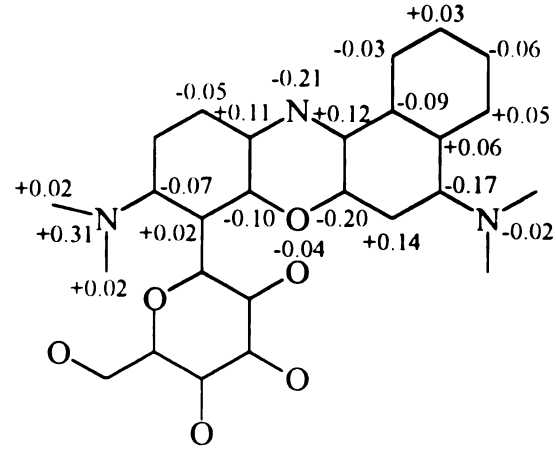

(b)

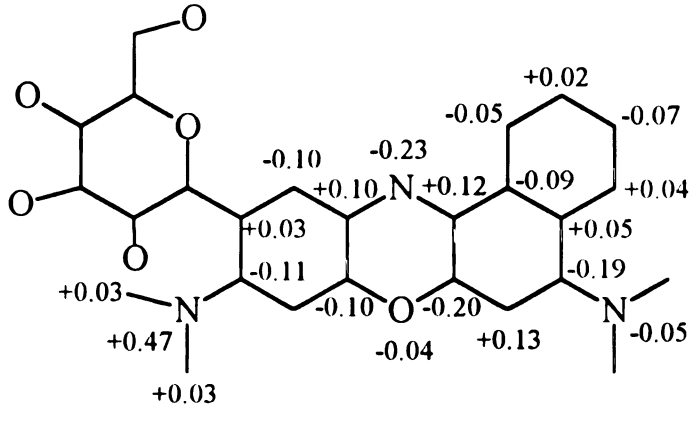

(c)

Figure 2.8. Calculated change in electron distribution between the singlet excited state (S_1) and the ground state (S_0) for phenoxazine and glycosylphenoxazines. Structure (a) is for phenoxazine, structure (b) is for 2-glycosylphenoxazine, and structure (c) is for 18-glycosylphenoxazine. A positive sign indicates a decrease in electron density upon excitation from the S_0 to S_1 electronic states. Protons are not shown, nor are values less than ±0.01.

Figure 2.9. Ca
T
fo
an
ch
co
an

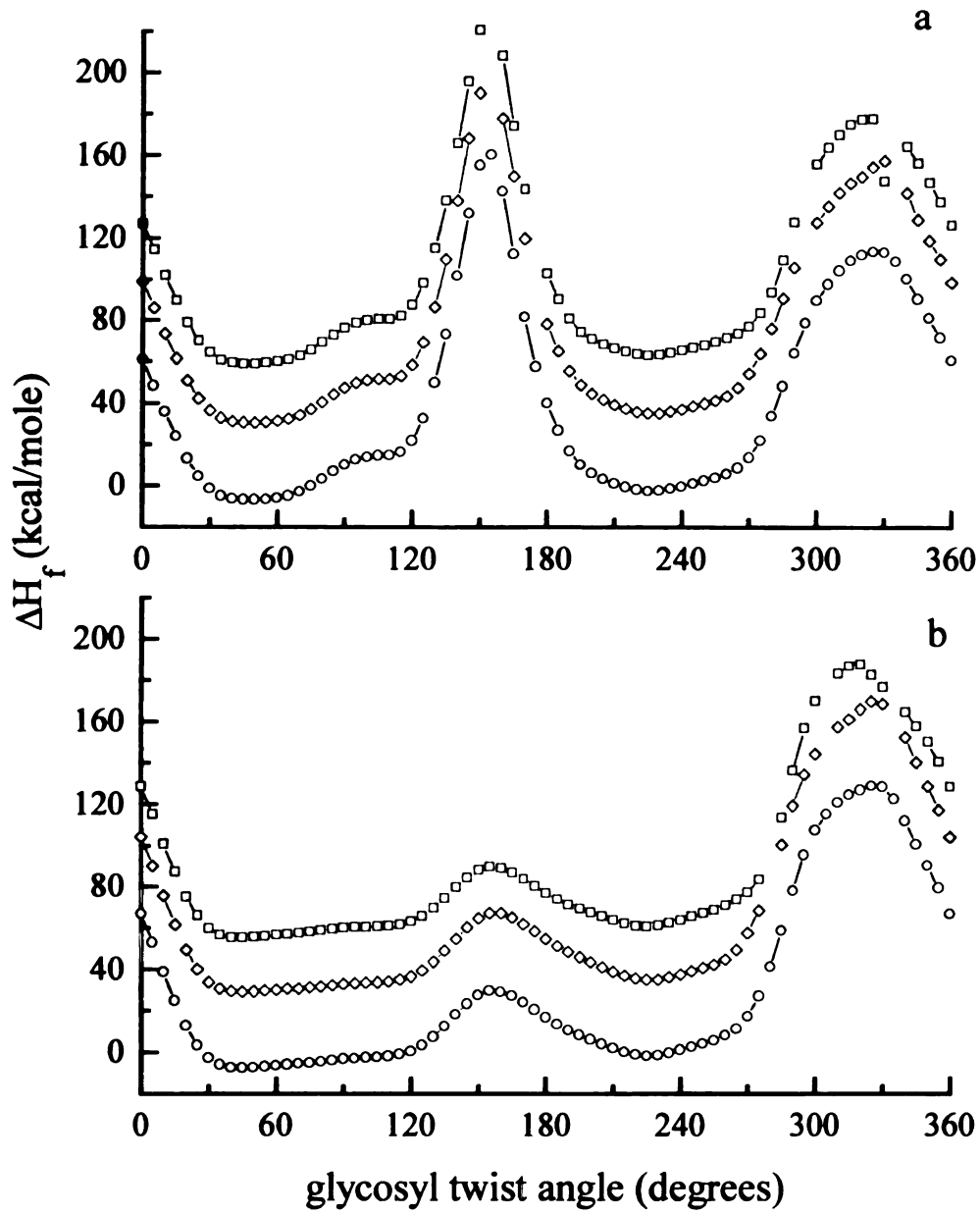

Figure 2.9. Calculated energy dependence of the glycosyl group rotation for the S_0 (O), T_1 (◊), and S_1 (□) states of glycosyl substituted oxazines. Tracings (a) are for 2-glycosyloxazine, and (b) are for the 18-glycosyl isomer. The dihedral angle is the angle made by the glycosyl group with respect to the oxazine chromophore. Missing points indicate a failure of the calculation to converge at the given dihedral angle. Relative energies at a given dihedral angle were $S_1 > T_1 > S_0$.

minima occurri

calculated barr

glycosyloxazin

calculated to h

glycosyloxazin

constrained to

significant the

calculated, indi

on the dihedra

calculations we

given dihedral a

calculation rout

and recalculate

previously disc

moiety through

discussed are a

Oxazo

and 18-glycos

rotational ison

for the oxazi

reference poi

chromophore

minima occurring at a 50° glycoside- chromophore dihedral angle in both isomers. The calculated barrier height reaches a local maximum of ~167 kcal/mole at 155° for 2-glycosyloxazine and ~37 kcal/mole for 18-glycosyloxazine. At 325°, the barrier height is calculated to be ~121 kcal/mole for 2-glycosyloxazine and ~136 kcal/mole for 18-glycosyloxazine. The heights of these barriers indicate that the glycoside moiety will be constrained to a relatively narrow range of angles and will not rotate freely. It is also significant the state ordering is consistent throughout the range of dihedral angles calculated, indicating that the linear optical response of the chromophore will not depend on the dihedral angle it makes with the glycoside group. It is noted that these calculations were performed using a calculation routine that determined the energy at a given dihedral angle without minimization of the complete structure. Recent advances in calculation routines allow minimization of the overall structure at each dihedral angle, and recalculated data provide qualitatively similar data to that discussed here. As previously discussed, it will not be possible to determine the position of the glycoside moiety through electronic absorption or emission experimental data. None of the results discussed are affected by this change in the calculation routine.

Oxazones and Phenoxazones. The electronic properties for oxazone, 2-glycosyl- and 18-glycosyloxazone, phenoxazone, 2-glycosyl and 18-glycosylphenoxazone and the rotational isomerization barriers for the glycosylated species have been computed. As for the oxazines and phenoxazines, oxazone and phenoxazone were calculated as a reference point to determine the effect of the addition of the glycoside moiety to the chromophore backbone. Table 2.3 shows the calculated properties for unsubstituted

Table 2-3. Calculated Properties of Oxazones and Glycosyloxazones

		energy relative to S_0 (cm^{-1})						
molecule	ΔH_f (kcal/mole)	T_1	S_1	T_2	S_2	$\mu(S_0)$ (D)	$\mu(T_1)$ (D)	$\mu(S_1)$ (D)

Table 2.3. Calculated Properties of Oxazones and Glycosyloxazones

		energy relative to S_0 (cm^{-1})						
molecule	ΔH_f (kcal/mole)	T_2	S_1	T_3	S_2	$\mu(S_0)$ (D)	$\mu(T_1)$ (D)	$\mu(S_1)$ (D)
oxazone	33.17	27177	27479	29030	31661	4.04	5.69	4.40
2-glycosyloxazone	-196.49	27653	27410	28810	31454	6.57	7.89	5.46
18-glycosyloxazone	-200.36	27836	27896	28710	31697	4.10	5.99	5.26
phenoxazone	47.43	29291	27873	31143	33203	3.41	4.26	4.09
2-glycosylphenoxazone	-182.95	29167	27778	30981	32637	3.81	4.68	4.30
18-glycosylphenoxazone	-185.77	28732	28212	30818	32717	4.52	5.24	4.97

oxazone and

moments for

for 2-glycosyl

than the grou

molecules has

charge distribu

any of the he

causes an incre

chromophores

The

glycosyloxazon

oxazines, the i

oxazone chron

of a twisted te

energy on sub

role in the tra

amino group p

than for the o

ordering, with

singlet state (S

large ($\Delta E(S_2$-S

for 18-glycosy

oxazone and phenoxazone and the glycosylated chromophores. The calculated dipole moments for these molecules follow a trend of increasing polarity on excitation, except for 2-glycosyloxazone, where the S_1 state is calculated to have a smaller dipole moment than the ground state. The calculated dipole moment of the triplet state in these molecules has the largest value in the oxazone calculations, but examination of the charge distribution of the T_1 state does not reveal a substantial charge accumulation for any of the heteroatom sites. Glycoside substitution at both the 2- and 18- positions causes an increase in the magnitude of the dipole moment compared to the unsubstituted chromophores.

The AM1/CI calculated electronic state orderings for oxazone, 2-glycosyloxazone, and 18-glycosyloxazone are shown in Figure 2.10. In contrast to the oxazines, the increase in the calculated $S_0 \leftrightarrow S_1$ transition energy on substitution for the oxazone chromophore is comparatively small, despite the sterically mediated formation of a twisted terminal amino group in the glycosylated species. The increase in transition energy on substitution indicates that the rotated amino group does in fact play a small role in the transition, but because of the inherent asymmetry in the chromophore, the amino group plays a comparatively smaller role in determining the energy of the S_1 state than for the oxazine species.[33] Oxazone and substituted oxazones have similar state ordering, with the triplet state T_1 being found between the ground (S_0) and excited singlet state (S_1). For all species, the energy separation between the S_2 and S_1 states is large ($\Delta E(S_2\text{-}S_1)$ = 4181 cm^{-1} for oxazone, 4044 cm^{-1} for 2-glycosyloxazone, 3801 cm^{-1} for 18-glycosyloxazone), so that the dominant optical transition will be $S_0 \leftrightarrow S_1$. The


30000
S_2
30000
S_2
30000
S_2

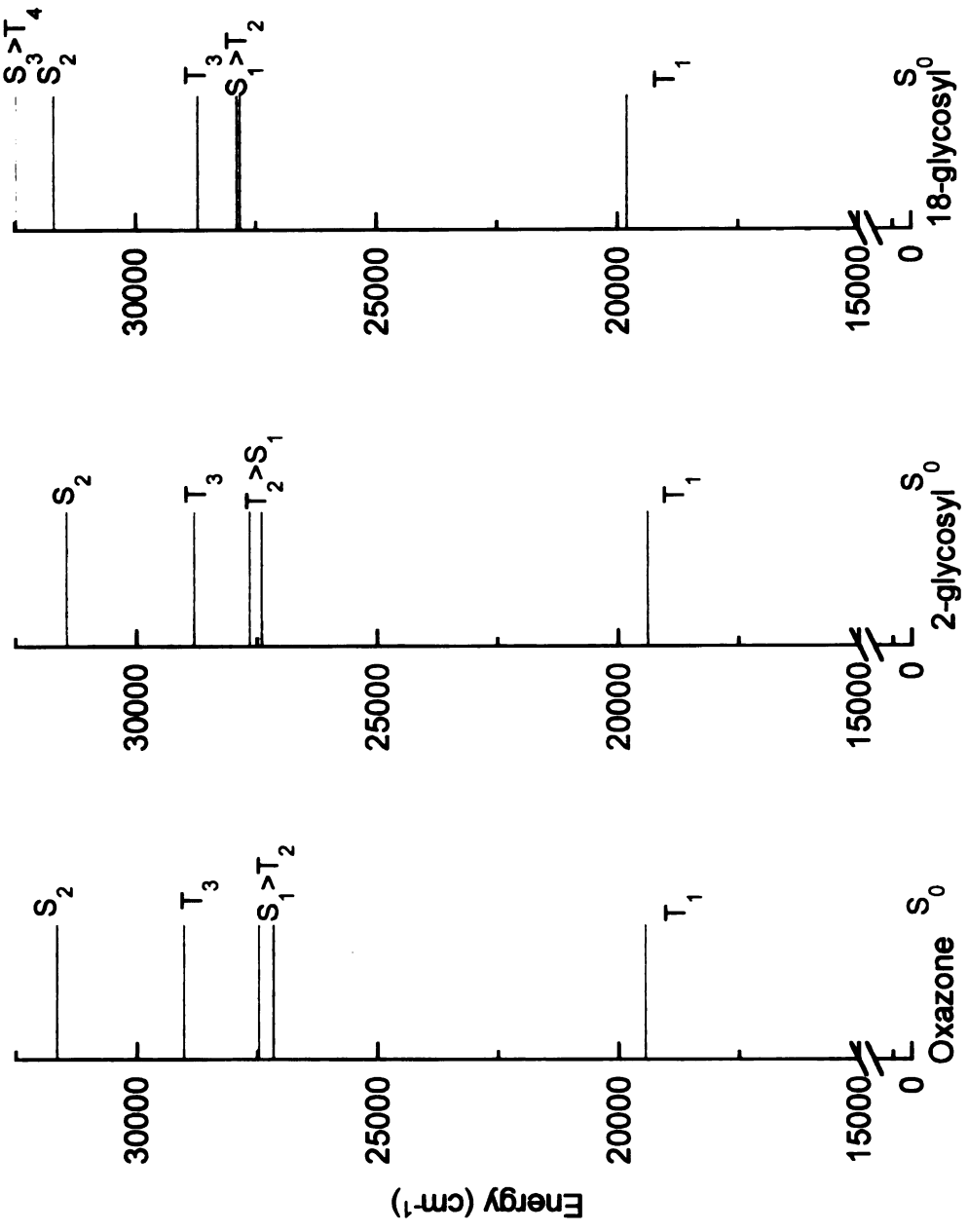

Figure 2.10. Oxazone and glycosyloxazone electronic state ordering determined from AM1 calculations using configuration interaction (CI).

energy separa

all species). s

the oxazines.

cm^{-1}, in 2-gly

$\Delta E(S_1\text{-}T_2)$ =

species the S

glycosylated p

energy separa

The phenoxaz

^{1}, 20802 cm

glycosylpheno

similar, with

phenoxazones

larger energy

modification

and that the

steric constra

contrast to th

The s

the glycosyla

213 show th

series, respec

energy separation between the S_1 and T_1 states is large ($\Delta E(S_1\text{-}T_1)$ = 8000 ± 100 cm^{-1} for all species), so that intersystem crossing from the S_1 to T_1 state not expected, but, as for the oxazines, the T_2 is in close energetic proximity to S_1. In oxazone, $\Delta E(S_1\text{-}T_2)$ = 302 cm^{-1}, in 2-glycosyloxazone the $\Delta E(S_1\text{-}T_2)$ = -243 cm^{-1} and in 18-glycosyloxazone the $\Delta E(S_1\text{-}T_2)$ = 60 cm^{-1}. In close analogy to the oxazines, these values indicate that for all species the S_1 and T_2 electronic states are essentially degenerate. The phenoxazone and glycosylated phenoxazones exhibit state ordering similar to that for the oxazones, but the energy separations between states is greater than for the oxazone series (Figure 2.11). The phenoxazone species have a T_1 state between S_0 and S_1, with $\Delta E(T_1\text{-}S_0)$ =20662 cm^{-1}, 20802 cm^{-1}, and 21129 cm^{-1} for phenoxazine, 2-glycosylphenoxazone and 18-glycosylphenoxazone, respectively. The energy differences between S_1 and S_0 are also similar, with $\Delta E(S_1\text{-}S_0)$ = 27872 cm^{-1}, 27778 cm^{-1}, and 28212 cm^{-1} respectively. For the phenoxazones, the T_2 state is higher in energy than the S_1 state and is also separated by a larger energy than is seen for the oxazones. These calculations suggest that glycoside modification of phenoxazone does not affect the electronic state ordering substantially, and that the optical response of all species will be largely similar, irrespective of the steric constraints imposed by the glycosyl moiety. This prediction is in significant contrast to that for the oxazines.

The state dependent electron density distributions for oxazone, phenoxazone, and the glycosylated forms of these chromophores have been determined. Figures 2.12 and 2.13 show the change in electron distribution for the oxazone series and phenoxazine series, respectively. It is important to note that these molecules do not undergo state

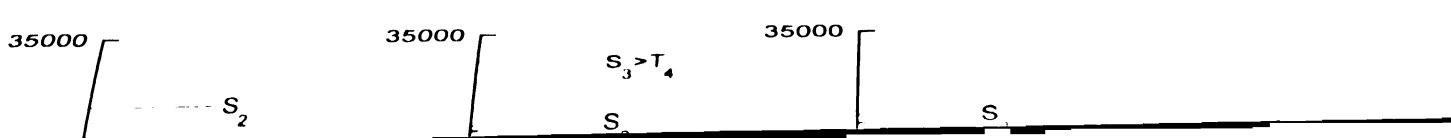
35000
S_2
35000
$S_3 > T_4$
S_2
35000
S

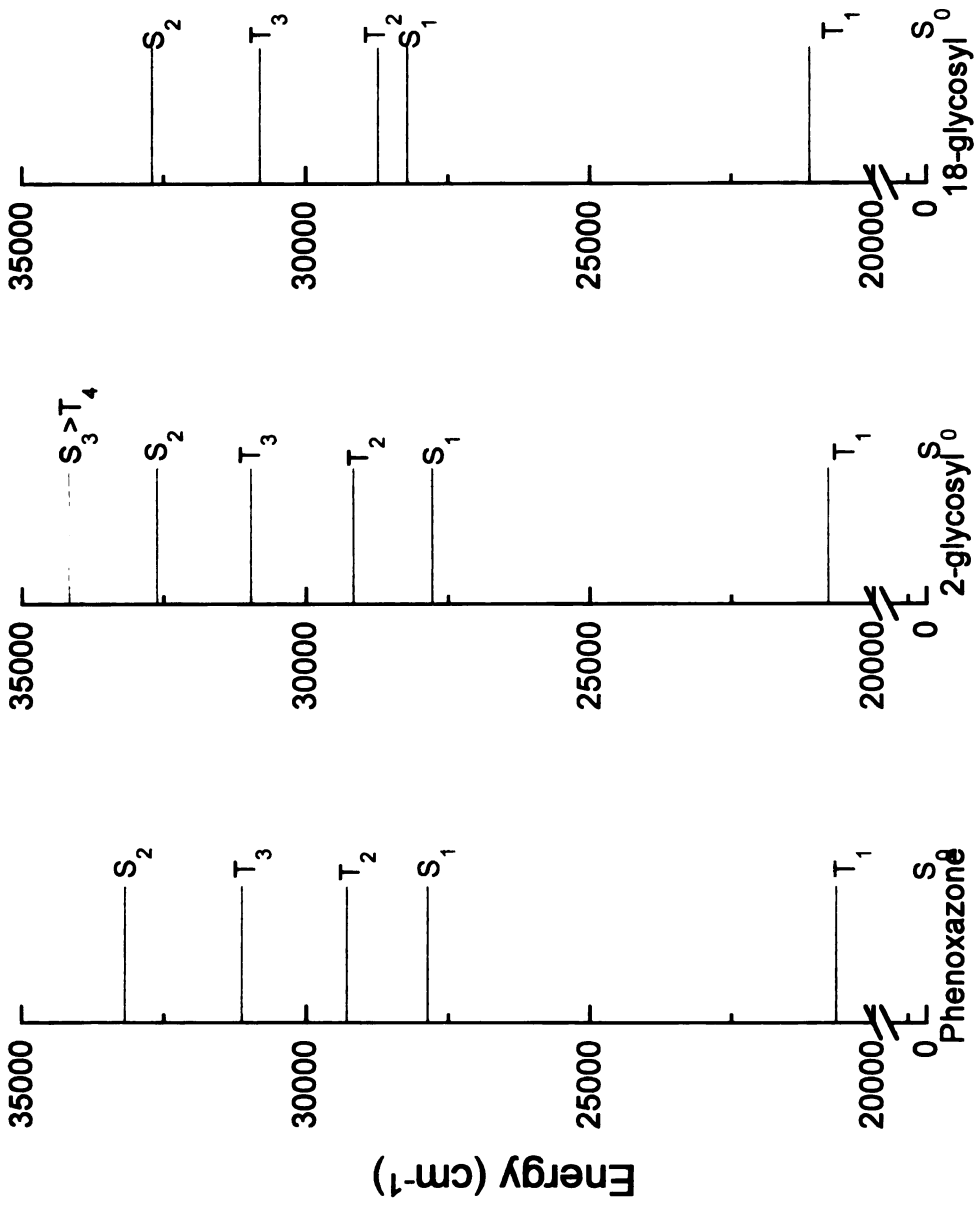

Figure 2.11. Phenoxazone and glycosylphenoxazone electronic state ordering determined from AM1 calculations using configuration interaction (CI).

Figure 2.12.

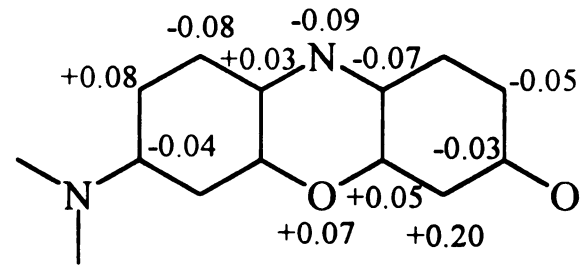

(a)

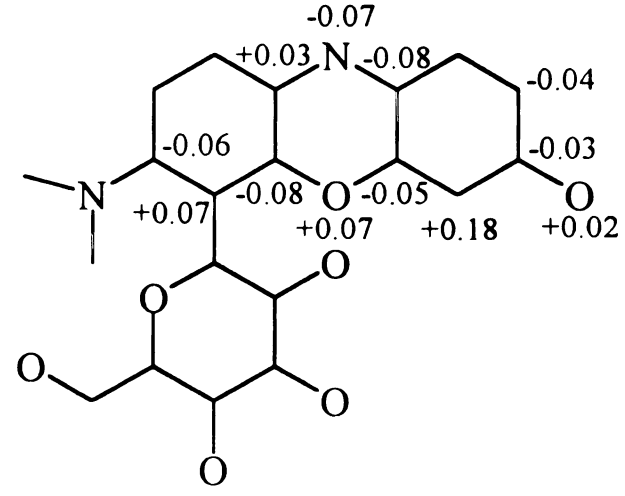

(b)

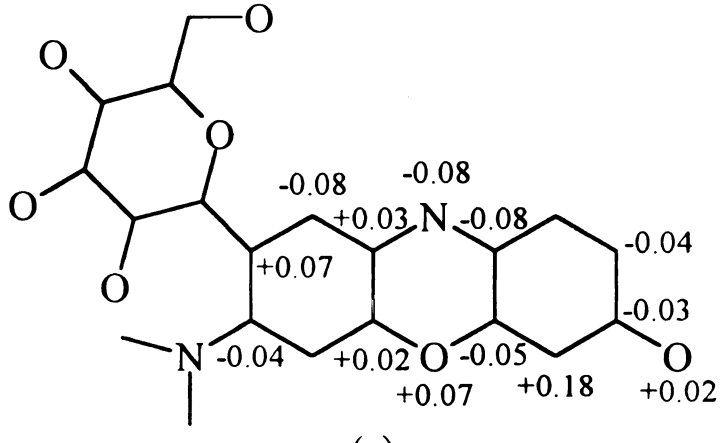

(c)

Figure 2.12. Calculated change in electron distribution between the singlet excited state (S_1) and the ground state (S_0) for oxazone and glycosyloxazones. Structure (a) is for oxazone, structure (b) is for 2-glycosyloxazone, and structure (c) is for 18-glycosyloxazone. A positive sign indicates a decrease in electron distribution upon excitation from the S_0 to S_1 electronic states. Protons are not shown, nor are values less than ±0.01.

Figure 2.13

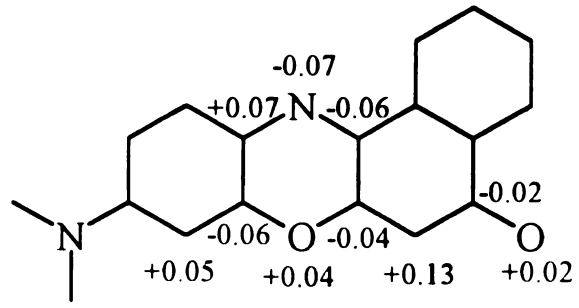

(a)

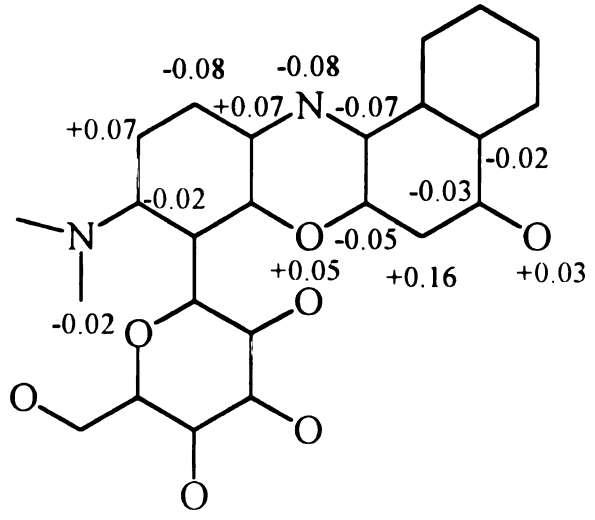

(b)

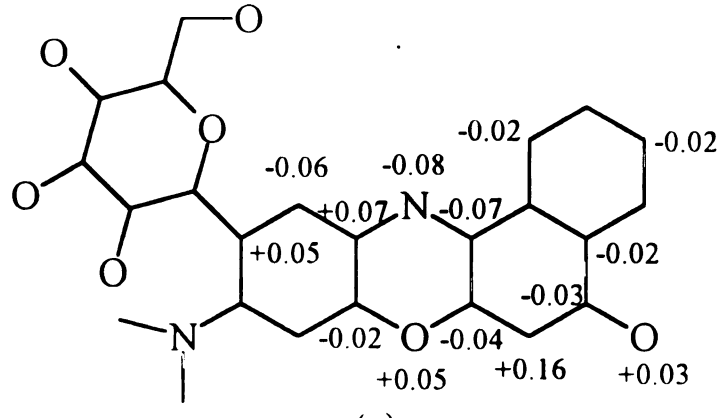

(c)

Figure 2.13. Calculated change in electron distribution between the singlet excited state (S_1) and the ground state (S_0) for phenoxazone and glycosylphenoxazones. Structure (a) is for phenoxazone, structure (b) is for 2-glycosylphenoxazone, and structure (c) is for 18-glycosylphenoxazone. A positive sign indicates a decrease in electron density upon excitation from the S_0 to S_1 electronic states. Protons are not shown, nor are values less than ±0.01.

dependent

oxazone ch

electron de

behaves si

consonant

glycoside m

excitation, a

these molecu

The

oxazone chr

the calculat

glycosyloxaz

glycoside-chr

-184 kcal

glycosyloxaz

kcal/mole f

magnitude o

range and w

the oxazine

angles calcul

that these ca

energy at a g

advances in

dependent charging on atoms in the chromophore or in the glycoside moiety. The oxazone chromophore (Fig. 2.12a) does not exhibit a significant spatial modulation of electron density on excitation, and the glycosyl modified chromophore (Fig. 2.12b,c), behaves similarly. The phenoxazone calculations, (Figs. 2.13) predict behavior consonant with that of the oxazones. As with carminic acid and the oxazines, the glycoside moiety does not undergo any change in electron density distribution upon excitation, and thus the role of this substituent in determining the optical response of these molecules is steric rather than electronic.

The isomerization barrier of the glycoside moiety about its bond with the oxazone chromophore is qualitatively similar to that of the oxazines. Figures 2.14 show the calculated isomerization barriers for 2-glycosyloxazone (Fig. 2.14a) and 18-glycosyloxazone (Fig. 2.14b). For these molecules, the energetic minima occur at a ~50° glycoside-chromophore dihedral angle. The barrier height reaches a local maximum of ~184 kcal/mole at 155° for 2-glycosyloxazone and ~40 kcal/mole for 18-glycosyloxazone. At a dihedral angle of 325°, the barrier height is calculated to be ~125 kcal/mole for 2-glycosyloxazone and ~134 kcal/mole for 18-glycosyloxazone. The magnitude of these barriers indicate that the glycoside moiety is constrained to a narrow range and will not freely rotate, as was observed in the oxazine calculations. As seen in the oxazine calculations, the state ordering is constant throughout the range of dihedral angles calculated, with T_1 being between S_0 and S_1 in both oxazone isomers. It is noted that these calculations were performed using a calculation routine that determined the energy at a given dihedral angle without minimization of the complete structure. Recent advances in calculation routines allow minimization of the overall structure at each

Figure 2.14.

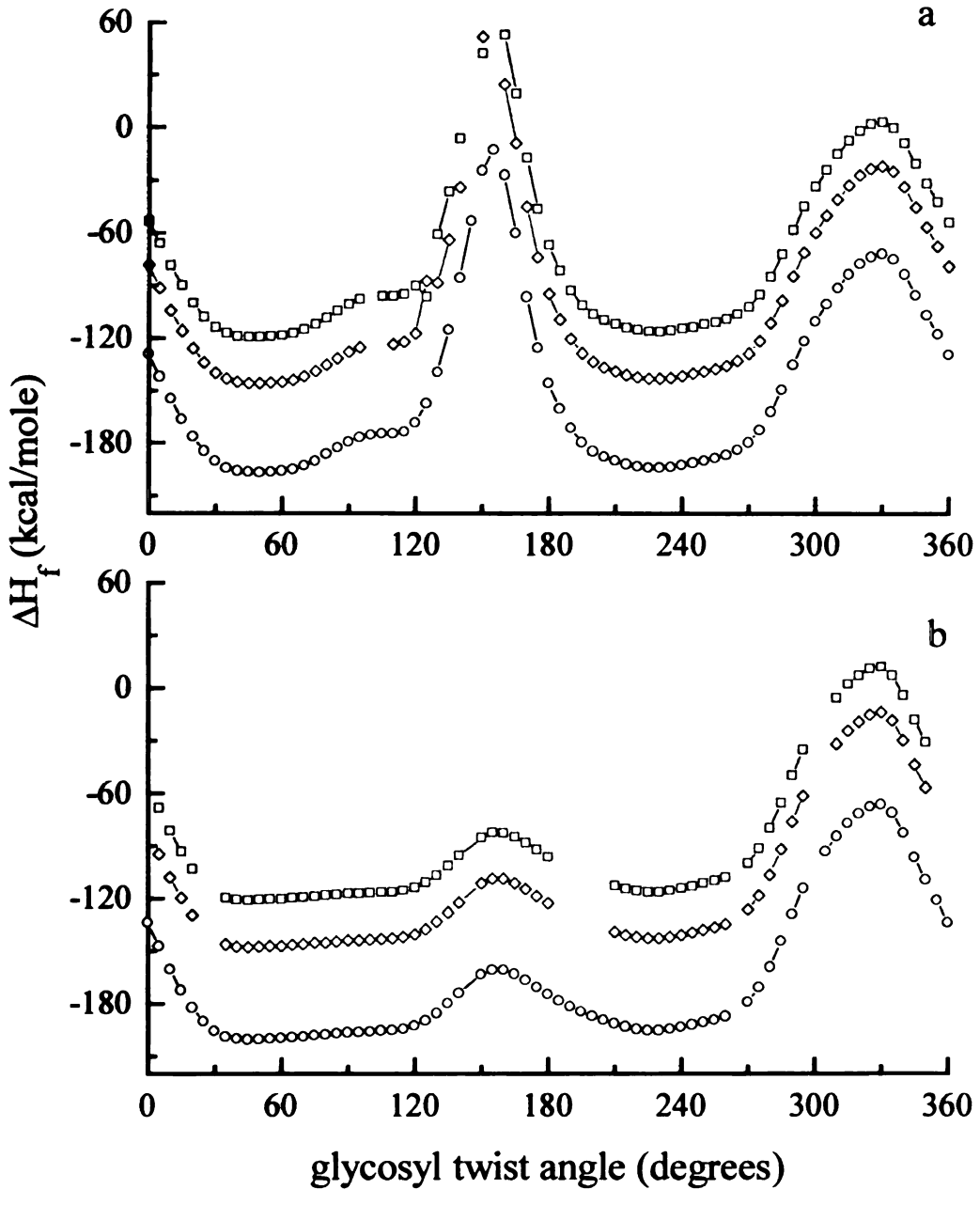

Figure 2.14. Calculated energy dependence of the glycosyl group rotation for the S_0 (O), T_1 (◊), and S_1 (□) states of glycosyl substituted oxazones. Tracings (a) are for 2-glycosyloxazone, and (b) ar for the 18-glycosyl isomer. The dihedral angle is the angle made by the glycosyl group with respect to the oxazone chromophore. Missing points indicate a failure of the calculation to converge at the given dihedral angle. Relative energies at a given dihedral angle were $S_1 > T_1 > S_0$.

dihedral angl

to that disc

chromophore

the results d

dihedral angle, and recalculated data for carminic acid provide qualitatively similar data to that discussed here. These data indicate that the linear optical response of the chromophore will not depend on the rotational position of the glycoside group. None of the results discussed are affected by this change in the calculation routine.

2.4. Con

In t

correspondi

molecules p

the $S_0 \leftrightarrow S$

singlet state

response of

associated w

predict that

from an exc

The formati

interference

calculations

will not dep

way as do t

chromophor

factors. A

responses o

chromopho

2.4. Conclusions

In this chapter, the electronic properties of several unsubstituted and corresponding glycosylated chromophores have been calculated. The results for all molecules predict that the main spectroscopic features that will be observed arise from the $S_0 \leftrightarrow S_1$ transition, and that other transitions originating from S_0 to higher excited singlet states will not be overlapped with the $S_0 \leftrightarrow S_1$ transition. The linear optical response of carminic acid is pH dependent[29-32] due to reordering of electronic states associated with the extent to which the molecule is protonated. These calculations predict that glycosylated oxazines will exhibit state dependent dynamical behavior arising from an excitation-induced accumulation of electron density at the heterocyclic nitrogen. The formation of a TICT S_1 state in the glycosylated oxazines is a direct result of steric interference between the terminal amino group and the glycoside moiety. These calculations predict that the optical and dynamical response of glycosylated oxazones will not depend on state-dependent changes in electron density distributions in the same way as do the glycosylated oxazines. The presence of the glycoside moiety on these chromophores will affect their linear response through steric rather than electronic factors. An important consequence of this calculated prediction is that the optical responses of these chromophores will not depend on the dihedral angle between the chromophore and the glycoside substituent.

2.5. Lite

1. McMorro

2. McMorro

3. Morris, D

4. Butler, R

5. Weaver, 8956.

6. Hambir, S

7. Jiang, Y

8. Jiang, Y

9. Blanchar

10. Awad, N

11. Blancha

12. Blancha

13. Blancha

14. Blancha

15. Blancha

16. Pan, B.

17. Chakra

18. Thomp

19. Bogusl

20. Li, T. N

2.5. Literature Cited

1. McMorrow, D; Lotshaw, W. T. *Chem. Phys. Lett.*, **1993**, *201*, 369.

2. McMorrow, D.; Lotshaw, W. T. *J. Phys. Chem.*, **1991**, *95*, 10395.

3. Morris, D. L. Jr.; Gustafson, T. L. *J. Phys. Chem.*, **1994**, *98*, 6725.

4. Butler, R. M.; Lynn, M. A.; Gustafson, T. L. *J. Phys. Chem.*, **1993**, *97*, 2609.

5. Weaver, W. L.; Huston, L. A.; Iwata, K.; Gustafson, T. L. *J. Phys. Chem.*, **1992**, *96*, 8956.

6. Hambir, S. A.; Jiang, Y.; Blanchard, G. J. *J. Chem. Phys.*, **1993**, *98*, 6075.

7. Jiang, Y.; Blanchard, G. J. *J. Phys. Chem.*, **1994**, *98*, 9411.

8. Jiang, Y.; McCarthy, P. K.; Blanchard, G. J. *Chem. Phys.*, **1994**, *183*, 249.

9. Blanchard, G. J. *J. Chem. Phys.*, **1991**, *95*, 6317.

10. Awad, M. M.; McCarthy, P. K.; Blanchard, G. J. *J. Phys. Chem.*, **1994**, *98*, 1454.

11. Blanchard, G. J.; Cihal, C. A. *J. Phys. Chem.*, **1988**, *92*, 5950.

12. Blanchard, G. J. *J. Phys. Chem.*, **1988**, *92*, 6303.

13. Blanchard, G. J. *J. Phys. Chem.*, **1989**, *93*, 4315.

14. Blanchard, G. J. *J. Phys. Chem.*, **1991**, *95*, 5293.

15. Blanchard, G. J. *Anal. Chem.*, **1989**, *61*, 2394.

16. Pan, B; Chakraborty, R; Berglund, K. A. *J. Crystal Growth*, **1993**, *130*, 587.

17. Chakraborty, R.; Berglund, K. A. *J. Crystal Growth*, **1992**, *125*, 81.

18. Thompson, S. G.; Burd, J. F. *Antimicro. Agents Chemother.*, **1980**, *18*, 264.

19. Boguslaski, R. C.; Burd, J. F.; Denning, C. E. *J. Clin. Sci.*, **1980**, *1*, 215.

20. Li, T. M.; Benovic, J. L.; Burd, J. F. *Anal. Biochem.*, **1981**, *118*, 102.

21 Burd, J

22 Dewar,
1985, *J*

23 Dewar,

24 Stewart

25 Dewar,

26 Dewar,

27 Allinger

28 McCart

29 Schwin

30 Stapelfe

31 Jorgens

32 Rasimas

33 Blancha

34 Majumd
1991, 9

35 Wang,
3736

36 Hicks, J
Lett., 1

37 Wang,

38 Sen, R
Lett., 1

39 Kajimo

21. Burd, J. F. *Meth. Enzymol.*, **1981**, *74C*, 79.

22. Dewar, M. J. S.; Zoebisch, E. G.; Healy, E. F.; Stewart, J. J. P. *J. Am. Chem. Soc.* **1985**, *107*, 3902.

23. Dewar, M. J. S.; Dieter, K. M. *J. Am. Chem. Soc.*, **1986**, *108*, 8075.

24. Stewart, J. J. P. *J. Comput.-Aided Mol. Des.*, **1990**, *4*, 1.

25. Dewar, M. J. S.; Thiel, W. *J. Am. Chem. Soc.*, **1977**, *99*, 4899.

26. Dewar, M. J. S.; Thiel, W. *J. Am. Chem. Soc.*, **1977**, *99*, 4907.

27. Allinger, N. L. *J. Am. Chem. Soc.*, **1977**, *99*, 8127.

28. McCarthy, P. K.; Blanchard, G. J. *J. Phys. Chem.*, **1993**, *97*, 12205.

29. Schwing-Weill, M. J.; Weschler, S. *Analusis*, **1986**, *14*, 290.

30. Stapelfeldt, H.; Jun, H.; Skibsted, L. H. *Food Chemistry*, **1993**, *48*, 1.

31. Jorgensen, K.; Skibsted, L. H. *Food Chemistry*, **1991**, *40*, 25.

32. Rasimas, J. P.; Berglund, K. A.; Blanchard, G. J. *J. Phys. Chem.*, **1996**, *100*, 7220.

33. Blanchard, G. J. *Chem. Phys.*, **1989**, *138*, 365.

34. Majumdar, D.; Sen, R.; Bhattacharyya, K.; Bhattacharyya, S. K. *J. Phys. Chem.*, **1991**, *95*, 4324.

35. Wang, Y.; McAuliffe, M.; Novak, F.; Eisenthal, K. B. *J. Phys. Chem.*, **1981**, *85*, 3736.

36. Hicks, J. M.; Vandersall, M. T.; Sitzmann, E. V.; Eisenthal, K. B. *Chem. Phys. Lett.*, **1987**, *135*, 413.

37. Wang, Y.; Eisenthal, K. B. *J. Chem. Phys.*, **1982**, *77*, 6076.

38. Sen, R.; Majumdar, D.; Bhattacharyya, S. P.; Bhattacharyya, S. N. *Chem. Phys. Lett.*, **1991**, *181*, 288.

39. Kajimoto, O.; Nayuki, T.; Kobayashi, T. *Chem. Phys. Lett.*, **1993**, *209*, 357.

A Time

Ultrafast kir

the fluoresc

The resoruf

(NaR) in *t*-b

two solvent

responses o

of the chrom

signals rec

measuremen

ionic associa

chromophor

deprotonati

significant r

Chapter 3

A Time Resolved Spectroscopic Study of Solution Phase Ionic Association and Dissociation

Summary

Ultrafast kinetic spectroscopies have been used to study the ionic exchange behavior of the fluorescent probe molecule resorufin in a binary solution of *n*-butanol and *t*-butanol. The resorufin chromophore, an organic anion, is associated with its sodium counter-ion (NaR) in *t*-butanol and is fully dissociated (R^-) in *n*-butanol. In a binary solution of the two solvents, both the associated and dissociated forms are present. The linear responses of these two species differ significantly and the populations of the two forms of the chromophore can be excited and monitored selectively. It has been shown that the signals recovered from ground state recovery and spontaneous emission lifetime measurements can be explained quantitatively using a kinetic model that accounts for ionic association and dissociation in both the ground and excited electronic states of the chromophore. The rates of this dissociation are qualitatively similar to protonation and deprotonation times reported for a variety of other polar organic molecules, implying the significant role of a pre-dissociative complex in the equilibrium system.

3.1. Int

Des
research-sca
interactions
extensive r
decades and
held to be t
between inc
times, the r
relaxation p
information
all of our p
experiment
properties
distances
molecule,
excitation
solvents, t
electrolyte
have show
dielectric
responsib

3.1. Introduction

Despite the fact that solutions are the medium of choice for many industrial- and research-scale chemical processes, our fundamental understanding of the intermolecular interactions that give rise to this phase of matter remains limited. There has been extensive research interest in liquid phase molecular interactions over the past two decades and much of this work has focused on neat solvents because they are widely held to be the simplest starting points for such investigations. Because the interactions between individual molecules in solution occur frequently and have short persistence times, the most common approach to the examination of solvation and solution phase relaxation processes has been to use a spectroscopically active probe molecule and infer information about the surrounding medium from its transient optical response. Virtually all of our present understanding of solution phase dynamics stems from spectroscopic experiments on (dilute) probe molecules. Depending on the structural and/or optical properties of the probe molecule, intermolecular interactions can be probed over distances ranging from several Å up through the longest dimension of the probe molecule,[1,2] and even toward 50 Å for experiments that are sensitive to electronic excitation transport.[3] In addition to the large body of experimental data on single solvents, there is also a less extensive literature concerned with binary solvent and electrolyte containing systems.[4-10] These studies on the more complex binary solutions have shown that the bulk properties of binary solvent systems, such as viscosity or dielectric constant, are not necessarily good indicators of the molecular scale interactions responsible for the dynamical behavior of dissolved probe molecules. This is not a

surprising re

significantly

molecule.

focused on

Rece

a significant

transient spe

butanol sys

molecule re

association

examine th

dissociated

centered at

resorufin i

associated

470 nm an

forms of th

kinetic mea

system, bo

measurem

molecule i

reported H

molecule

surprising result because the discrete molecular nature of the solvent can give rise to a significantly non-uniform environment over the length scale sensed by the probe molecule. Much of the present effort in research on solvent-solute interactions is focused on understanding organization and relaxation on this very short length scale.

Recently, it has been shown that, if the binary system is chosen carefully, there is a significant amount of information on local organization that can be derived from transient spectroscopic experiments.[11] In the work reported here, the binary *n*-butanol/*t*-butanol system has been investigated using the well-characterized fluorescent probe molecule resorufin.[12-21] The primary motivation for this work is to understand the association and dissociation kinetics of this probe molecule so that we can use it to examine the molecular onset of crystallization from solution.[11] Resorufin exists in its dissociated form, as the free anion R^- in primary alcohols, with an absorption maximum centered at ~ 580 nm and a prominent emission band centered at ~ 600 nm. In *t*-butanol, resorufin is almost completely associated with its Na^+ counter-ion (NaR). The associated form of resorufin is characterized by a broad absorption band centered at ~ 470 nm and a comparatively less intense emission maximum at ~ 550 nm. The two forms of this probe molecule are spectroscopically resolved well enough so that direct kinetic measurements can be made on each specie. In the binary *n*-butanol/*t*-butanol system, both R^- and NaR are present, and through a family of transient spectroscopic measurements, we can determine the ionic association and dissociation rate(s) for this molecule in both the ground and excited electronic states of the chromophore. The data reported here indicate that the time constants for association and dissociation of this molecule depend on the electronic state of the chromophore but lie within the 10^{-11} s -

10^9 s wind

number of

acids and b

kinetic info

discussed a

steady state

points to th

anion

3.2. Ex

Ste

using a Hi

bandpass

excitation a

the binary

Pic

ground-stat

only an ou

shown in F

Antares 76

MHz repe

power at 5

produce

10^{-9} s window. Interestingly, these time constants are entirely consistent with a large number of reports on solution phase protonation/deprotonation of a variety of organic acids and bases.[22] Presented below are the experimental methods used to extract the kinetic information as well as the model used to interpret these data. These results are discussed and compared to the equilibrium information on this system available from steady state absorption measurements. The comparison of kinetic and equilibrium data points to the role of a pre-dissociative complex between the Na^+ cation and the resorufin anion.

3.2. Experimental

Steady state absorption and emission spectra: Absorption spectra were acquired using a Hitachi U-4000 UV-Visible absorption spectrometer operating with a 2 nm bandpass. Emission spectra were recorded on a Hitachi F-4500 fluorimeter using 10 nm excitation and emission bandpasses. The absorption and emission spectra of resorufin in the binary butanol solvent are shown in Figure 3.1.

Picosecond Pump-Probe Spectroscopy. The spectrometer used to measure the ground-state recovery times of NaR and R^- has been described in detail previously,[23] and only an outline of the system is presented here. A schematic of the spectrometer is shown in Figure 3.2. The light source is a mode locked CW Nd:YAG laser (Coherent Antares 76-S) that produces 30 W average power at 1064 nm with 100 ps pulses at 76 MHz repetition rate. The 1064 nm light is frequency doubled to produce > 3 W average power at 532 nm. The second harmonic and residual fundamental light are mixed to produce ~1.2 W average power at 355 nm with the same pulse width and repetition rate

Figure 3 1

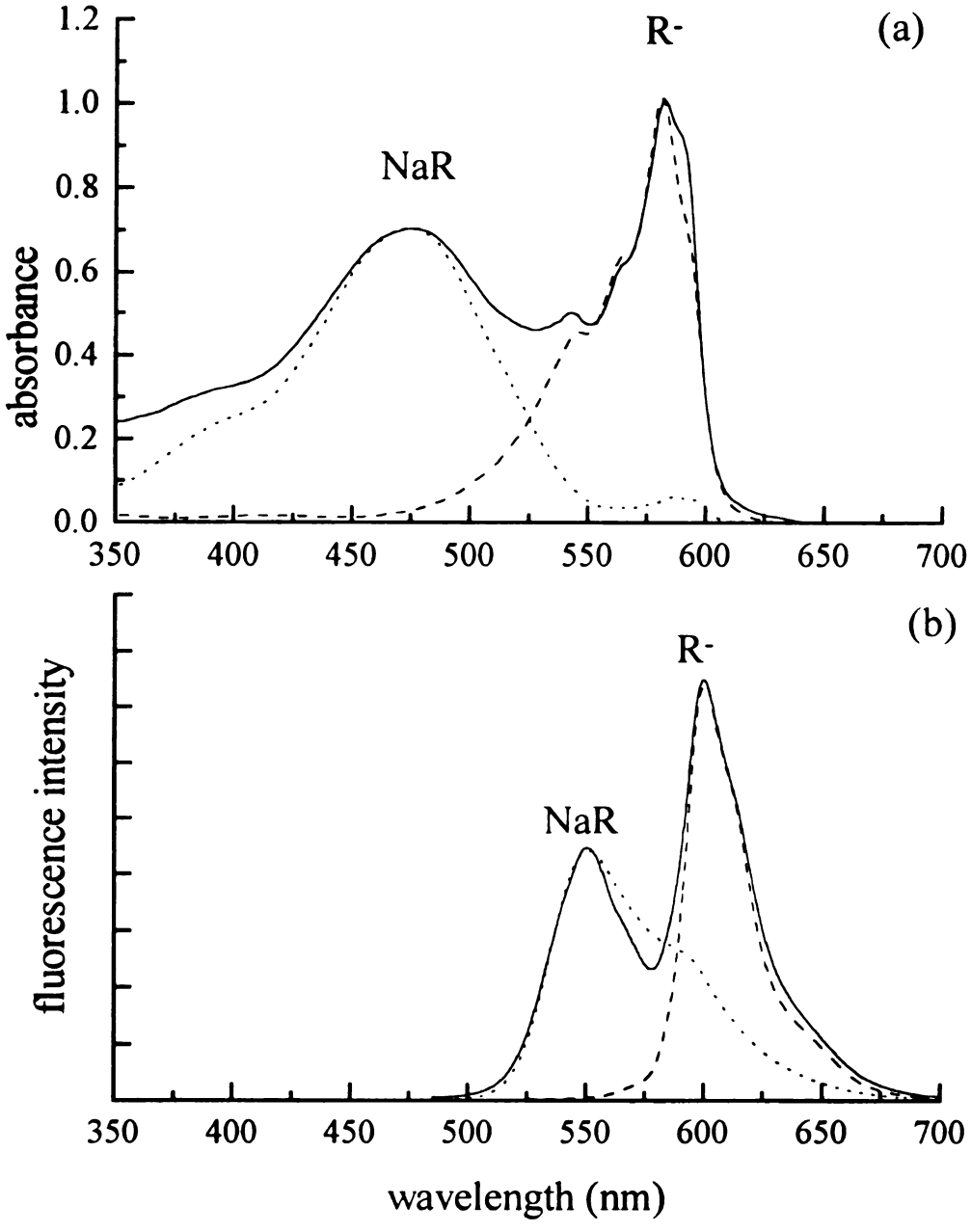

Figure 3.1. The linear absorption and emission spectra observed for 25 μM resorufin in butanols. Figure 3.1(a) are the absorption spectra for resorufin in neat *t*-butanol (dotted tracing), in neat *n*-butanol (dashed tracing), and in the mixed butanols (solid tracing). Figure 3.1(b) are the fluorescence spectra for resorufin in neat *t*-butanol (dotted tracing), neat *n*-butanol (dashed tracing), and in the mixed butanols (solid tracing). All spectra are normalized for presentation purposes.

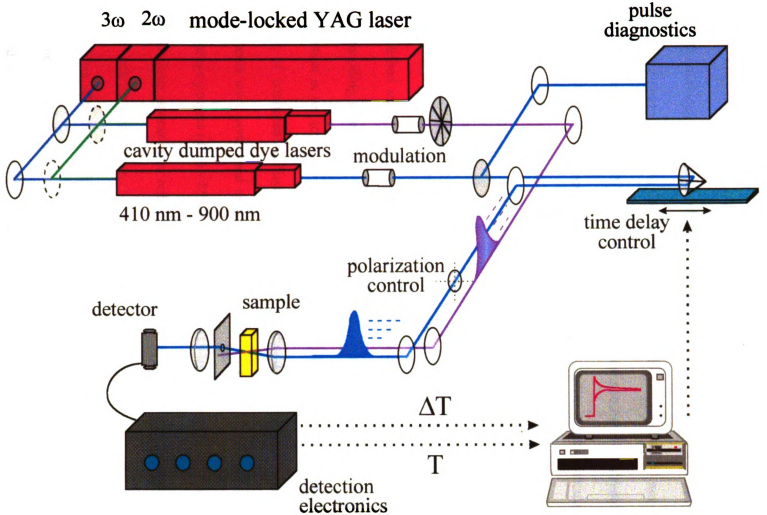

Figure 3.2. Picosecond Pump-probe spectrometer.

as the fundamental. The second and/or third harmonic output of the source laser is used to pump two dye lasers synchronously (Coherent 701-3). For dye laser operation near 470 nm, Stilbene 420 dye (Exciton) pumped with 355 nm light is used. For operation near 580 nm the dye used is Rhodamine 6G (Kodak) and it is pumped with 532 nm light. Because the pump and probe dye lasers can be operated in either the 470 nm - 475 nm range or in the 580 nm - 585 nm range independent of one another, the complete matrix of ground state recovery measurements on the R˙/NaR system can be executed. Both dye lasers are cavity dumped at ~8 MHz and the pulses from each yield second order autocorrelation traces of ~7 ps FWHM. The time resolution of this spectrometer is determined by the cross-correlation of the two laser pulse trains, which is typically 10 ps FWHM. Detection of the transient depletion signals generated by the ~ nJ laser pulses is accomplished using a radio- and audio-frequency triple modulation, shot noise limited signal encoding scheme.[24-26] For all ground state recovery measurements, the probe laser polarization is set to 54.7° with respect to the pump laser polarization to ensure the absence of rotational diffusion contributions to the data. Ground state recovery experiments were performed using a pump laser operating at either 470 nm or 580 nm with average powers of 20 - 25 mW at the sample (~15 μm focused beam diameter), and the probe laser operating at either 475 nm or 585 nm with ~150 μW average power co-focused with the pump laser.

Time Correlated Single Photon Counting (TCSPC) Spectrometer: The spectrometer used to measure the spontaneous lifetimes of NaR and R˙ has also been described in detail before.[27,28] A schematic diagram of this system is shown in Figure 3.3. For excitation at 470 nm, light pulses from the UV pumped dye laser described

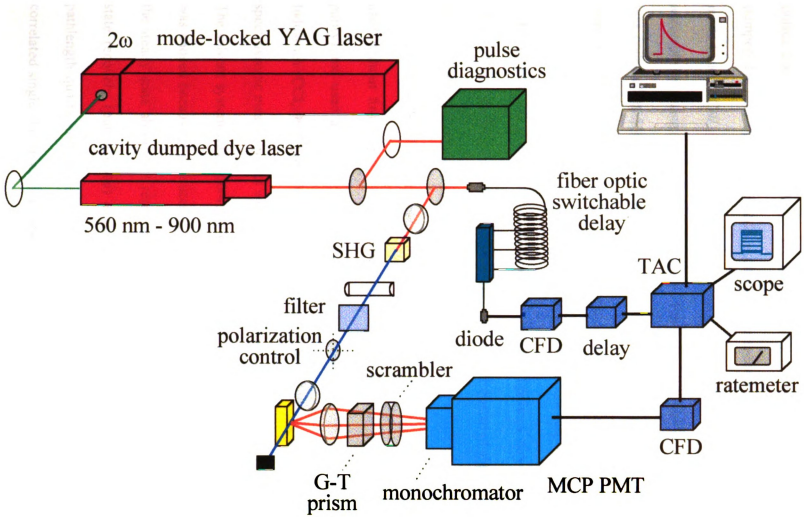

Figure 3.3. Time correlated single photon counting spectrometer.

above are used with a cavity dumping rate of 4 MHz. For excitation at 580 nm, the light pulses used to excite the sample are generated by a cavity-dumped, synchronously pumped dye laser (Coherent 702-2) excited by the second harmonic of the output of a mode-locked CW Nd:YAG laser (Quantronix 416). Excitation at 580 nm was accomplished using Rhodamine 6G (Kodak). For both excitation wavelengths, emission was collected at 550 nm and at 600 nm. For all samples, fluorescence was collected using a 10 nm (FWHM) detection bandwidth at a polarization of 54.7° with respect to the polarization of the excitation pulse. The typical instrument response function is ~40 ps FWHM for this system, and the measured fluorescence lifetimes vary from ~300 ps to ~1 ns. The experimental excited state lifetime data are not obscured significantly by the instrumental response function.

Chemicals: Sodium Resorufin was obtained from Aldrich (99+% purity) and used without further purification. The *n*-butanol was obtained from Aldrich (99+% purity) and used as received. The *t*-butanol was obtained from Columbus Chemical Industries (CCI, 99% purity) and was used as received. All resorufin solutions used for spectroscopic measurements were made to a total chromophore concentration of 25 μM. The solvent system was a 60/40 (v/v) solution of *n*-butanol and *t*-butanol. This system was chosen because it produced similar concentrations of NaR and R^- as measured by the steady state absorption responses of the two species (*vide infra*). For all ground state recovery (pump-probe) experiments, the sample was flowed through a 1 mm pathlength quartz flow cell to minimize thermal contributions to the signal. For time correlated single photon counting experiments, a 1 cm pathlength quartz sample cuvette was placed in a temperature-controlled heat sink (brass block). All experiments were

performed at 27°C, with the sample temperature being held constant to within ± 0.5°C (Neslab Endocal bath and RTE-110 cooler).

Data Reduction: Data from the pump-probe and TCSPC experiments were fit to a sum of exponential decays using Microcal Origin software. The data were fit using the following (general) procedure. First, the maximum value of the cross-correlation (CC, pump-probe measurements) or instrumental response function (IRF, TCSPC measurements) was used to establish the reference start time for each run. The experimental signals (GSR or TCSPC) were registered in time to correspond with the appropriate instrumental response to establish the time zero of the experiment. A normalized data set was then fit to a sum of exponentials. The data were fit from a point were the intensity of the CC/IRF was < 5% of the total signal to ensure that any contribution to the signal from the instrumental response did not affect the fit. The data have not been deconvoluted from the cross correlation or instrumental response function because the ion exchange and population decay dynamics of interest here are significantly longer than the response functions.

3.3. Kinetic Model

While there is a significant body of literature concerned with the thermodynamic aspects of ionic association and dissociation, this chapter describes the direct measurement of the kinetics of these processes. Accordingly, the resorufin/butanols system is considered in the context of a set of coupled first order reactions.[29] As shown in Figure 3.4, there exists a series of rate constants associated with the depopulation of

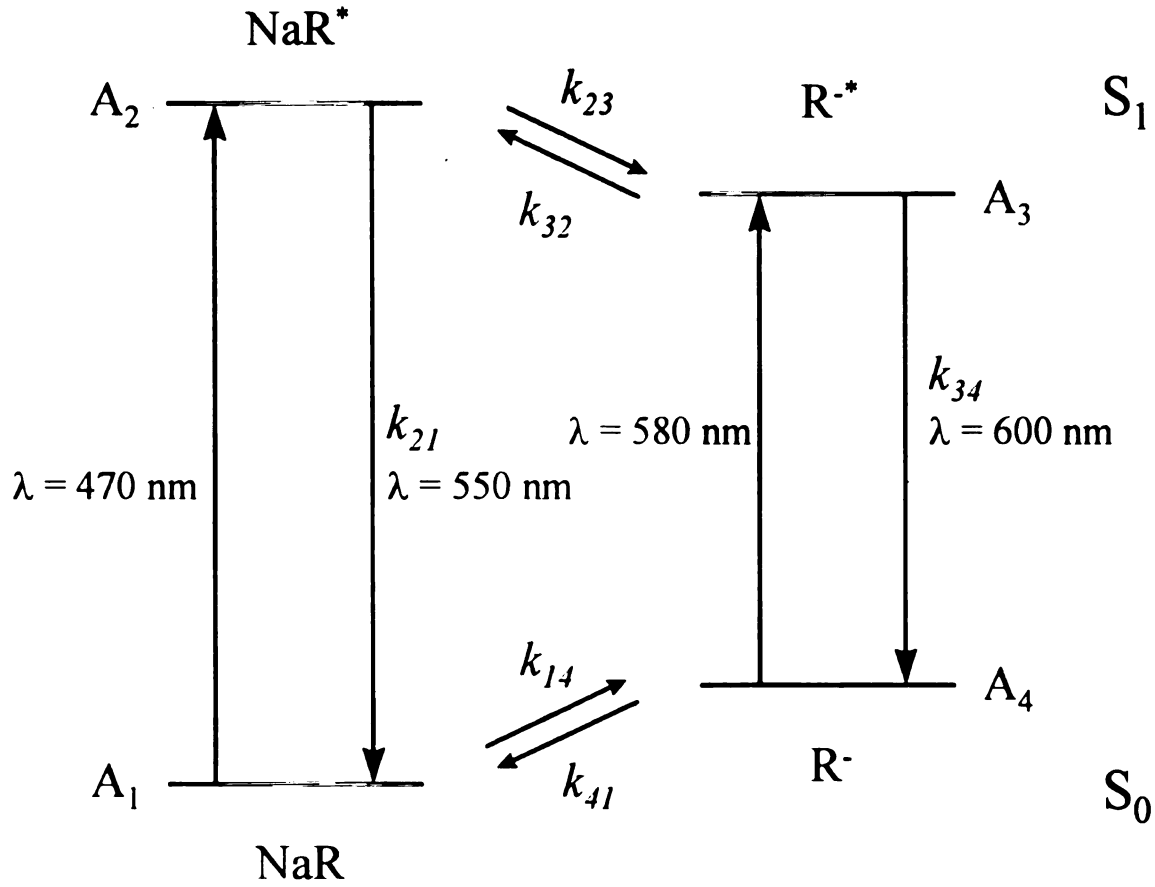

Figure 3.4. Schematic energy level diagram indicating the states for associated resorufin (NaR) and dissociated resorufin (R^-). State A_1 represents the ground state (S_0) of NaR, state A_2 is the lowest excited singlet state (S_1) of NaR, state A_3 is the lowest excited singlet state of R^-, and state A_4 is the ground state of R^-. The rate constant for spontaneous emission of NaR is k_{21} and for R^- is k_{34}. Ionic exchange rate constants between the excited state species are k_{23} and k_{32}. Ionic exchange rate constants between the ground state species are k_{14} and k_{41}.

the excited states as well as an equilibrium between the ground state forms of resorufin. The time course of each state in Figure 3.4 is described using the following expressions:

$$\frac{d}{dt}A_1 = k_{21}\cdot A_2 + k_{41}\cdot A_4 - k_{14}\cdot A_1 \qquad [3.1]$$

$$\frac{d}{dt}A_2 = k_{32}\cdot A_3 - (k_{21} + k_{23})\cdot A_2 \qquad [3.2]$$

$$\frac{d}{dt}A_3 = k_{23}\cdot A_2 - (k_{32} + k_{34})\cdot A_3 \qquad [3.3]$$

$$\frac{d}{dt}A_4 = k_{34}\cdot A_3 + k_{14}\cdot A_1 - k_{41}\cdot A_4 \qquad [3.4]$$

$$\sum A = 1 \qquad [3.5]$$

where, for these experiments, ground state NaR corresponds to A_1, the NaR first excited singlet state is A_2, the first excited singlet state of R^- is A_3, and ground state R^- is A_4 (Figure 3.4). Rate constants for ionic exchange and spontaneous population decay are included in this scheme. For example, deactivation of A_2 to A_1 occurs at a rate determined by the rate constant k_{21}, while excited state association/dissociation between states A_2 and A_3 proceeds according to rate constants k_{23} and k_{32}. Terms for the excitation rate constants have not been included, since these processes are essentially instantaneous and are determined by the laser pulses used ($\leq$ 10 ps). This series of coupled differential equations (3.1 - 3.5) represents a simplification of the general case where there exist four species, each capable of interconversion with any of the others.[29] For this system, the functional form of the population evolution for each state A will be a sum of exponential decays,[29]

$$A_i(t) = \sum_{r=1}^{4} B_{ir} \exp(\lambda_r t) \qquad [3.6]$$

where the subscript r indicates the coupling of species i to the other species r and the terms λ are permutations of the rate constants k. It is this same functional form to which the experimental data are fit. For this system (Figure 3.4), the non-trivial terms λ are given by:

$$\lambda_1 = \tfrac{1}{2}[-k_{21} - k_{23} - k_{32} - k_{34} - \sqrt{(k_{21} + k_{23} + k_{32} + k_{34})^2 - 4(k_{21}k_{32} + k_{21}k_{34} + k_{23}k_{34})}] \qquad [3.7]$$

$$\lambda_2 = \tfrac{1}{2}[-k_{21} - k_{23} - k_{32} - k_{34} + \sqrt{(k_{21} + k_{23} + k_{32} + k_{34})^2 - 4(k_{21}k_{32} + k_{21}k_{34} + k_{23}k_{34})}] \qquad [3.8]$$

$$\lambda_3 = -k_{14} - k_{41} \qquad [3.9]$$

It is these terms that are extracted from the experimental data and, from these λ values, the rate constants k_{ij} were determined. A prediction of this model is that, for all of the measurements made, it is expected there to be only three time constants and, in fact, this condition is observed experimentally.

3.4. Results and Discussion

The ground state recovery data and spontaneous emission decay data for the resorufin chromophore in the binary butanol system offer a unique opportunity for understanding the kinetics of solution phase ionic association and dissociation. Because the absorption and emission responses of NaR and R^- are resolved from one another sufficiently, it is possible to examine the population dynamics of all species (ground and excited state NaR and R^-) as a function of initial population conditions. Specifically, the

S_1 state of NaR can be populated by excitation at 470 nm and the spontaneous depopulation of this state can be monitored by TCSPC, collecting at 550 nm, formation and depopulation of S_1 R^- (TCSPC, collection at 600 nm), population recovery of S_0 NaR (GSR, probe at 475 nm) or population build-up of S_0 R^- (GSR, probe at 585 nm). The initial population can be placed in S_1 R^-, with monitoring of the population of the other states. The data for two groups of experiments is presented below, where the initial excitation condition is varied and the population evolution of all states is monitored. The measurements reported below on resorufin in the binary butanol system exhibit an apparently wide range of functionalities, depending on the species excited and the state monitored. For all measurements, however, the functional form of the data can be accounted for within the framework of the kinetic model presented above, where there are three distinct regimes for the experimental decay time constants, λ_1, λ_2, and λ_3.

Before discussing the measured kinetic responses, it should be made clear that the chemical process monitored is not proton exchange, but counter-ion (Na^+) exchange. This argument is based on the availability of protons in each of the solvents, the concentration of the resorufin compared to the free proton concentration, and the assignment of the absorption bands for this chromophore. The autoprotolysis constant for *n*-butanol is $10^{-21.8}$, [30] implying that [*n*-$BuOH_2^+$] = 1.26×10^{-11} M for the neat solvent. By comparison, the autoprotolysis constant for *t*-butanol is $10^{-28.5}$, [31] yielding [*t*-$BuOH_2^+$] = 5.62×10^{-15} M. The presence of ~10^{-5} M Na^+ and R^- in solution will perturb the equilibrium concentrations of the dissociated solvent species, but the extent of this perturbation is not the focus of this work, nor is it believed that this effect contributes measurably to the experimental data (*vide infra*). The important conclusion from these

autoprotolysis data is that *t*-butanol is a significantly weaker acid than *n*-butanol, and thus, greater protonation of the resorufin is expected in *n*-butanol than in *t*-butanol. Simple pH-dependent measurements of resorufin in pH 3 and pH 10 water demonstrate that the deprotonated form of resorufin, R^-, absorbs at 580 nm, and the protonated form absorbs at 470 nm. The absorption spectroscopic data in the alcohols indicate that the free anion (R^-) dominates in *n*-butanol, and a specie with an absorption response identical to the protonated form of resorufin is dominant in *t*-butanol. Given the low concentration of labile protons in both *n*- and *t*- butanol as well as their dielectric constants (ε_0 = 12.7 for *t*-butanol and ε_0 = 17.5 for *n*-butanol), it is believed that, in *t*-butanol, it is not the protonated form, HR, but the cation-associated form NaR, that is responsible for the observed absorption resonance. The functional form of the experimental linear response data bounding K_{eq} for dissociation are inconsistent with a protonation argument as well. These data will be presented below along with a comparison of the results from the kinetic and steady-state (equilibrium) experiments.

Before presenting this comparison, the kinetic and steady-state data are described separately. The simulations presented in conjunction with the experimental data below were performed using optimized values for the rate constants k_{ij}. Following presentation of the data these values will be discussed in detail.

Excitation of NaR at 470 nm. Excitation of the resorufin chromophore at 470 nm populates, initially, the first excited singlet state (S_1) of the associated form of this molecule (NaR) (A_2 = 1). The population recovery of the ground state (S_0) NaR (A_1) is monitored via transient bleaching recovery at 475 nm, S_1 NaR (A_2) relaxation via fluorescence decay at 550 nm, population and relaxation of S_1 R^- (A_3) by fluorescence

intensity decay at 600 nm and S_0 R^- (A_4) population by ground state recovery of the R^- absorption band at 580 nm. These data are presented in Figures 3.5 and 3.6. The picture that emerges from the excited state relaxation data is that dissociation of S_1 NaR is efficient based on the short time required to detect a response from S_1 R^- (Figure 3.5b). Despite the short time required for population of S_1 of R^-, it is clear that there is an onset to this signal compared to the monotonic depopulation of S_1 NaR (Figure 3.5a). No attempt is made to quantify this slight difference in risetime, only its presence is noted. This finding implies the possible existence of an intermediate dissociative complex, and a discussion of this point is found below. Consistent with simulations of A_i using Eqs. 3.1 - 3.5, (Fig 3.7), the population of S_1 NaR decays more rapidly than the population of S_1 R^- when S_1 NaR is the species excited initially. These simulations are based on the measured spontaneous emission rate constants (k_{21} and k_{34}) for each state (A_2 and A_3) in the neat butanols. For the ground state recovery measurements (Figures 3.6), the simulated responses reported in Figure 3.7 are the negative of the experimental $\Delta T/T$ signals, and this sign difference is the result of the detection modulation scheme used for the pump-probe measurements.[24-26] In agreement with the model, population recovery of S_0 R^- (Figure 3.6b) is significantly more rapid than for S_0 NaR (Figure 3.6a). The difference in the time course of these populations is the direct result of the dissociation equilibrium operating in this system. A distinct rise time is noted for the ground state recovery signal for NaR (Figure 3.6a), and this contribution to the signal is not predicted by the model. Attempts at changing the initial population conditions of the simulation cannot reproduce the form of this response, and it is believed to arise from spectral overlap. In other words, the ground state recovery (transient bleaching)

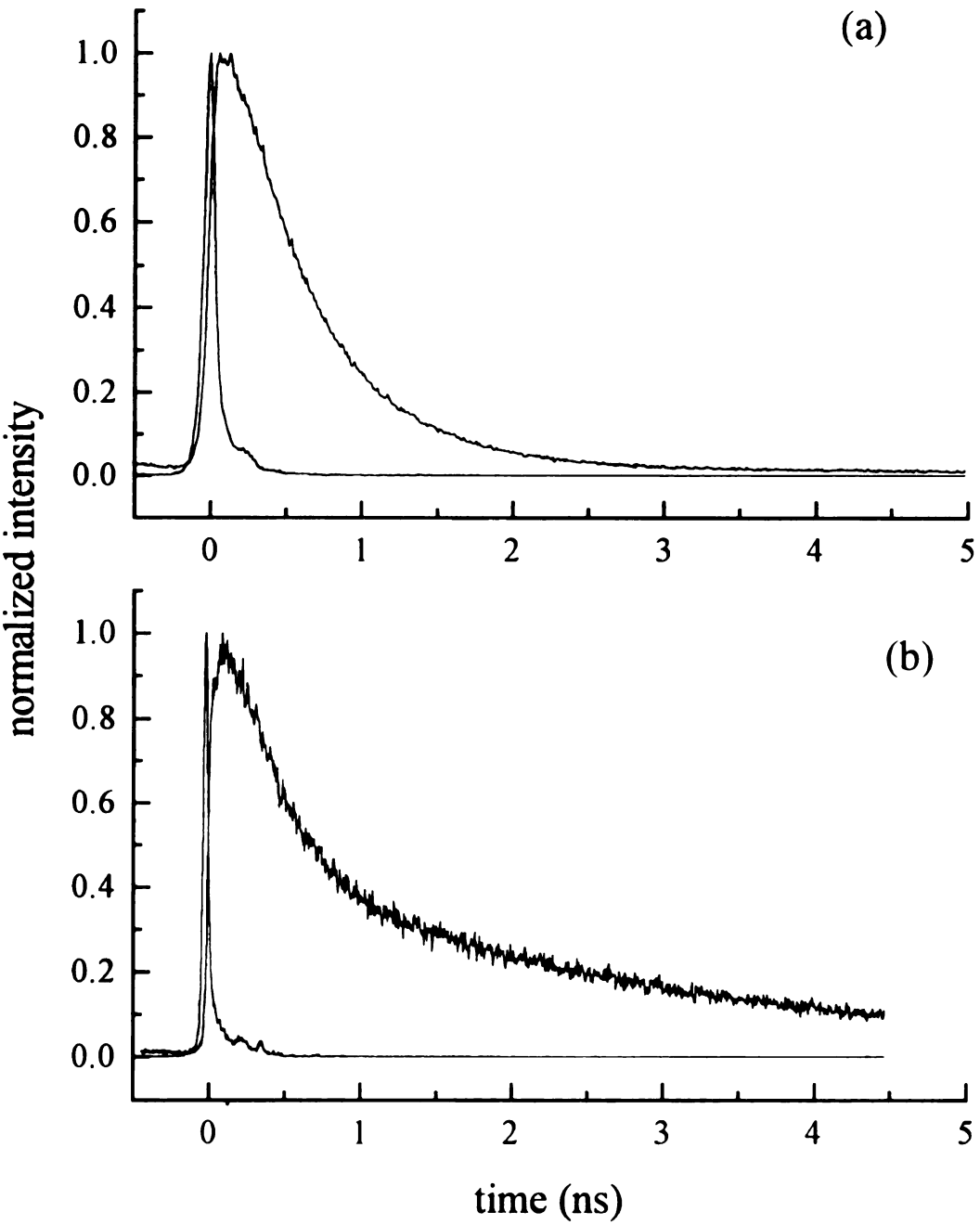

Figure 3.5. Fluorescence (spontaneous emission) lifetime of NaR using an excitation wavelength of 470 nm. Trace (a) is the lifetime decay observed at an emission wavelength of 550 nm (NaR), and trace (b) is the decay observed at an emission wavelength of 600 nm ($R^{\cdot}$). The instrumental response function indicates zero delay time, and its intensity has been normalized to the maximum intensity of the lifetime decay.

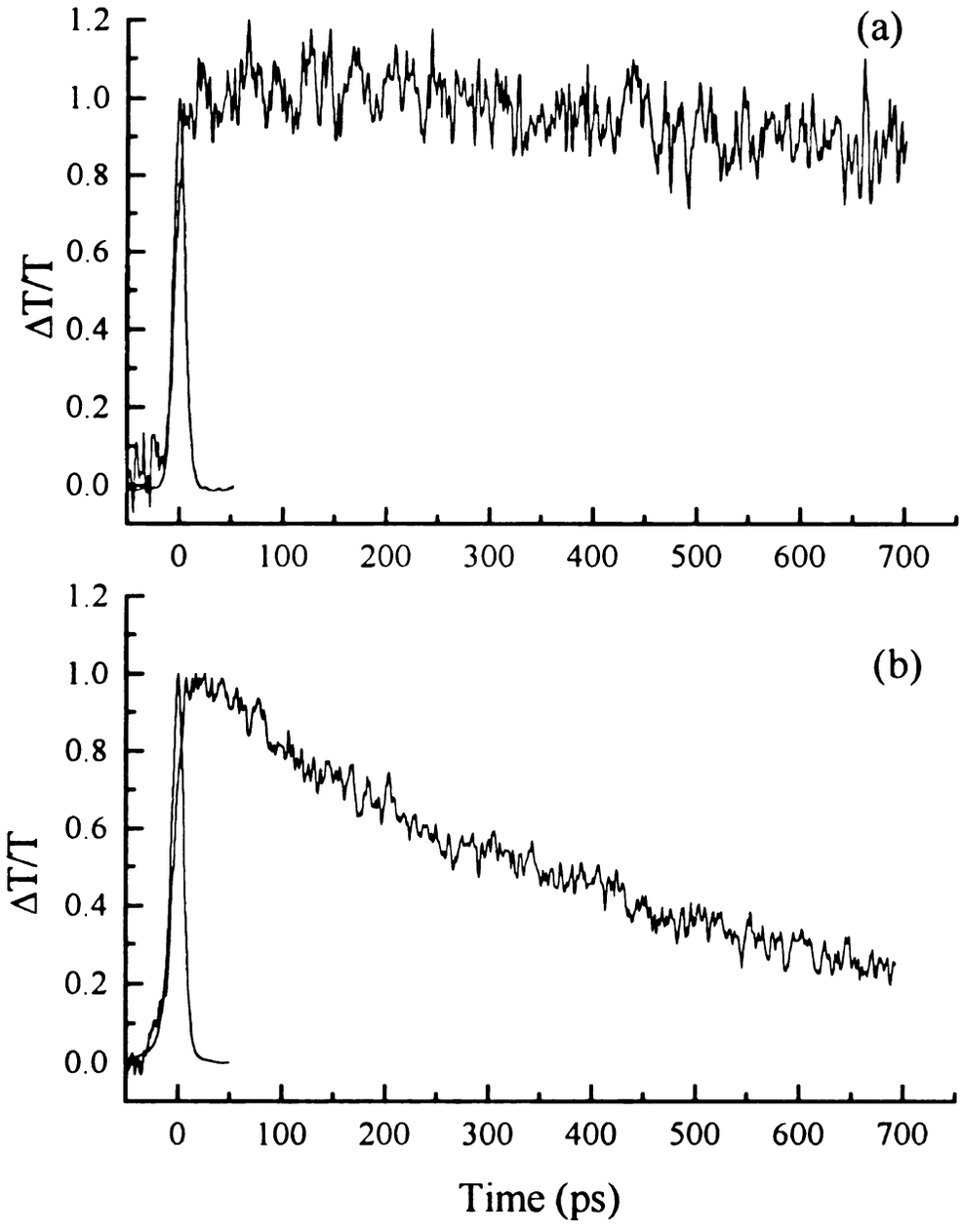

Figure 3.6. Ground state recovery (GSR) of resorufin observed using a pump wavelength of 470 nm. Tracing (a) is the GSR observed with a probe wavelength of 470 nm, which monitors the population recovery of species NaR. Tracing (b) is the GSR observed with a probe wavelength of 580 nm, which monitors the population recovery of species $R^{\cdot}$. The instrumental response function indicates zero delay time, and its intensity has been normalized to the maximum intensity of the GSR scan.

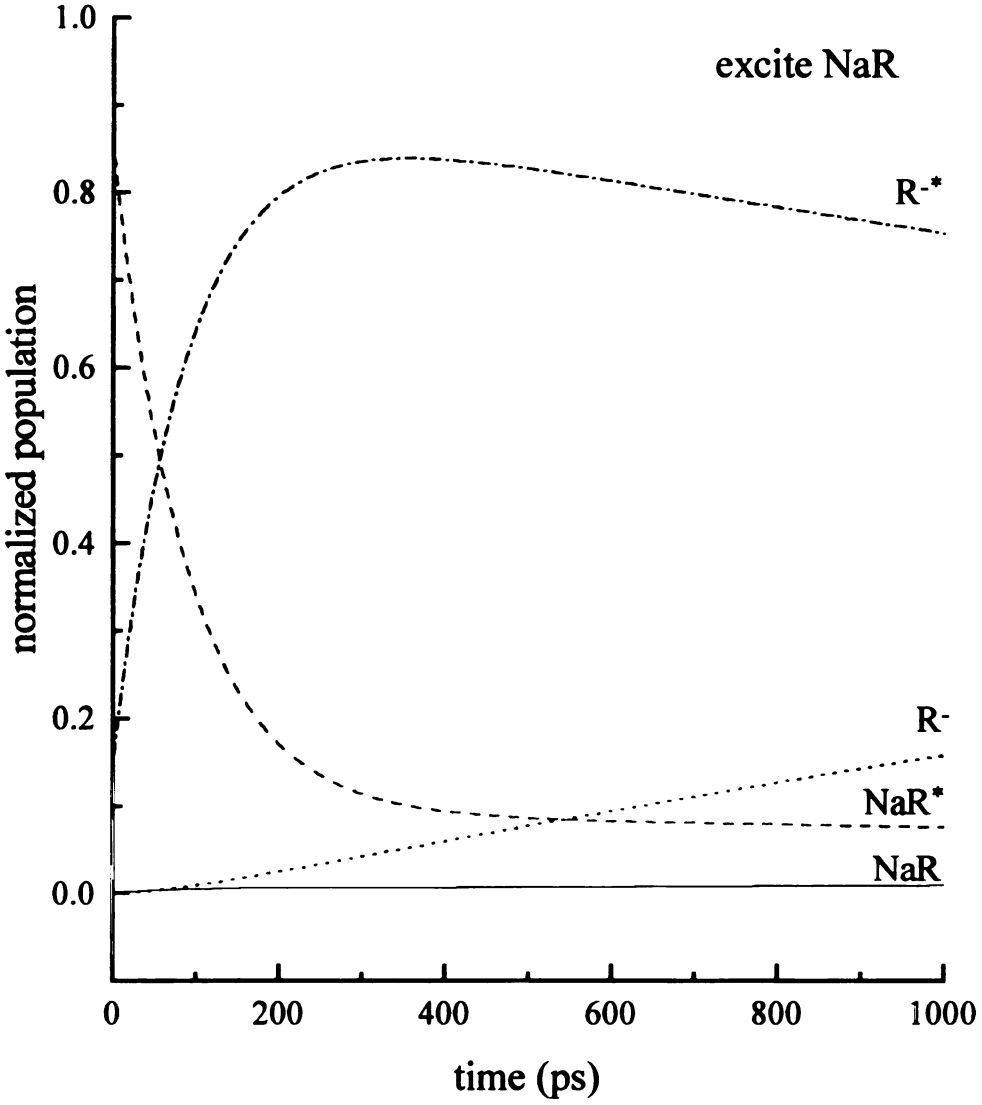

Figure 3.7. Kinetic simulations of the population dynamics of resorufin as modeled in equations 3.1-3.5. Plot shows the time course of the populations when pumped by 470 nm light, which initially populates only state A_2 (NaR^*). Initial population of state A_2 =0.85, of state A_3=0.15. A detailed discussion of these simulations is found in the text.

Table 3.1. Measured spontaneous emission times (SPE) and ground state recovery (GSR) times for resorufin in a binary butanol system. Wavelengths indicated represent the pump (excitation) wavelength and the probed (emission or ground state recovery) wavelength. All measurements of SPE times used time correlated single photon counting spectroscopy, measurements of GSR times were obtained using pump/probe spectroscopy. All measurements were performed at 300.0 ± 0.1 K. The τ_2 value was determined by measurement of τ_{fl} for resorufin in *n*-butanol and *t*-butanol and was also the best fit value for the complex decays reported for the mixed solvent system.

measurement and wavelengths (nm)	τ_1 (ps)	τ_2 (ps)
SPE (470/550)	595 ± 5	4600
SPE (470/600)	514 ± 27	4600
SPE (580/600)	389 ± 54	4600
GSR (470/470)	20 ± 5	4600
GSR (470/580)	432 ± 45	4600
GSR (580/470)		~ constant
GSR (580/580)	38 ± 6	4600

response at 475 nm comes mostly from NaR absorption, but there is a contribution from the band tail of R^- (Figure 3.1). From these experimental data, in conjunction with the model, three decay constant values (λ_i^{-1}) are extracted that can be related to the rate constants k_{ij} (Table 3.1).

Excitation of R^- at 580 nm. R^- was excited selectively and the population evolution of the ground and excited states of both R^- and NaR were monitored. These data in are presented in Figures 3.8 and 3.9. The excited state lifetime data is shown in Figure 3.8 and the ground state recovery measurements for R^- and NaR in Figure 3.9. The population evolution of S_1 R^- (Figure 3.8b) is particularly interesting because of the significant intensity increase that occurs well after excitation. This response is not predicted by the model in the limit that S_1 R^- is excited selectively, and this response is accounted in terms of spectral overlap between S_0 NaR and R^- (Figure 3.1). If spectral overlap is incorporated into the kinetic model (Figure 3.10) through the initial condition $A_2(0) = 0.85$, $A_3(0) = 0.15$, yielding model kinetic responses consonant with the data presented in Figures 3.8. It is also noted that the excitation of R^- at 580 nm and the observation of emission at 550 nm (Figure 3.8a) demonstrates unambiguously the existence of an equilibrium condition between S_1 NaR and S_1 R^- and places an important limit on the relative energies of the two S_1 species. In analogy to excitation of NaR at 470 nm, the experimental ground state recovery measurements are the negative of the model simulations presented in Figure 3.10. For these measurements, it is found that the recovery time of S_0 R^- is significantly faster than that for S_0 NaR (Figures 3.9). Also, the presence of a build-up in bleaching intensity of the NaR band subsequent to excitation of R^- must be accounted for in terms of spectral overlap. The magnitude of the bleaching

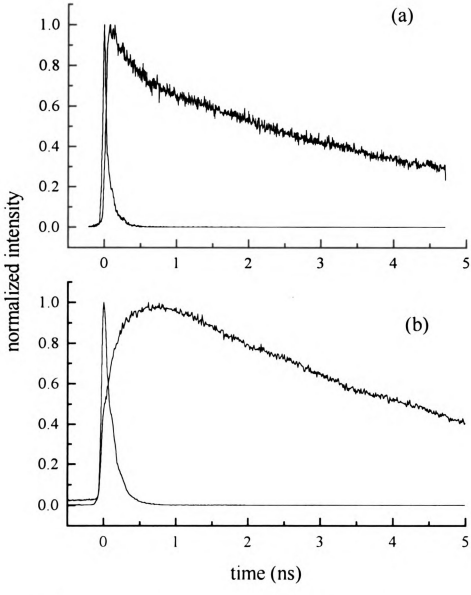

Figure 3.8. Fluorescence (spontaneous emission) lifetime of $R^{\cdot}$ using an excitation wavelength of 580 nm. Trace (a) is the lifetime decay observed at an emission wavelength of 550 nm (NaR), and trace (b) is the decay observed at an emission wavelength of 600 nm ($R^{\cdot}$). The instrumental response function indicates zero delay time, and its intensity has been normalized to the maximum intensity of the lifetime decay.

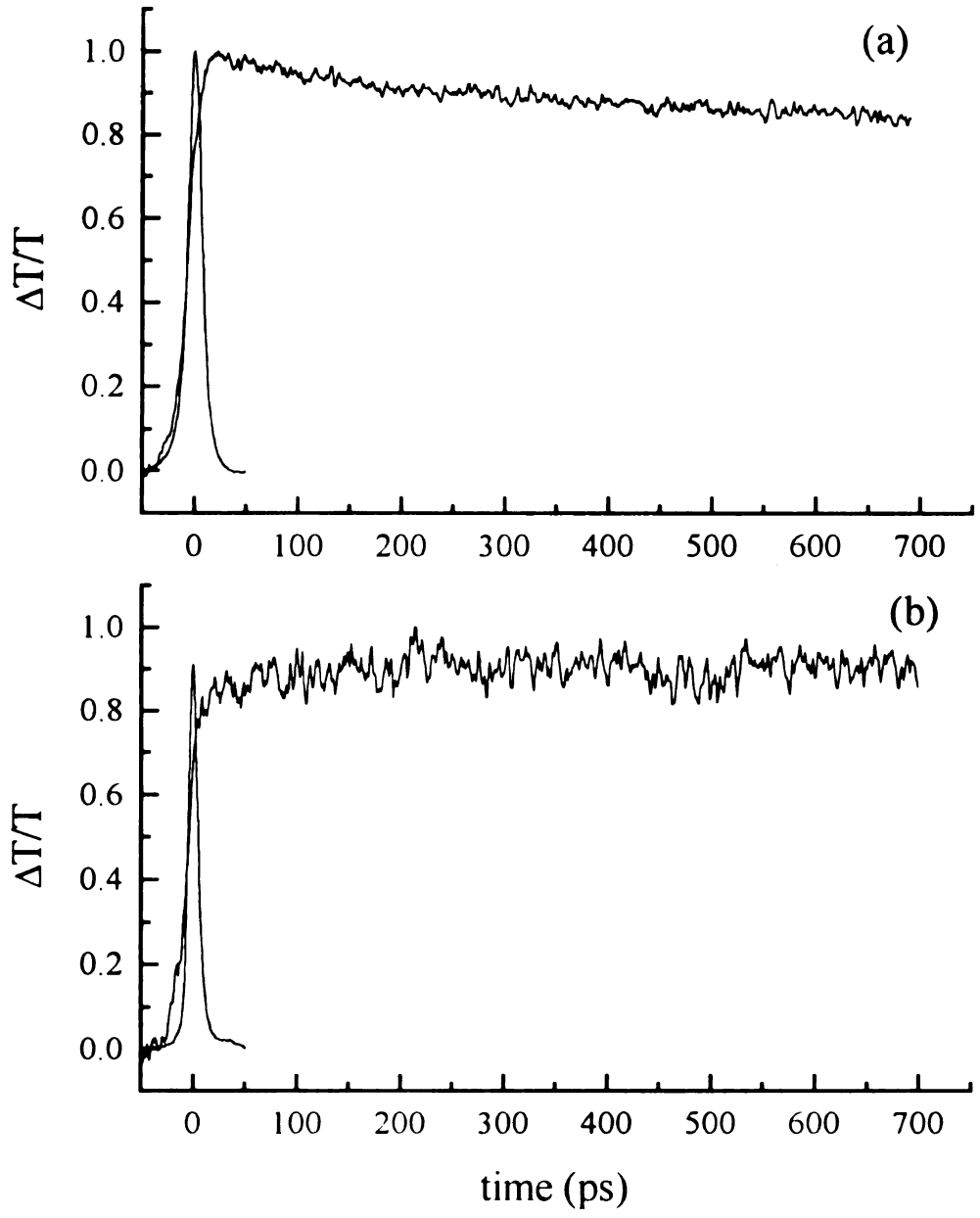

Figure 3.9. Ground state recovery (GSR) of resorufin observed using a pump wavelength of 580 nm. Tracing (a) is the GSR observed at 580 nm, which monitors the population recovery of species R^-. Tracing (b) is the GSR observed at 470 nm, which monitors the population recovery of species NaR. The instrumental response function indicates zero delay time, and its intensity has been normalized to the maximum intensity of the GSR scan.

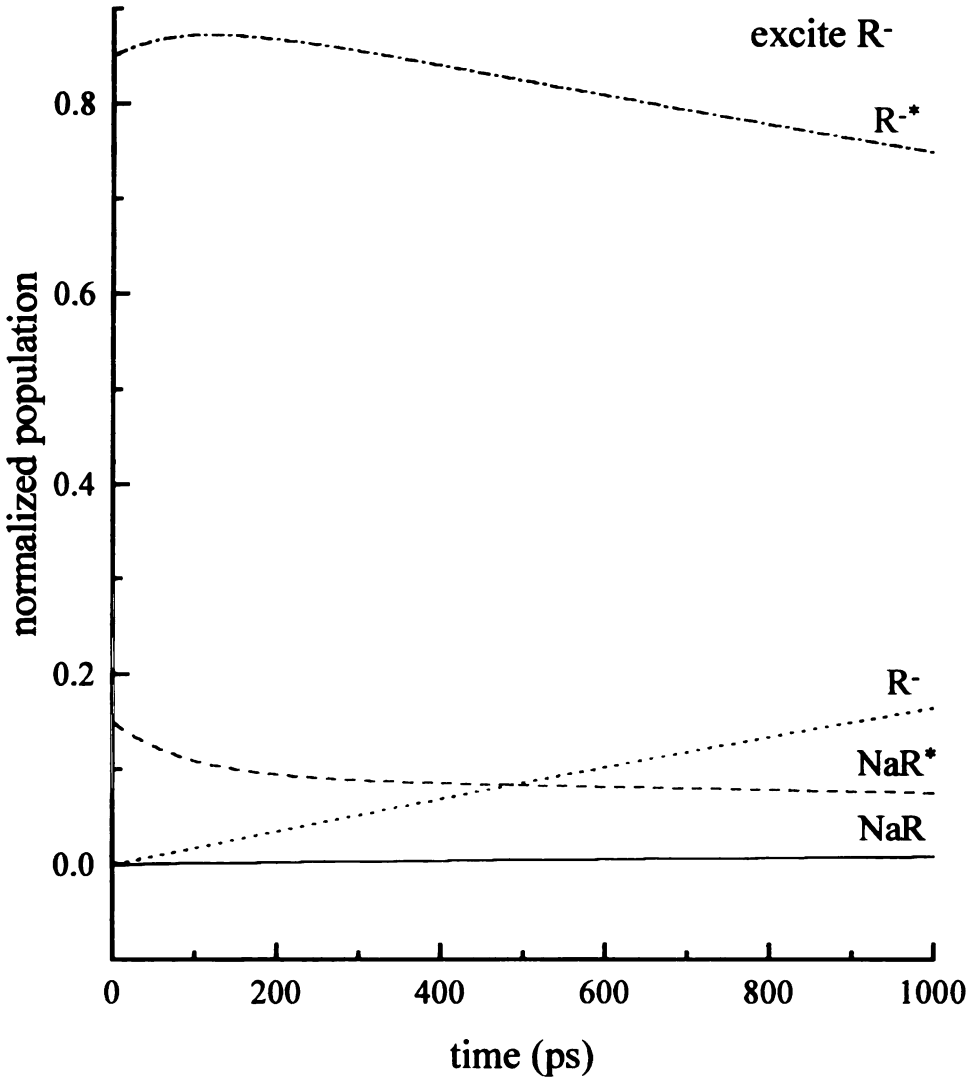

Figure 3.10. Kinetic simulations of the population dynamics of resorufin as modeled in equations 3.1-3.5. Plot shows the time course of the populations when pumped with 580 nm light, which initially populates only state A_3 (R^{-*}). Initial population of state A_2 =0.15, of state A_3=0.85. A detailed discussion of these simulations is found in the text.

signal for S_0 NaR has not been quantified, but it is significantly smaller than that measured for S_0 R^-. This difference is due, in part, to the pump laser intensity available at 470 nm compared to that available at 580 nm and also, in part, to the comparatively weaker molar absorptivity of the NaR absorption band.

The relative values of the decay time constants derived from our experimental data and their chemical significance is now addressed. Inspection of the experimental decay time constants (Table 3.1) reveals three distinct values, corresponding to λ_1^{-1}, λ_2^{-1} and λ_3^{-1}. Three time regimes are measured in these experiments, a fast component at $\cong$ 25 ps, a slower component at $\cong$ 500 ps, and a long time component at $\cong$ 4500 ps. The value of λ_2^{-1} is assigned to be $\cong$ 4500 ps based on the functional form of Equation 3.8 compared to Equation 3.7. There remains, however, ambiguity in the assignment of the experimental values corresponding to λ_1^{-1} and λ_3^{-1}. Given the experimental data alone, this ambiguity cannot be resolved, but in concert with simulations of Equations 3.1 - 3.5 (Figures 3.5 and 3.8), bounds can be placed on the values of λ_1^{-1} and λ_3^{-1} that are consistent with the experimental data. The simulated time evolution of the populations for states A_1 - A_4 are presented in Figures 3.5 and 3.8 and, as described above, are in agreement with the experimental data. For these simulations values used for k_{21} (2×10^8 s^{-1}) and k_{34} (2×10^8 s^{-1}) were derived from spontaneous emission lifetime measurements of resorufin in the two neat solvents *n*-butanol and *t*-butanol. In order to obtain the form of the simulations consistent with the experimental data, $k_{23} = 3\times10^{10}$ s^{-1}, $k_{32} = 2\times10^9$ s^{-1}, $k_{41} = 1\times10^8$ s^{-1} and $k_{14} = 2\times10^9$ s^{-1} were used. This set of rate constants yields $\lambda_1^{-1} = 31$ ps, $\lambda_2^{-1} = 5000$ ps, and $\lambda_3^{-1} = 476$ ps. It is also possible, in principle, using the appropriate set of rate constants, to obtain values of $\lambda_1^{-1} \sim 500$ ps and $\lambda_3^{-1} \sim 25$ ps, but for this set of

rate constants, the functional forms of the population evolution of A_1 - A_4 are not in agreement with the experimental data. Thus, based on the experimental signals and the set of rate constants that produce simulations in agreement with these data, $\lambda_1^{-1} \sim 30$ ps and $\lambda_3^{-1} \sim 500$ ps. This assignment is critical to the understanding of the ion exchange dynamics in this system because it places limits on the rates of dissociation and association in each electronic state of resorufin.

For the ground state ionic equilibrium, it is observed that the concentrations of R^- and NaR are different by a factor of ~3 ($[RH] \cong 3[R^-]$), based on the absorptivities of the R^- (ε = 97,000 L/mol-cm) and NaR (ε = of 33,000 L/mol-cm) bands and their relative band intensities (integrated areas) in the 60/40 butanols solution used here. It is noted that the absorptivity we report here for R^- is slightly higher than that reported previously[20] and attribute this small difference to the higher precision available with the absorption spectrometer used here. In addition, the transient data yield best fit values for k_{14} (2×10^9 s^{-1}) and k_{41} (1×10^8 s^{-1}). At this point it is important to compare these kinetic results to those achieved using steady state absorption measurements. As discussed above, the equilibrium process of interest is

$$NaR \rightleftharpoons Na^+ + R^- \qquad [3.i]$$

For this reaction, the equilibrium constant for dissociation can be measured directly,

$$K_{eq} = \frac{[Na^+][R^-]}{[NaR]} \qquad [3.10]$$

From our initial conditions that $[Na^+] = [R^-]$ and both $[R^-]$ and [NaR] can be measured from absorption measurements. Thus a plot of the ratios of the absorbances for each

specie as a function of initial resorufin concentration provides a function from which Keq can be estimated. Figure 3.11 represents a plot of $[A_{R^-}]/[A_{NaR}]$ vs. initial concentration of NaR. The two lines indicate the calculated dependence of the absorbance ratio on initial concentration for two different values of K_{eq} that bound the experimental data. It is clear that the experimental data are of a functional form similar to, but not identical to, that used in the calculated functions. An implication of this finding is that there may be an intermediate complex that is neither fully dissociated nor associated. Additional support for this possibility is found in the comparison of the equilibrium data to the kinetic rate constants.

The K_{eq} determined from steady state data lies in the range 1.4×10^{-5} M $\leq K_{eq} \leq$ 7×10^{-5} M while the kinetic association/dissociation rate constants imply a value of ~ 20 for the exchange process sensed in the ground state and ~ 10 in the excited state. These kinetic rate constant ratios are unitless, and thus a direct comparison to the equilibrium value is not easily achieved. However, the differences in both magnitude and units for the kinetic and equilibrium treatments can be understood in the context of the system being more complicated than a simple ionic dissociation. It is clear that Coulombic forces will play a significant role in the processes we measure and thus it is likely inaccurate to consider these dynamics as exchange between two limiting cases (fully dissociated and tightly associated). A more realistic treatment includes the existence of a pre-associative (or pre-dissociative) intermediate state, and the correspondence between the kinetic and equilibrium results in such a system can be understood as

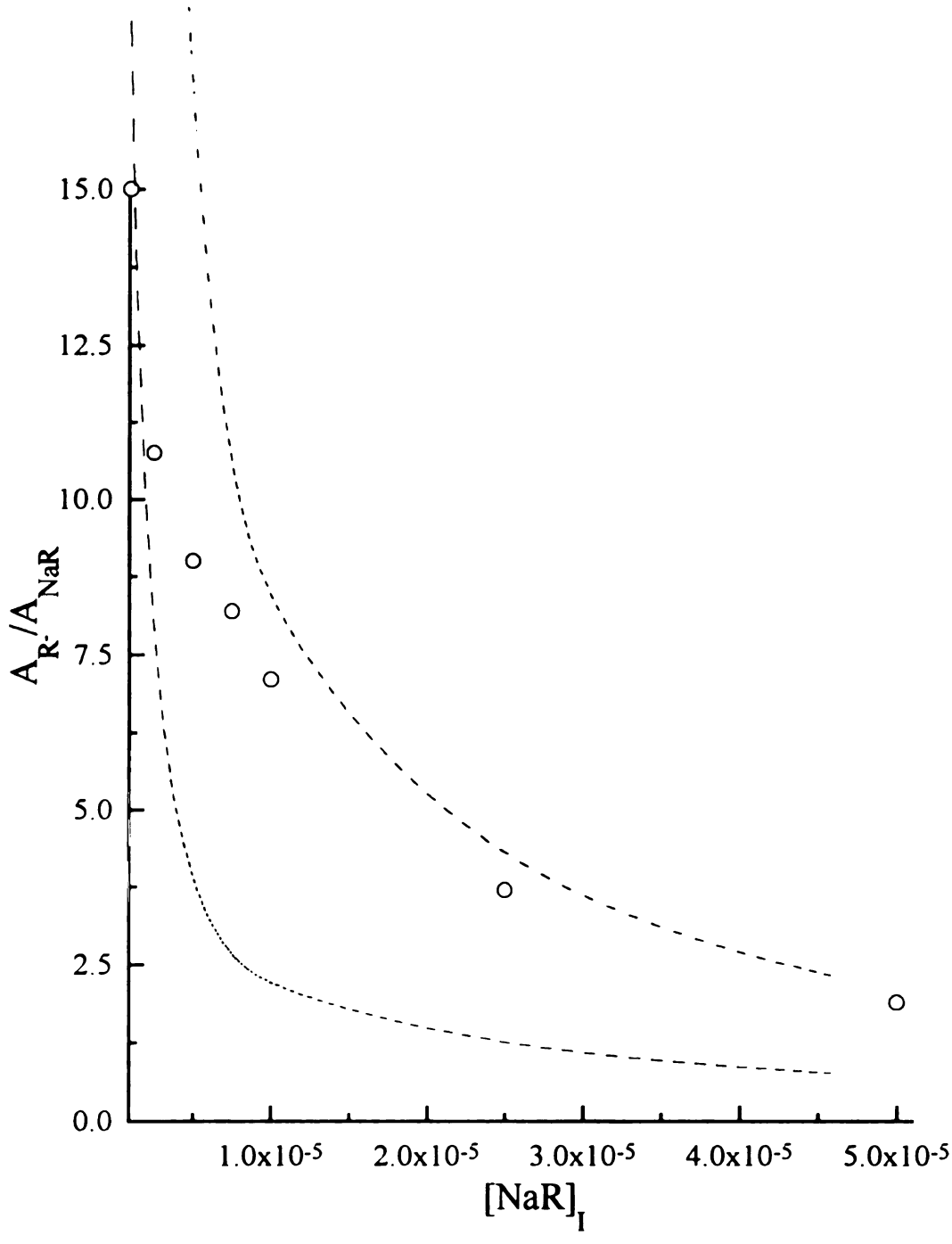

Figure 3.11. Ratio of absorbances for the two forms of the chromophore as a function of initial chromophore concentration. Lines are calculated absorbance ratios for two values of K_{eq}. See text for a discussion.

$$NaR \underset{k1r}{\overset{k1f}{\rightleftharpoons}} [Na\cdots\cdots R] \underset{k2r}{\overset{k2f}{\rightleftharpoons}} Na^{+} + R^{-} \qquad [3.ii]$$

where the relevant equilibrium expression is derived as the product of two distinct steps

$$k_1 = \frac{k_{1f}}{k_{1r}} = \frac{[Na\cdots R]}{[NaR]}$$

$$k_2 = \frac{k_{2f}}{k_{2r}} = \frac{[Na^+][R^-]}{[Na\cdots R]} \qquad [3.11]$$

$$K_{eq} = k_1 k_2$$

The intermediate specie Na••••R is defined as the pre-associative/dissociative complex, rate constants can be identified for the formation and loss of the complex from either the tightly bound form or the fully dissociated form. The formation constant k_1 is the ratio of the rate constants k_{1f} and k_{1r}, and the dissociation constant k_2 is likewise the ratio of the rate constants k_{2f} and k_{2r}. The apparent difference between the kinetic and equilibrium results arises by understanding that the kinetics experiments monitor the disappearance of the species, and not the static distribution. Thus the k_{14} rate constant in the kinetic model corresponds to k_{1f} in Equation 3.11, and k_{41} in the kinetic model corresponds to k_{2r} in Equation 3.11. The difference between K_{eq} and $[k_{14}/k_{41}]$ is the ratio $[k_{2f}/k_{1r}]$ and it is not possible to elucidate the constituents of K_{eq} beyond this point due to an inability to detect the complex explicitly. While a logical expectation might be that the steady state response of the complex should be intermediate between that of NaR and R^-, it is not possible to detect or resolve its presence for two reasons. First, the spectral overlap of the linear responses of NaR and R^- obscure this intermediate region

and second, the steady state concentration of this specie is unknown. There are possible hints of the presence of additional bands in the linear response in Figures 3.1, and these features *may* be associated with the complex postulated.

It is instructive to compare these kinetic data for association and dissociation to those available for similar reactions. The most common association/dissociation process studied so far has been proton exchange.[32-36] It is common in the treatment of such data to consider the presence of a partially associated complex, as done here, and the time constants found for protonation and deprotonation are, by and large, consonant with those that have been found here for Na^+ association and dissociation. The primary implications of this finding are two-fold. The first is that the role of the intermediate complex is crucial in accounting for the observed fast rate constants. In other words, the state-dependent k_{2r} rate constant measured indicates that the overall equilibrium process we measure is not diffusion limited. This result is not surprising due to the strength of the Coulombic interactions between the ionic constituents in the dissociated form. The second implication arising from the similarity of Na^+ and H^+ dissociation is that the mass of the ion does not play a deterministic role in the process. If inertial considerations were important then one would expect a difference of a factor of ~23 due to the difference in mass of the two moieties. If that were the case, then Coulombic interactions are implicated as the mediating force in dissociative equilibria. Thus the observed dynamics are not consistent with either a completely inertial or a completely diffusive mechanism for the dissociation. Further evidence in support of importance of Coulombic forces in these equilibrium processes is the significant state-dependence measured in the exchange rate constants.

3.5. Conclusions

The association and dissociation dynamics have been measured for the probe molecule resorufin in a binary butanol solvent system. Measurements of both the ground and excited state dynamics for both the associated and dissociated form of the probe molecule demonstrate that there is rapid exchange of sodium ions between NaR and R^- in both the S_0 and S_1 states of each form. Comparison of the kinetic and equilibrium data demonstrates the important role of an unresolved pre-associative/dissociative complex for this system. Despite the outwardly complicated kinetic responses measured, there are three distinct temporal regimes associated with this family of data, and the physical significance of these data can be understood in the context of a simple kinetic model. Comparison of this model with the experimental data reveals that the associative and dissociative kinetics observed are state dependent, with the onset of dissociation being achieved a factor of ~ 10 faster for S_1 resorufin than for S_0 resorufin. This difference in kinetic responses for the two states to changes is attributed to changes in electron densities associated with excitation of the two species of resorufin. An important general conclusion of this work is that, even at comparatively low chromophore concentrations (25 μM here) the dynamics of ionic exchange can mediate the observed optical response significantly. Because these dynamics occur on a time scale similar to that measured for molecular reorientation in moderately viscous liquids, it is possible that there is some interplay between molecular reorientation and ionic exchange processes.

3.6. Literature Cited

1. Jiang, Y.; Blanchard, G. J. *J. Phys. Chem.*, **1994**, *98*, 9411.

2. Jiang, Y.; Blanchard, G. J. *J. Phys. Chem.*, **1995**, *99*, 7904.

3. Fleming, G. R. Chemical Applications of Ultrafast Spectroscopy, Oxford University Press, 1986, and references therein.

4. Blanchard, G. J. *Anal. Chem.*, **1989**, *61*, 2394.

5. Beddard, G. S.; Doust, T.; Hudales, J. *Nature*, **1981**, *294*, 145.

6. Hartman, R. S.; Konitsky, W. M.; Waldeck, D. H. *J. Am. Chem. Soc.*, **1993**, *115*, 9692 and references therein.

7. Christensen, R. L.; Drake, R. C.; Phillips, D. *J. Phys. Chem.*, **1986**, *90*, 5960.

8. Gudgin-Templeton, E. F.; Kenney-Wallace, G. A. *J. Phys. Chem.*, **1986**, *90*, 2896.

9. Gudgin-Templeton, E. F.; Kenney-Wallace, G. A. *J. Phys. Chem.*, **1986**, *90*, 5441.

10. Dutt, G. B.; Doriaswamy, S. *J. Chem. Phys.*, **1992**, *96*, 2475.

11. Rasimas, J. P.; Berglund, K. A.; Blanchard, G. J. *J. Phys. Chem.*, **1996**, *100*, 7220.

12. Spears, K. G.; Steinmetz, K. M. *J. Phys. Chem.*, **1985**, *89*, 3623.

13. Gudgin-Templeton, E. F.; Quitevis, E. L.; Kenney-Wallace, G. A. *J. Phys. Chem.*, **1985**, *89*, 3238.

14. Walsh, C. A.; Berg, M.; Narasimhan, L. R.; Fayer, M. D. *Chem. Phys. Lett.*, **1986**, *130*, 6.

15. Renn, A.; Bucher, S. E.; Meixner, A. J.; Meister, E. C.; Wild, U. P. *J. Lumin.*, **1988**, *39*, 181.

16. Renge, I. *Chem. Phys.*, **1992**, *167*, 173.

17. Zollfrank, J.; Friederich, J. *J. Phys. Chem.*, **1992**, *96*, 7889.

18. Yu, J.; Berg, M. *Chem. Phys. Lett.*, **1993**, *208*, 315.

19. Kindervater, H. W.; Deeg, F. W.; Brauchle, C. *J. Lumin.*, **1995**, *64*, 231.

20. Blanchard, G. J.; Cihal, C. A. *J. Phys. Chem.*, **1988**, *92*, 5950.

21. Root, L. J.; Stillinger, F. H. *Phys. Rev. B*, **1990**, *41*, 2348.

22. Arnaut, L. G.; Formosinho, S. J. *J. Photochem. Photobiol. A*, **1993**, *75*, 1.

23. Jiang, Y.; Hambir, S. A.; Blanchard, G. J. *Opt. Commun.*, **1993**, *99*, 216.

24. Bado, P.; Wilson, S. B.; Wilson, K. R. *Rev. Sci. Instrum.*, **1982**, *53*, 706.

25. Andor, L,; Lorincz, A.; Siemion, J.; Smith, D. D.; Rice, S. A. *Rev. Sci. Instrum.*, **1984**, *55*, 64.

26. Blanchard, G. J.; Wirth, M. J. *Anal. Chem.*, **1986**, *58*, 532.

27. Holtom, G. R. *Proc. SPIE*, **1990**, *1204*, 2.

28. DeWitt, L.; Blanchard, G. J.; LeGoff, E.; Benz, M. E.; Liao, J. H.; Kanatzidis, M. G. *J. Am. Chem. Soc.*, **1993**, *115*, 12158.

29. Matsen, F. A.; Franklin, J. L. *J. Am. Chem. Soc.*, **1950**, *72*, 3337.

30. Kreshkov, A.; Aldarova, R.; Smolova, N. T. *Zh. Fiz. Khim.*, **1969**, *43*, 2846.

31. Kolthoff, I. M.; Chantooni, M. K. *Anal. Chem.*, **1979**, *51*, 1301.

32. Formosinho, S. J.; Arnaut, L. G. *J. Photochem. Photobiol. A: Chem.*, **1993**, *75*, 1.

33. Arnaut, L. G.; Formosinho, S. J. *J. Photochem. Photobiol. A: Chem.*, **1993**, *75*, 21.

34. Pines, E.; Huppert, D.; Agmon, N. *J. Chem. Phys.*, **1988**, *88*, 5620.

35. Webb, S. P.; Philips, L. A.; Yeh, S. W.; Tolbert, L. M.; Clark, J. H. *J. Phys. Chem.*, **1986**, *90*, 5154.

36. Anthon, D. W.; Clark, J. H. *J. Phys. Chem.*, **1987**, *91*, 3530.

Chapter 4

A Study of the Fluorescence and Reorientation Dynamics of Carminic Acid in Primary Alcohols

Summary

The fluorescence lifetime and reorientation dynamics of carminic acid in primary aliphatic alcohols and water have been studied to develop an understanding of its dynamic properties. The fluorescence response exhibits a biexponential decay, which is attributed to emission from two stable conformers of carminic acid. The reorientation behavior of carminic acid depends sensitively on the chemical identity of the solvent. The dynamical response of carminic acid is predicted by the Debye-Stokes-Einstein (DSE) equation with a sticking boundary condition for water, methanol, ethanol and *n*-propanol. In the higher alcohols, carminic acid reorientation follows DSE behavior in the slip limit. These data, taken collectively, indicate that carminic acid interacts strongly with polar solvents and that the structural degrees of freedom available to this probe molecule do not affect its dynamical responses over a time scale of several nanoseconds.

4.1. Introduction

This ultimate goal of the research presented in this dissertation is development of an understanding of local organization in binary solution phase systems, especially those in which one of the constituents can self-assemble into a crystalline solid at sufficiently high concentration. The approach taken in this work to gain a molecular-scale understanding of solution phase self-assembly is to use a "tailor-made impurity" fluorescent probe molecule that incorporates in the crystalline matrix without altering the crystal structure to any significant extent. The transient fluorescent and motional characteristics of the appropriate probe molecule can provide information on the details of crystal formation from solution. In order to make these studies feasible, it is first necessary to understand the intrinsic properties of the probe molecule in comparatively simpler neat solvent systems. It is these initial experimental studies reported here. This work on the probe molecule carminic acid [1-4] ((7-α-D-glycopyranosyl) 9,10-dihydro-3,5,6,8-tetrahydroxy-1-methyl-9,10-dioxo-2-anthracene carboxylic acid, Figure 4.1) demonstrates that, while the fluorescence and dynamical responses of this molecule are complicated, they can be understood, and this molecule can be used to probe the elementary stages of crystallization from solution.

4.2. Experimental

Chemicals: Carminic acid was obtained from Aldrich (99% purity) and used without further purification. All *n*-alcohol solvents were obtained from Aldrich (99+% purity) and, except for methanol and ethanol, were used as received. Methanol and ethanol were dried over Mg turnings and distilled prior to use. Distilled, deionized water

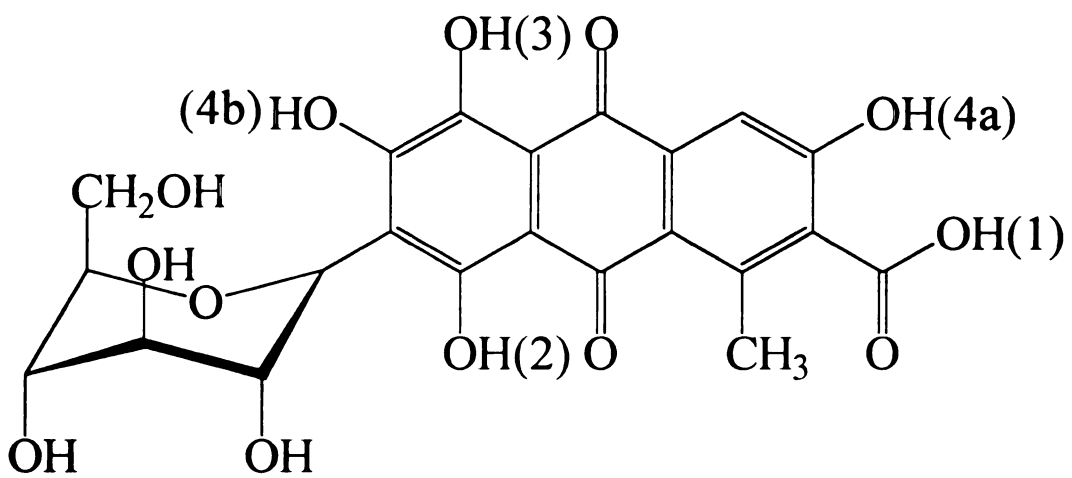

Figure 4.1. The structure of carminic acid. pK_{a1}=2.81, pK_{a2}=5.43, pK_{a3}=8.10 (pKa values from reference 4).

was used for aqueous experiments. All carminic acid solutions used for dynamical and lifetime measurements were 30 μM. This concentration was found to be sufficiently low that no aggregation or other cooperative effects could be detected. For all transient measurements, the sample cuvette was placed in a temperature-controlled heat sink (brass block) whose temperature was maintained at 300 ± 0.5 K (Neslab Endocal).

Steady state absorption and emission spectra: Absorption spectra were acquired using a Hitachi U-4000 UV-Visible absorption spectrometer operating with a 2 nm bandpass. Emission spectra were recorded on a Hitachi F-4500 fluorimeter using 10 nm excitation and emission bandpasses. The absorption and emission spectra of carminic acid in methanol are shown in Figure 4.2. These linear responses are virtually identical for all solvents we examined, save for variations in fluorescence quantum yield and fluorescence lifetime.

Time Correlated Single Photon Counting (TCSPC) Spectrometer: The spectrometer used for the lifetime and dynamical measurements of carminic acid has been described in detail before (Chapter 3, Figure 3.3). The light pulses used to excite the sample are generated with a cavity-dumped, synchronously pumped dye laser (Coherent 702-2) excited by the second harmonic of the output of a CW mode-locked Nd:YAG laser (Quantronix 416). Carminic acid was excited at 310 nm (Kiton Red, Exciton, with $LiIO_3$ SHG) or 550 nm (Pyromethine 570, Exciton), and fluorescence was collected at 575 nm using a 10 nm (FWHM) bandwidth. Fluorescence was collected at polarizations of 0^0, 54.7^0,and 90^0 with respect to the polarization of the excitation pulse. Instrument response time is ~40 ps FWHM, and the fluorescence lifetimes vary from ~75 ps to ~1

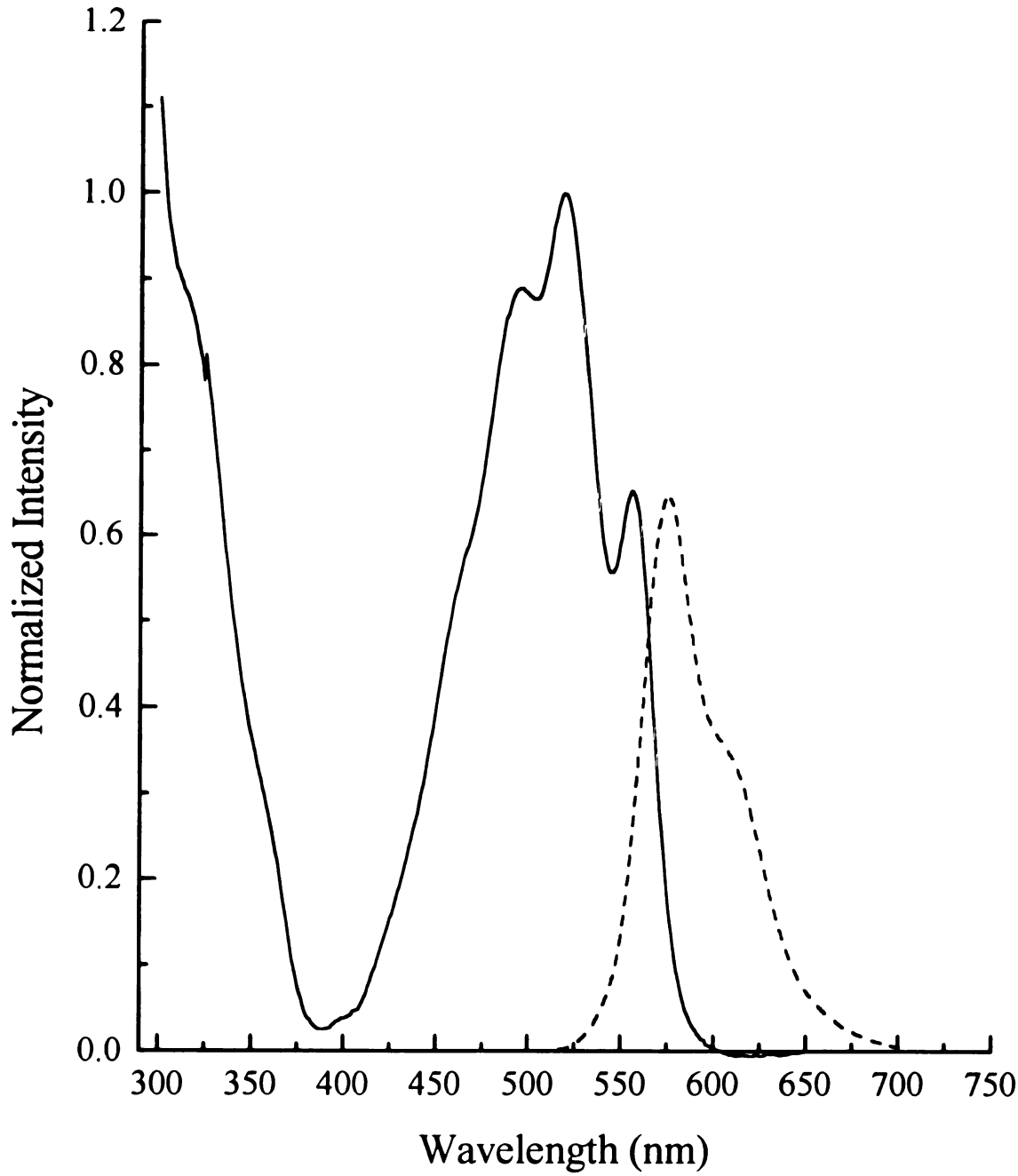

Figure 4.2. Absorption and emission spectra of carminic acid in methanol. The emission band is normalized to the leading edge absorption feature for presentation only, and is not indicative of any measurement of the fluorescence quantum yield.

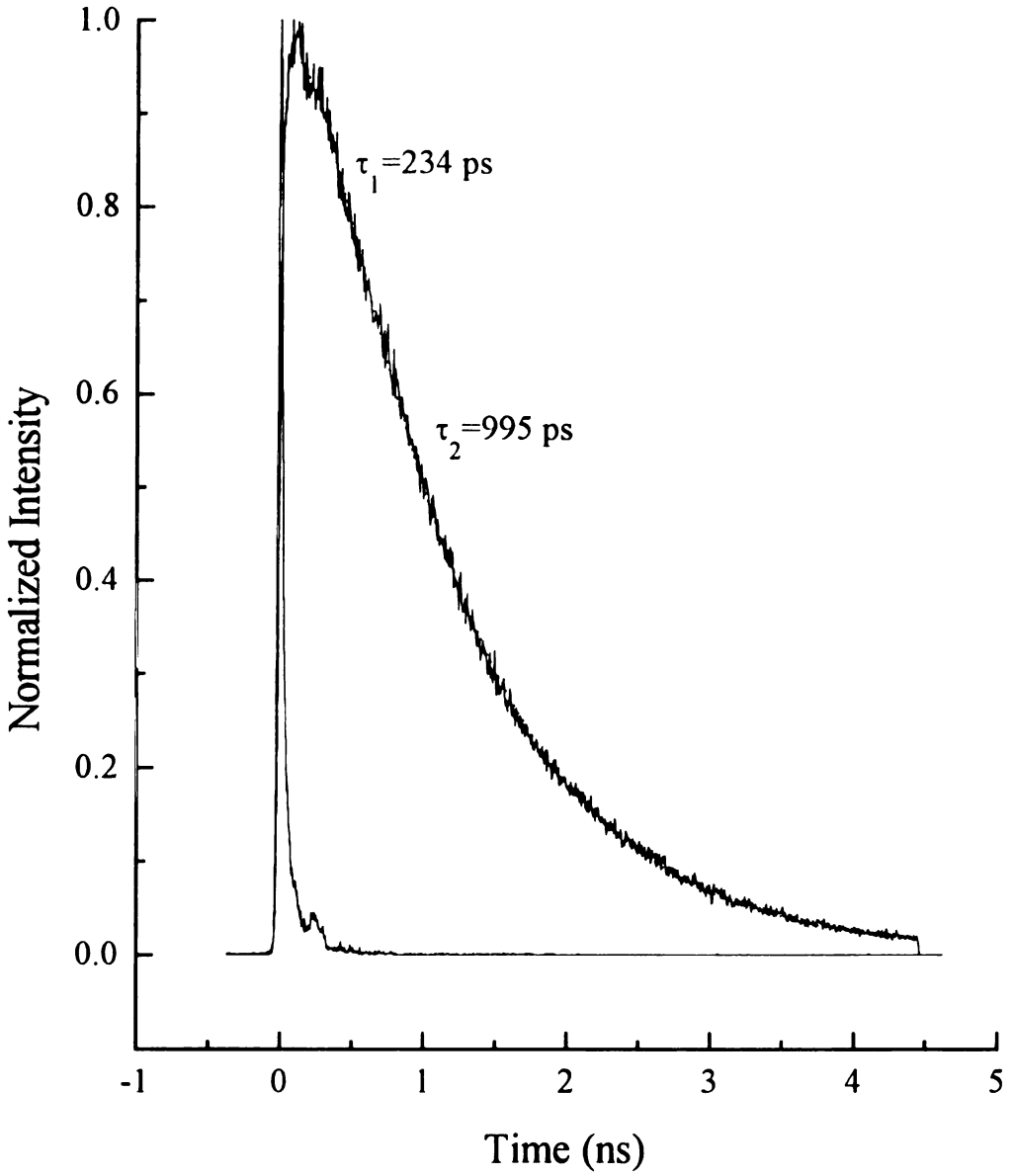

Figure 4.3. Fluorescence intensity decay for carminic acid in methanol, with the response function. The two time constants refer to regressions of the data to the function $f(t) = A_1 \exp(-t/\tau_1) + A_2 \exp(-t/\tau_2)$.

ns. A typical lifetime scan, together with the instrumental response function, is shown for carminic acid in methanol in Figure 4.3.

4.3. Results and Discussion

This work is concerned with understanding the intrinsic properties of the probe molecule carminic acid and, additionally, the dependence of its dynamical behavior on its local environment. Carminic acid was chosen for this work because of its pendant glycosyl moiety, which is ultimately expected to allow carminic acid to act as a "tailor-made impurity" probe molecule by incorporation into the elementary complexes preceding the formation of β-D-glucose crystals from aqueous solution. While carminic acid is suited to this application, there is very little experimental information available in the literature concerning its optical properties.[1-3] In order to understand the fundamental behavior of carminic acid, its fluorescence lifetime and rotational diffusion behavior in a series of *n*-alcohols and water have been studied. The results on carminic acid in water have been included to provide a frame of reference for the data presented here with respect to subsequent experiments in aqueous solutions. It is found that the fluorescence lifetime of carminic acid exhibits a double exponential decay functionality and this response is determined by steric rather than electronic or solvation effects. The reorientation behavior of carminic acid is also more complicated than simple theoretical models predict, and we discuss the reasons for this complexity in terms of largely frictional solvent-solute interactions.

Fluorescence Lifetimes: Fluorescence lifetimes of carminic acid in the *n*-alcohols methanol through *n*-butanol, *n*-hexanol, *n*-octanol, and water are shown in Table 4.1,

Table 4.1. Absorption maxima, solvent viscosities, fluorescence lifetimes, anisotropies and reorientation times for carminic acid.

Solvent	Absorption maximum (nm)	η, cP [a]	$\tau_{fl}(1)$ (ps)	$\tau_{fl}(2)$ (ps)	R(0)	τ_{OR} (ps)
MeOH	496	0.576	221 ± 25	963 ± 22	0.17 ± 0.02	244 ± 29
EtOH	496	1.032	75 ± 5	996 ± 18	0.14 ± 0.01	402 ± 20
1-PrOH	496	1.796	204 ± 16	1127 ± 46	0.15 ± 0.01	547 ± 55
1-BuOH	496	2.377	275 ± 43	1023 ± 23	0.13 ± 0.01	589 ± 37
1-HxOH	496	4.146	504 ± 17	1327 ± 28	0.11 ± 0.01	694 ± 79
1-OtOH	496	6.878	937 ± 76	2299 ± 240	0.10 ± 0.02	900 ± 72
H_2O	525	0.837 [b]	153 ± 6	---	0.10 ± 0.01	175 ± 15

[a] From Ref. 12.
[b] From Lange's Handbook of Chemistry, 13th Edition, McGraw-Hill, New York, 1985.

Solvent abbreviations: MeOH = methanol, EtOH = ethanol, 1-PrOH = 1-propanol, 1-BuOH = 1-butanol, 1-HxOH = 1-hexanol, 1-OtOH = 1-octanol

along with previously determined solvent viscosities.[5] All experimental decay times reported are best-fit values from regression of the data, using the maximum of the instrumental response function as the zero time. Because the fluorescence lifetimes are significantly longer than the instrument response function, deconvolution of the response function from the data did not alter the fitted parameters. The uncertainties reported for each value are 95% confidence intervals for at least six individual determinations.

There are two noteworthy features contained in these data. The first is that the fluorescence intensity of carminic acid decays in time with a double exponential functionality in the *n*-alcohols. Only one lifetime was recovered for carminic acid in water (153 ps). For water, the second component in the carminic acid fluorescence population decay is unresolvably fast. The second important point is that both components of this population relaxation are sensitive to the bulk viscosity of the solvent. It is necessary to focus first on the functionality of the carminic acid fluorescence decay in the *n*-alcohols. For most chromophores, spontaneous emission intensity decays as a single exponential in time. More complicated functionalities, *i.e.* multiple or non-exponential decays, suggest contributions from any of a number of photophysical processes that can complicate the interpretation of dynamical data. The steady state and dynamical fluorescence response of carminic acid have been investigated in detail to eliminate several possible causes for the observed double exponential fluorescence decay behavior. It is possible that a transient spectral shift is responsible for the apparent double exponential relaxation behavior, and this possibility has been investigated. The data presented in Figure 4.4 are time-resolved fluorescence spectra of carminic acid in 1-propanol. These data are time slices of individual time-domain decays

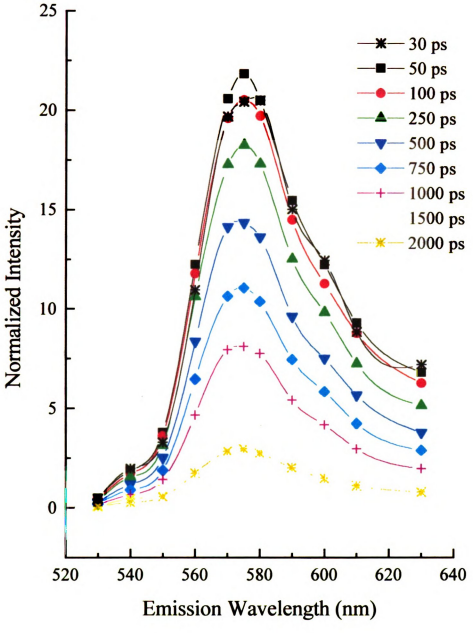

Figure 4.4. Fluorescence spectra of carminic acid in 1-propanol as a function of time after excitation. Data were taken in the time domain, at 10 nm wavelength intervals using a 10 nm FWHM detector bandpass. Intensities of the individual time were normalized to the steady state frequency domain fluorescence at 3 ns after excitation.

that have been normalized to the steady-state fluorescence spectrum at a time long after excitation (3 ns). The lifetimes for each time scan are the same to within the experimental uncertainty for all emission wavelengths we measure (530 nm to 630 nm at 10 nm intervals). Since spectral shifts in coumarins have been observed occurrring over a 50 to 100 ps time interval in 1-propanol, an analogous response for carminic acid would be expected if a spectral relaxation process dominates the observed response.[6,7] No frequency-domain spectral dynamics for carminic acid are observed, and therefore the observed double exponential fluorescence intensity decay cannot be explained on the basis of a solvent reorganization[6,7] or intramolecular relaxation[8,9] process. To check for any contributions to the fluorescence response from internal conversion ($S_2 \rightarrow S_1$ relaxation), the fluorescence lifetime of carminic acid was measured in methanol, exciting at both 310 nm and at 550 nm. Excitation at 310 nm accesses the carminic acid S_2 state and the S_1 state is excited by 550 nm light. According to Kasha's rule, excitation to a singlet state higher than S_1 will relax nonradiatively to the S_1 state. If internal conversion requires a measurable amount of time in carminic acid then any excitation energy-dependence in the dynamic fluorescence response should reflect this relaxation. Previously, such a difference has been observed for excitation of two different electronic states in the thiophene oligomer 3',4'-dibutyl-2,2',5',2"-terthiophene,[10] however in carminic acid identical fluorescence relaxation times are observed for excitation at 310 nm and 550 nm. Thus, internal conversion from S_2 to S_1 does not account for the observed double exponential fluorescence intensity decay observed experimentally.

With the most likely explanations for the observed fluorescence intensity decay functionality eliminated, the effect of molecular structural rotational freedom on the

carminic acid fluorescence response is considered. In Chapter 2 the isomerization barrier for rotation of the glycosyl group about its tethering bond to the chromophore[11] was described. Because the isomerization barrier between these two conformers is large (~90 kcal/mol), it is expected that a contribution from each conformer should be observed, if they are distinguishable. In other words, because of the large isomerization barrier, the two conformers are essentially "trapped" for the duration of the lifetime measurements. It is also worth consideration that the different components of the fluorescence population decay arise from carminic acid molecules protonated to different extents. Because the first pK_a of carminic acid is small (pK_{a1} = 2.8), we can expect a contribution from both the fully protonated and the monodeprotonated forms of carminic acid. If multiple forms existed in alcohol solution, however, it would be observed that the fractional contribution from each decay would vary with the wavelength of observation because deprotonation of carminic acid causes a significant change in the $S_0 \leftrightarrow S_1$ transition energy.[11] This is not observed experimentally. In addition, the reorientation dynamics of the two species would be different because the protonated form of carminic acid is neutral and the monodeprotonated form is charged. Only a single component is observed in all of the carminic acid rotational diffusion measurements (*vide infra*). It is noted, however, that in water, the majority of carminic acid (~98%) is in the monodeprotonated form (H_3CA^-) whereas for the *n*-alcohols dissociation is significantly less important due to the small autoprotolysis constants characteristic of this family of solvents. The observation of a single exponential decay for carminic acid in water could be accounted for by the fact that, in water, emission from a different species is detected.

Both of the decays seen in the fluorescence lifetime data exhibit a solvent viscosity dependence, as seen in Figure 4.5. Both the fast and slow lifetimes increase with increasing solvent viscosity, except in methanol. It is believed that the origin of this viscosity dependence lies in the ability of the chromophore to maintain a rigid, close to planar structure.[12] There is significant rotational freedom available the glycosyl moiety with respect to the chromophore. While the isomerization barrier is large between the two conformers, there remains ~30 degrees of rotational freedom available to the sugar group. Despite the fact that the chromophore is energetically decoupled from the glycosyl group, both of these functionalities contain permanent dipole moments. It is well established that an oscillatory dipole moment in close proximity to a chromophore can modulate the relaxation pathways available to the chromophore significantly.[13-16] For carminic acid, the motional freedom of the glycosyl moiety with respect to the chromophore will be determined to a significant extent by the viscosity of its immediate environment. Thus the ability of the glycosyl moiety to provide a nonradiative relaxation pathway to the chromophore is decreased in high viscosity solvents and the measured lifetime is increased. In addition, fast lifetime components of 221 ± 25 and 75 ± 5 ps for methanol and ethanol, respectively, are noted. These data do not follow a smooth viscosity-dependent trend, as do the data for other alcohols. The cause of these apparent anomalies with respect to the overall increase in lifetime with increasing solvent viscosity is not clear based on the information at hand, but a possibile explanation is offered. It is possible that the ethanol used contained a small amount of adventitious water, which would cause a decrease in solvent viscosity and a subsequent decrease in lifetime. The ethanol lifetime, however, is shorter than observed for water. Based on the previous

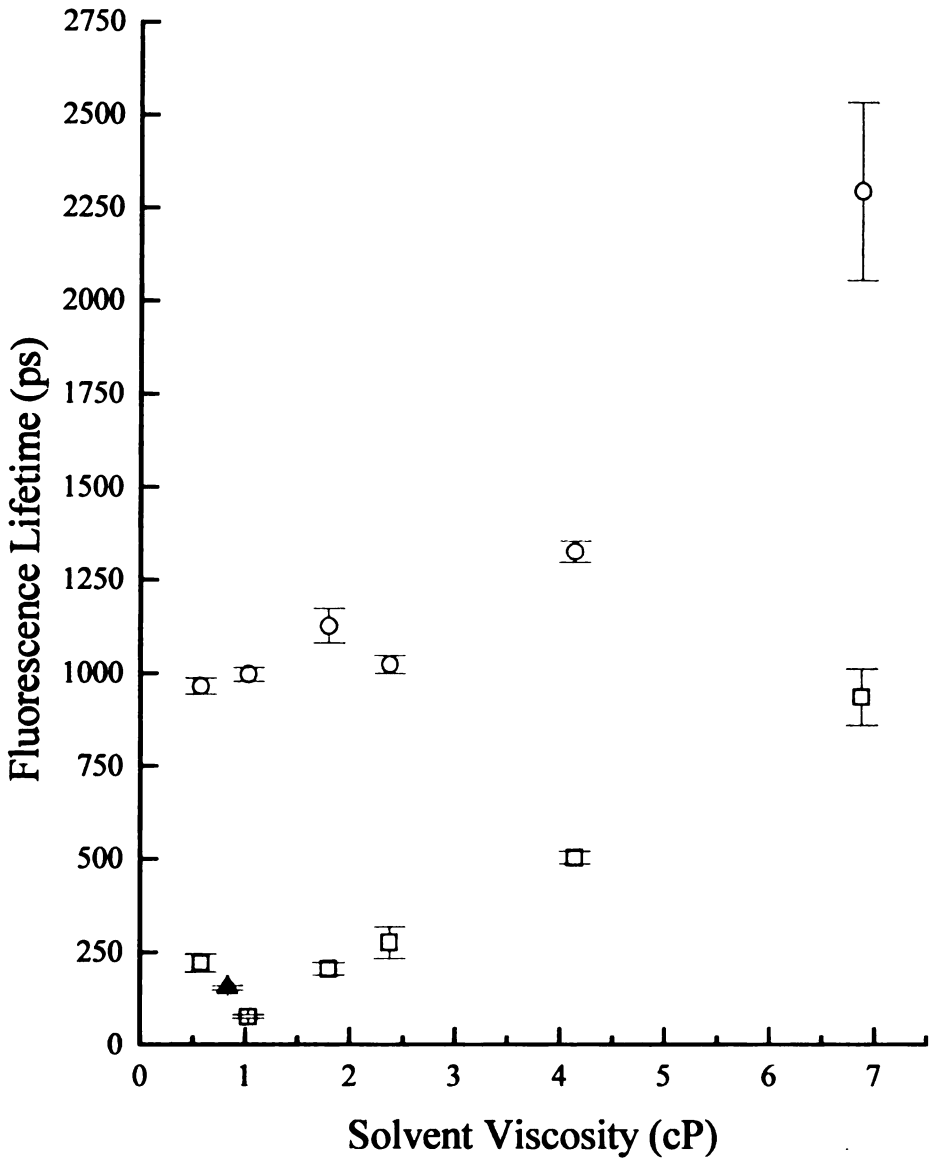

Figure 4.5. Solvent bulk viscosity dependence of fluorescence lifetime for carminic acid.

discussion of different forms of carminic acid being present in equilibrium, it is possible that this is an observation of lifetimes due to emission from two forms in a complicated equilibrium. The autoprotolysis constants for these solvents ($K_{a,\ water} = 1 \times 10^{-14}$, $K_{a,\ MeOH} = 2 \times 10^{-17}$, $K_{a,\ EtOH} = 8 \times 10^{-20}$)[17] follow a smooth trend, however, arguing against such an affect.

Rotational Diffusion Measurements: The (S_1) reorientation times of carminic acid in the *n*-alcohols and water are reported in Table 4.1. Fluorescence intensity decays were collected at polarizations of 0° ($I_{\parallel}(t)$) and 90° ($I_{\perp}(t)$) relative to the (vertical) exciting laser polarization. These data were used to generate the induced orientational anisotropy function, R(t), according to Equation 4.1,

$$R(t) = \frac{I_{\parallel}(t) - I_{\perp}(t)}{I_{\parallel}(t) + 2I_{\perp}(t)} \qquad [4.1]$$

For all measurements, R(t) decayed as a single exponential. No nonexponential or multiple exponential behavior could be resolved. The reported zero-time anisotropy values are from the regression of the data for times greater than 50 ps after excitation, and the uncertainties reported for each quantity are 95% confidence intervals for six or more individual determinations.

There are a variety of ways to interpret the information contained in rotational diffusion measurements, with the method of interpretation being determined largely by the form of the experimental R(t) function. In principle, the R(t) function can contain up to five exponential decays, depending on the orientation(s) of the excited and emitting transition dipole moments, and the shape of the volume swept out by the rotating probe molecule.[18,19] For the comparatively small number of cases where more than one

exponential decay time constant can be extracted from experimental R(t) data, it is possible to obtain direct information on the shape of the volume swept out by the probe molecule due to its rotor shape.[20] Multiple exponential decays are seen in R(t) in only a limited number of cases, however, and the most common form of R(t) is that of a single exponential decay, as reported here for carminic acid. There are essentially two quantities that can be extracted from the experimental single exponential R(t) data. These are the relative angle of the excited and emitting transition moments, (R(0)) and the time constant of the decay of R(t), τ_{OR}. The information content of R(0) is not considered in this work because, for carminic acid, R(0) is essentially solvent-independent and thus little information on intermolecular interactions is available from this quantity. In order to obtain information on the rotor shape of the reorienting molecule, more than two parameters are required. If these are not available, one is left to approximate the effective rotor shape of the probe molecule based on its structure. The rotational diffusion behavior of many molecules in many solvents has been approximated well (usually to within a factor of two) using the modified Debye-Stokes-Einstein equation.[5,21-35]

$$\tau_{OR} = \frac{\eta V f}{kTS} \qquad [4.2]$$

where τ_{OR} is the probe molecule orientational relaxation time, η is the solvent bulk viscosity, V is the probe molecule hydrodynamic volume, *S* is a shape factor that corrects for the nonspherical shape of the probe molecule, calculated from Perrin's equations[36] to be 0.727 for carminic acid based on the min/max axial ratio $\rho = 0.42$ (*vide infra*), *k* is the Boltzmann constant, and T is the temperature. The friction coefficient, *f*, is equal to 1

for the "sticking" boundary condition and, for the slipping boundary condition, f varies between 0 and 1, depending on the effective ellipsoidal shape of the reorienting molecule.[18,37] It should be noted that the calculation of S requires the assumption of an effective rotor shape. For this work, carminic acid has been modeled as a prolate ellipsoid based on its molecular structure. A point of ambiguity common to interpreting reorientation measurements of large, labile probe molecules lies in the determination of their molecular volumes. The molecular volume of carminic acid is determined by the method of van der Waals increments[38] to be 366 Å^3, but this calculation does not explicitly account for the additional void volume which must be accounted for because of the non-planarity of the glycosyl moiety with respect to the chromophore. Previous calculations predicted that the angle between the glycosyl group and the chromophore is ~55°, so this additional volume is significant. Molecular models show that dimensions of ~15Å x ~15Å x ~6.2Å carminic acid are appropriate, suggesting the volume for the ellipsoid of rotation (730 Å^3) is significantly larger than predicted by the method of van der Waals increments. It is recognized that there are a variety of methods available to estimate molecular volume, and that each means has its advantages and disadvantages. Experience indicates that the method of van der Waals increments predicts the volume of rigid probe molecules reasonably well for non-polar solvents, and somewhat less well for polar solvents. This method does not predict the hydrodynamic volumes of labile molecules as well because of its inability to account for any functionally excluded volume that arises from conformational variation of the probe molecule. Despite the limitation in the ability to determine molecular volumes accurately, the modified DSE model predicts a linear relationship between solvent viscosity and measured reorientation times. The

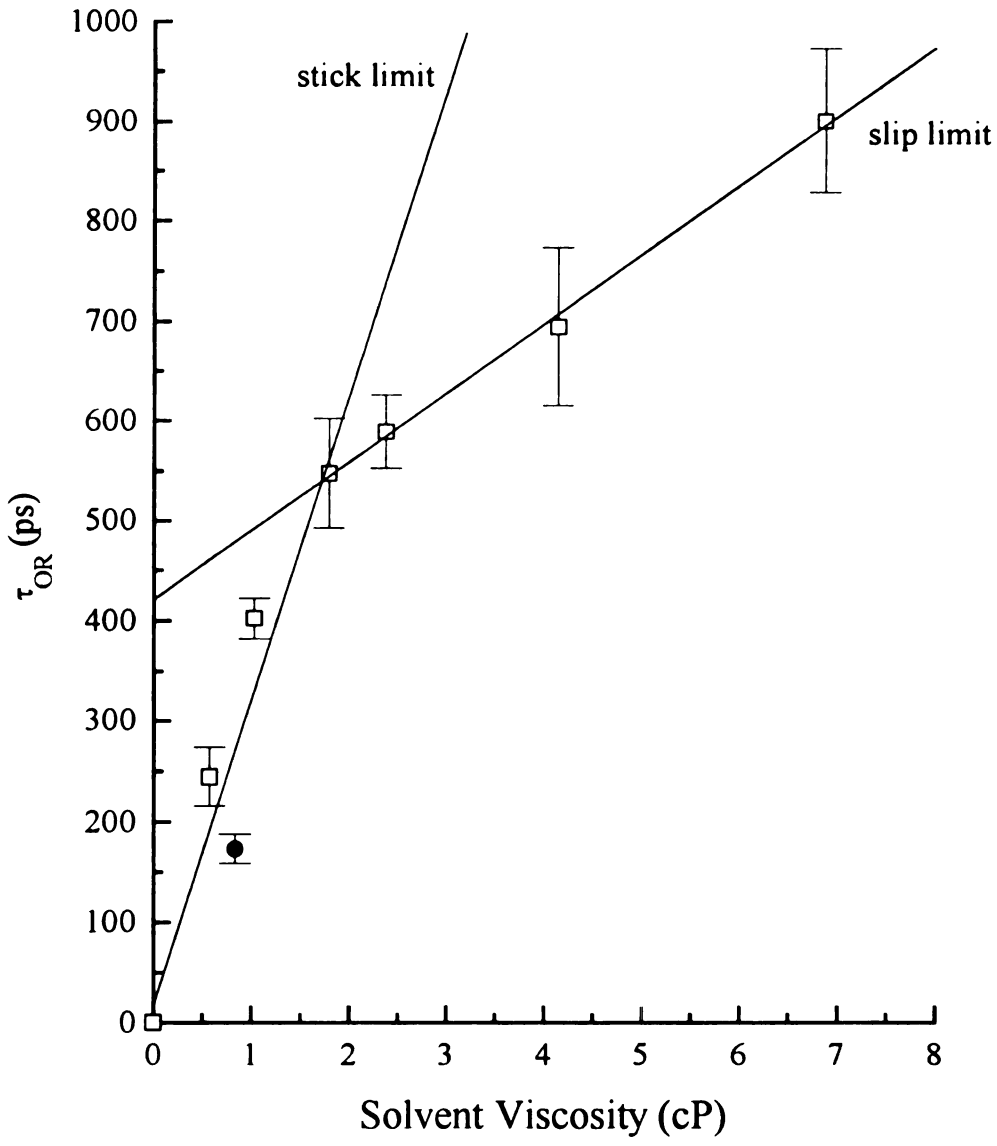

Figure 4.6. Solvent bulk viscosity dependence of the reorientation time, τ_{OR}, for carminic in water (●) and the *n*-alcohols (□). The solid lines indicate the best fit lines for the data points. See text for a discussion of these data.

data presented in Figure 4.6 for rotational diffusion of carminic acid in the *n*-alcohols and water demonstrate that the relationship between reorientation time and solvent bulk viscosity is curvilinear for the chemical systems we report here. It is clearly not physically reasonable to model these data in the context of a solvent-dependent change in the volume of the carminic acid molecule, and any contribution to the reorientation data from dielectric friction would scale monotonically with increasing alcohol aliphatic chain length.[39-42] In order to understand these data, it is necessary to consider the boundary condition for the solvent-solute interaction to be dependent on the identity of the solvent. There is ample precedent in the literature for changes in this boundary condition as a function of solvent identity.[20,43,44] Two distinct linear regions can be identified in the viscosity-dependence of the carminic acid reorientation times. The first region, for the solvents water, methanol, ethanol and 1-propanol, exhibits a linear viscosity-reorientation time relationship. For the solvents 1-butanol, 1-hexanol, and 1-octanol, the viscosity-reorientation time relationship is also linear, but with a significantly smaller slope. The change of slope is accounted for in the τ_{OR} - η dependence in the context of a change in the frictional boundary condition for the solvent-solute interactions. The slope of the linear relationship between reorientation time and viscosity is related to the effective volume of the probe molecule,

$$\frac{\tau_{OR}}{\eta} = \frac{V_{eff}}{kT}$$
$$V_{eff} = V_{vdW} \cdot f \cdot \frac{1}{S} \qquad [4.3]$$

From the estimate of V_{vdW} = 730 Å^3, and a shape factor S = 0.727, a stick-limit (f=1) V_{eff} = 1237 Å^3 is calculated. The experimental data yield V_{eff} = 1257 ± 113 Å^3 for carminic

acid reorientation in water, methanol, ethanol and 1-propanol. τ_{OR} for carminic acid in water does not follow exactly the trend seen in the alcohols. As discussed above, in water carminic acid exists primarily in its monodeprotonated form (-1 charge) while for the alcohols, the dominant form is the neutral, fully protonated molecule. The reorientation dynamics of carminic acid appear to be affected to only a modest extent by the presence of the charge. In the slip limit, where f = 0.294,[18] a V_{eff} = 364 Å^3 is calculated, and experimentally V_{eff} = 286 ± 20 Å^3 is measured for carminic acid in 1-butanol, 1-hexanol and 1-octanol. The predictions of the modified DSE model are considered to be in good agreement with the experimental data. This change in the frictional interaction between carminic acid and the surrounding solvent is an expected result for a probe molecule that can interact strongly with the surrounding solvent. Because of the number of polar functionalities on the carminic acid molecule it is very likely that hydrogen bonding between the solvent and the solute is significant. The solvent molecules in closest proximity to the carminic acid molecule will likely be oriented predominantly with their hydroxyl functionalities toward the probe molecule and their aliphatic groups oriented away from the molecule, toward the bulk solvent. For small polar solvent molecules, this "aliphatic screening" of the probe molecule will not be as important as it will be for the larger solvents. As the solvent size increases, the solvent-solute complex will thus appear less polar to the bulk solvent, and a more slip-like boundary condition is to be expected. This argument does not necessarily imply direct solvent attachment to the solute,[45,46] but rather a bias in the average orientation of the solvent molecules surrounding the solute.

4.4. Conclusions

The transient fluorescence and reorientation responses of the probe molecule carminic acid in water and a series of primary aliphatic alcohols have been examined. The fluorescence lifetime data indicate that, despite the structural degrees of freedom available to the pendant glycosyl moiety, the population relaxation dynamics of the chromophore can be interpreted in the context of two distinct conformers. It has been demonstrated that the double exponential decay of the fluorescence lifetime response is not consistent with a transient spectral shift, and is not accounted for by internal conversion. The rotational diffusion data for carminic acid in these same solvents show that, as the size of the solvent molecule increases, the frictional interaction(s) between carminic acid and its surroundings appear to decrease. This change in interaction between the probe molecule and the surrounding solvent is intrepreted in the context of strong intermolecular interactions. These data suggest collectively that carminic acid will be a useful and sensitive "tailor-made impurity" probe of solution phase self-assembly effects in glucose. Those experiments are presented in Chapter 5.

4.5. Literature Cited

1. Kirkbright, G. F.; West, T. S.; Woodward, C. *Talanta*, **1966**, *13*, 1637.

2. Jorgensen, K.; Skibsted, L. H. *Food Chemistry*, **1991**, *40*, 25.

3. Stapelfeldt, H.; Jun, H.; Skibsted, L. H. *Food Chemistry*, **1993**, *48*, 1.

4. Schwing-Weill, M. J.; Weschler, S. *Analusis*, **1986**, *14*, 290.

5. Blanchard, G. J. *J. Phys. Chem.*, **1988**, *92*, 6303.

6. Maroncelli, M; Fleming, G. R. *J. Chem. Phys.*, **1987**, *86*, 6221.

7. Jarzeba, W.; Walker, G. C.; Johnson, A. E.; Barbara, P. F. *Chem. Phys.*; **1991**, *152*, 57.

8. Blanchard, G. J. *J. Chem. Phys.*, **1991**, *95*, 6317.

9. Jiang, Y.; McCarthy, P. K.; Blanchard, G. J. *Chem. Phys.*, **1994**, *183*, 249.

10. DeWitt, L.; Blanchard, G. J.; LeGoff, E.; Benz, M. E.; Liao, J. H.; Kanatzidis, M. G. *J. Am. Chem. Soc.*, **1993**, *115*, 12158.

11. Rasimas, J. P., Blanchard, G. J. *J. Phys. Chem.*, **1994**, *98*, 12949.

12. Berlman, I. B. Handbook of Fluorescence Spectra of Aromatic Molecules, Academic, New York, 1971, p. 50.

13. Blanchard, G. J.; Heritage, J. P.; Baker, G. L.; Etemad, S. *Chem. Phys. Lett.*, **1989**, *158*, 329.

14. Nowak, M. J.; Blanchard, G. J.; Baker, G. L.; Etemad, S.; Soos, Z. G. *Phys. Rev. B*, **1990**, *41*, 7933.

15. Hambir, S. A.; Yang, T.; Blanchard, G. J.; Baker, G. L. *Chem. Phys. Lett.*, **1993**, *201*, 521.

16. Hambir, S. A.; Blanchard, G. J.; Baker, G. L. *Appl. Spectroscopy*, **1995**, *49*, 374.

17. Skoog, D. A., West, D. M. Fundamentals of Analytical Chemistry, Holt, Rinehart, and Winston, New York, **1976**, p. 257.

18. Hu, C-M.; Zwanzig, R. *J. Chem. Phys.*, **1974**, *60*, 4353.

19. Chuang, T. J.; Eisenthal, K. B. *J. Chem. Phys.*, **1972**, *57*, 5094.

20. Blanchard, G. J. *J. Chem. Phys.*, **1987**, *87*, 6802.

21. Porter, G., Sadkowski, P. J., Tredwell, C. J. *Chem. Phys. Lett.*, **1977**, *49*, 416.

22. Spears, K. G., Cramer, L. E. *Chem. Phys.*, **1978**, *30*, 1.

23. Millar, D. P., Shah, R., Zewail, A. H. *Chem. Phys. Lett.*, **1979**, *66*, 435.

24. Waldeck, D. H., Cross, A. J., Jr., McDonald, D. B., Fleming, G. R. *J. Chem. Phys.*, **1981**, *74*, 3381.

25. von Jena, A., Lessing, H. E. *Chem. Phys. Lett.*, **1981**, *78*, 187.

26. Spears, K. G., Steinmetz, K. M. *J. Phys. Chem.*, **1985**, *89*, 3623.

27. Templeton, E. F. G., Quitevis, E. L., Kenney-Wallace, G. A. *J. Phys. Chem.*, **1985**, *89*, 3238.

28. Debye, P. Polar Molecules, Chemical Catalog Co.: New York, 1929, p. 84.

29. Justus, B. L., Cox, A. J., Butz, K. W., Scott, G. W. *Chem. Phys.*, **1988**, *119*, 125.

30. Blanchard, G. J. *J. Phys. Chem.*, **1989**, *93*, 4315.

31. Quitevis, E. L., Horng, M-L. *J. Phys. Chem.*, **1990**, *94*, 5684.

32. Dutt, G. B., Doriswamy, S., Periasamy, N., Venkataraman, B. *J. Chem. Phys.*, **1990**, *93*, 8498.

33. Blanchard, G. J. *J. Phys. Chem.*, **1991**, *95*, 5293.

34. Alavi, D. S., Waldeck, D. H. *J. Phys. Chem.*, **1991**, *95*, 4848.

35. Vauthey, E. *Chem. Phys. Lett.*, **1993**, *216*, 530.

36. Perrin, F. *J. Phys. Radium*, **1934**, *5*, 497.

37. Youngren, G. K.; Acrivos, A. *J. Chem. Phys.*, **1975**, *63*, 3846.

38. Edward, J. T. *J. Chem. Educ.*, **1970**, *47*, 261.

39. Nee, T. W.; Zwanzig, R. *J. Chem. Phys.*, **1970**, *52*, 6353.

40. Madden, P.; Kivelson, D. *J. Phys. Chem.*, **1982**, *86*, 4244.

41. Kivelson, D.; Spears, K. G. *J. Phys. Chem.*, **1985**, *89*, 1999.

42. Philips, L. A.; Webb, S. P.; Clark, J. H. *J. Chem. Phys.*, **1985**, *83*, 5810.

43. Blanchard, G. J.; Wirth, M. J. *J. Phys. Chem.*, **1986**, *90*, 2521.

44. Jiang, Y.; Blanchard, G. J. *J. Phys. Chem.*, **1994**, *98*, 6436.

45. Blanchard, G. J. *Anal. Chem.*, **1989**, *61*, 2394.

46. Moog, R. S.; Bankert, D. L.; Maroncelli, M. *J. Phys. Chem.*, **1993**, *97*, 1496.

Chapter 5

A Molecular "Lock-and-Key" Approach to Detecting Solution Phase Self-Assembly. A Fluorescence and Absorption Study of Carminic Acid in Aqueous Glucose Solutions

Summary

A novel approach to the study of complex ternary systems is introduced, where a fluorescent chromophore contains a functionality that incorporates into pre-crystalline aggregates in concentrated solutions. The feasibility of this approach is demonstrated using carminic acid, a fluorescent molecule possessing a pendant glycosyl moiety, in aqueous glucose solutions. The steady state absorption and emission responses of carminic acid as well as its picosecond dynamical response are reported. These data, taken collectively, show that saturated glucose solutions exhibit anomalous molecular-scale organization, and that the persistence time of this organization is significantly less than a nanosecond. These results indicate that kinetic contributions to crystallization are expected to play an important, sometimes dominant role in this technologically important process. The presence of labile protons on the chromophore is also a potential factor in mediating aggregate formation in these systems.

5.1. Introduction

Many chemical reactions and large scale purifications are performed using compounds in solution. This is because properties of the solution such as polarity and temperature can be adjusted with comparative ease, and solution phase reactions provide a nominally homogeneous reaction medium. In addition to synthesis, the purification of many industrially important compounds by crystallization from solution is well established. Despite the obvious utility and widespread application of solution phase chemistry, surprisingly little is understood about the interactions between molecules that lead to crystallization from solution. Increased understanding of solution phase phenomena will provide the background for direct measurement of species leading to nucleation and growth. A reason for this lack of information is that there is no stable "structure" in solution that is amenable to study by techniques well suited to the examination of solid state organization. Thus, the examination of organization in liquids has been done largely by inference, and in only a limited number of cases are there data that reveal the presence of short range organization in solution.[1-8]

Because the interactions between molecules in solution fluctuate so rapidly, ultrafast laser technologies have found significant application to this field. For this type of measurement, the probe molecule is present in solution at a low concentration, and the information gathered from these measurements is related in some manner to the environment formed by the solvent around the solute. Interactions between the probe molecule and its surroundings are typically different than those experienced by a given solvent molecule in the neat medium. For this type of experiment, a short pulse of light

is used to initiate some condition at a well defined point in time, and an optical response of the probe molecule is then interrogated. These measurements introduce a perturbation to the equilibrium condition of the system and the kinetic information on how the system returns to its initial state is used to characterize the solution in some way. Examples of this approach are rotational diffusion,[9-19] transient spectral shift[20-29] and vibrational population relaxation measurements.[30-40] Rotational diffusion and vibrational population relaxation are mediated largely by intermolecular events such as dielectric and viscous frictional interactions and polar coupling effects. Transient spectral relaxation measurements rely on the mediation of intramolecular electronic or vibrational relaxation by intermolecular interactions to gain information about the solvent medium.[41,42] These experiments are valuable and can provide a great deal of insight into solvation processes provided the intrinsic intramolecular relaxation behavior of the probe molecule is well understood. Separation of the intramolecular probe molecule population relaxation dynamics from those determined by the solvent is not always straightforward. Despite these limitations, a wide variety of ultrafast laser spectroscopic measurements have provided significant insight into intermolecular interactions in solution.

The majority of studies on fundamental solvent-solute interactions have been performed in binary systems, where only the solvent and a small amount of the probe molecule are present. The rationale behind this approach is that a necessary prerequisite to understanding more complex processes is to first know the properties of the constituents individually. This approach does not take advantage of a great deal of widely applied chemistry where local organization occurs spontaneously. For many

chemical systems, where two components are present in significant amounts, "self-assembly" can occur, and it is this process that is the focus of this paper.

This work uses ternary solutions, where two constituents, one which is capable of crystallizing from solution, are present in significant amounts. The third component, the probe molecule, is used to detect and characterize organization within the quasi two-component system. There have been several other examinations of two-solvent systems using fluorescent probe molecules. Either the systems under examination did not exhibit a phase separation or, if they did, the location of the probe molecule in the system was not well defined.[43-50] The unique aspect of the approach reported here is that the probe molecule contains a functionality that allows its incorporation into the crystallizing system. It has been determined that this is the case by deliberately crystallizing glucose in the presence of small quantities (5 ppm) of the glycosylated chromophore and verifying that (colored) crystalline material is obtained. The information provided by using this "lock-and-key" approach[51] to probe molecule interactions with self-assembling systems offers insight into the local environment(s) formed by these complex solutions. In order to extract information from these measurements, an understanding of the optical response of the carminic acid chromophore must be achieved. With this understanding, the dynamical lifetime and reorientation data on carminic acid can be discussed in the context of local organization in aqueous glucose solutions. This work shows that, while incorporation of carminic acid into the pre-crystalline matrix does occur, the lifetimes of these aggregates are significantly less than the measured reorientation times. This finding implies that, prior to crystallization, these solutions are better treated as highly

dynamic, exchange mediated systems and not as micro-heterogeneous system where constituents can be treated as distinct moieties.

5.2. Experimental

Chemicals: Carminic acid was obtained from Aldrich (99% purity) and used without further purification. The structure of carminic acid, along with the relevant pK_a assignments has been shown in Figure 4.1. All solutions were prepared using triple-distilled, deionized water. Aqueous buffer solutions were prepared in a series of pH values ranging from pH 2.0 to pH 10.0. Solution pH was confirmed using a pH electrode (Orion Research Inc.). The ionic strength was made constant for all buffer solutions ($\mu = 0.50$). Anhydrous β-D-glucose was obtained from Fluka and used without further purification. All solutions were prepared at a carminic acid concentration of $1x10^{-5}$ M (5 ppm). It was found that this concentration is sufficiently low that no dye aggregation or other cooperative effects could be detected. Glucose solutions were prepared by weighing appropriate amounts of glucose and water, followed by heating to 70°C to ensure complete dissolution. For all transient fluorescence measurements, the sample quartz (Suprasil) cuvette was placed in a temperature controlled heat sink (brass block) whose temperature was maintained at 298 ± 0.05 K using a temperature controlled circulator (Neslab Endocal). Samples were stirred using a Teflon stirbar and magnetic stirrer to eliminate absorption-induced thermal gradients.

Steady state absorption and emission spectra: Absorption spectra were acquired using a Hitachi U-4000 UV-Visible absorption spectrometer operating with a 2 nm bandpass. Emission spectra were recorded on a Hitachi F-4500 fluorimeter using 10 nm

excitation and emission bandpasses. 25 scans were signal averaged for each emission spectrum.

Time Correlated Single Photon Counting (TCSPC) Spectrometer: The spectrometer used for the lifetime and dynamical measurements of carminic acid has been described in detail before (Chapter 3, Figure 3.3). The light pulses used to excite the sample are generated with a cavity-dumped, synchronously pumped dye laser (Coherent 702-2) excited by the second harmonic of the output of a mode-locked CW Nd:YAG laser (Quantronix 416). Carminic acid was excited at 310 nm (Kiton Red, Exciton, with $LiIO_3$ SHG), and fluorescence was collected at both 450 nm and 575 nm using a 10 nm (FWHM) detection bandwidth. Detection was accomplished using an MCP-PMT (Hamamatsu R2809). Fluorescence was collected at polarizations of 0°, 54.7°, and 90° with respect to the polarization of the (vertical) excitation pulse to determine both fluorescence lifetimes and rotational diffusion times. The typical instrument response function is ~ 40 ps FWHM for this system and the measured fluorescence lifetimes vary from ~200 ps to ~6 ns.

5.3. Results and Discussion

The objective of this work is to understand and characterize the elementary complexes that form between glucose molecules prior to nucleation and crystal growth in aqueous glucose solutions. Ultimately, it is hoped to correlate these complexes with the driving forces for nucleation and growth. Short range intermolecular interactions are monitored in the glucose/water solutions using a "tailor-made impurity" probe molecule, carminic acid. Carminic acid contains two distinct moieties, a chromophore and a

pendant glucose group. The data presented here demonstrate that the glucose functionality of carminic acid incorporates into the glucose-water matrix and thus the optical response of the chromophore senses local organization in the pre-crystallization environment. This is ensured by testing for incorporation in the crystalline limit, where glucose accepts up to 10 ppm carminic acid while retaining the ability to form a crystalline solid. At higher carminic acid concentrations, non-crystalline glucose is formed from saturated solution. There are three basic points considered in this work. These are the steady state linear response of carminic acid in aqueous buffer and glucose solutions, its fluorescence lifetime, and its reorientation behavior dependence on glucose concentration. Because of the structural and electronic complexity of carminic acid, it has been necessary to examine its intrinsic electronic response prior to using it as a probe of intermolecular organization (Chapter 2).[52] It is has been found here that the steady state linear response of carminic acid in glucose solutions changes with glucose concentration. These changes are attributed to the acid/base equilibria of the labile protons of the chromophore. Previous reports on carminic acid have indicated that it is a triprotic acid,[53] but the data presented demonstrate that it is a tetraprotic acid. The ground state pK_a of the fourth proton is sufficiently high that its contribution to the linear response is weak at pH 10. The species detected are fully protonated carminic acid (H_4CA) and several deprotonated forms ($H_{4-x}CA^{-x}$, x = 1-4). A comparison of the glucose concentration dependence to that seen for carminic acid in aqueous buffers shows that the steady state optical response of this molecule can be used to determine the pH of aqueous glucose solutions. The fluorescence lifetimes at two emission wavelengths of carminic acid exhibit a double exponential decay functionality, as was

previously observed for this probe molecule in *n*-alcohols (Chapter 4).[54] The rotational diffusion behavior of carminic acid reveals a glucose concentration-dependent change in the interactions between the probe molecule and its immediate surroundings. This behavior depends sensitively on the specific form of carminic acid detected.

Steady state absorption spectroscopy of carminic acid. The steady state absorption and emission responses of carminic acid in a series of aqueous buffers and aqueous glucose solutions have been studied. The data for the aqueous buffers is discussed first because of their utility in the assignment of carminic acid absorption and emission bands. Figure 5.1 shows the calculated α-fractions[55] for carminic acid, using the pK_a data for the first three dissociable protons as reported by Schwing-Weill and Weschler.[53] Noteworthy in this figure is the fact that there are likely to be at least two forms of carminic acid in solution for any pH between ~3 and ~9. Figure 5.2 shows the absorption spectra of 10^{-5} M carminic acid solutions in a series of aqueous buffers between pH 2 and pH 10. These spectra were not collected for wavelengths shorter than 350 nm because of significant absorption by the buffer solution constituents. The position of the absorption band near 500 nm depends on the pH of the solution, as indicated by the arrow. There is an isobestic point at ~505 nm, indicating that the spectral shift is caused by a pH-dependent shift in equilibrium between two carminic acid conjugate acid/base species. As the solution pH increases, the intensity of the band at 490 nm decreases and the intensity of the band at 540 nm increases correspondingly. At pH 2, the dominant form of carminic acid is the fully protonated species (H_4CA) (see Figure 5.2), and therefore the absorption band centered at 490 nm is assigned to H_4CA. Because the specie that absorbs at ~ 540 nm is related to the H_4CA band through an

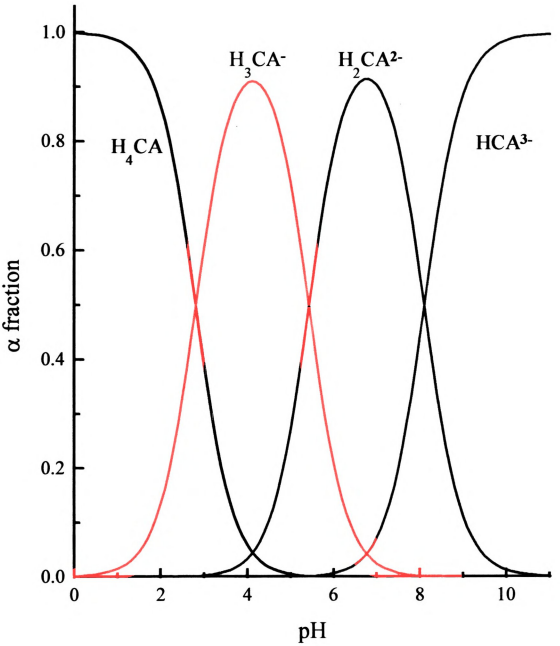

Figure 5.1. α-Fractions calculated for carminic acid (pK_a values from reference 53).

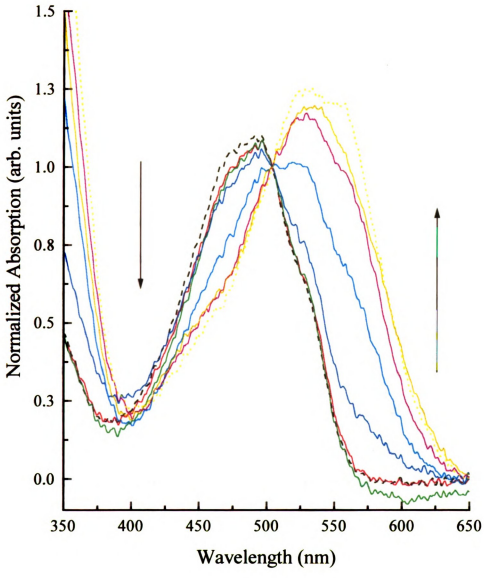

Figure 5.2. Linear absorption spectra for aqueous buffer solutions (pH 2 to pH 10) containing 10^{-5} M carminic acid. All buffers have a constant ionic strength of $\mu = 0.50$. The spectra have been normalized to the isobestic point at 505 nm.

isobestic point, it must necessarily be H_3CA^-. At pH 10, the dominant form of carminic acid is the triply deprotonated species (HCA^{3-}) (See Figure 5.1), and the 575 nm band is assigned to this form. It is noted that the HCA^{3-} band is not resolved from the H_3CA^- band, and it is almost certain that a contribution from H_2CA^{2-} is also present in the 550-575 nm region. Based on these data, it is clear that the ratio of the absorbance at 490 nm to that at 540 nm can be used to detect the pH of the medium surrounding the carminic acid chromophore.

The linear response of carminic acid in aqueous glucose solutions can be understood using the information gained from the aqueous buffer solutions. Figure 5.3 shows the absorption spectra for 10^{-5} M carminic acid in aqueous glucose solutions. The spectra were normalized to the isobestic point at 515 nm. There are three isobestic points apparent in these data; at 330 nm, 375 nm and 515 nm. Using the data obtained in aqueous buffers as a guide, we assign the absorption band centered at 490 nm to H_4CA. The band centered at 540 nm is due to H_3CA^- because these species are coupled through the isobestic point at 515 nm. As discussed above, the absorption shoulder at ~ 570 nm is due to HCA^{3-}. The absorption band centered at 350 nm must be due to H_3CA^- based on the isobestic point at 375 nm. It is likely, but not definite, that the absorption band centered at 325 nm is associated with H_2CA^{2-}, and that the band at 275 nm has at least some contribution from all of the carminic acid forms. Because the data for absorbance in aqueous buffers cut off at 350 nm, it was not possible to assign the specie(s) that absorb(s) at 275 nm.

Figure 5.4 shows an expanded region of the data from Figure 5.3. A comparison of these data to those acquired in aqueous buffers (Figure 5.2) reveals several

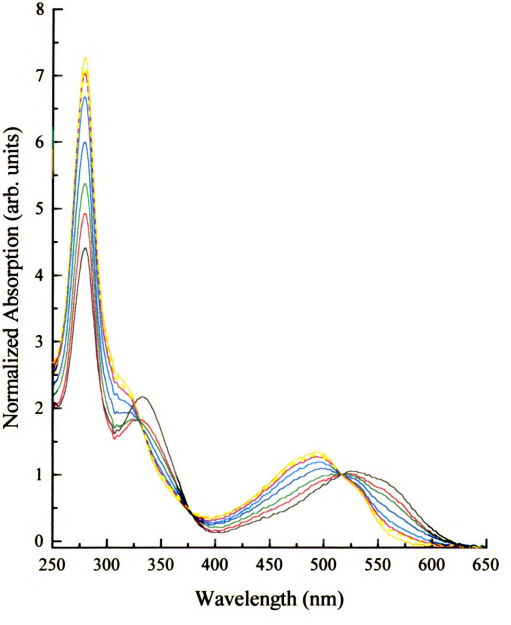

Figure 5.3. Linear absorption spectra between 250 nm and 650 nm for aqueous glucose solutions containing 10^{-5} M carminic acid. Spectra are normalized to isobestic point at 515 nm. The dashed tracing represents a saturated glucose solution.

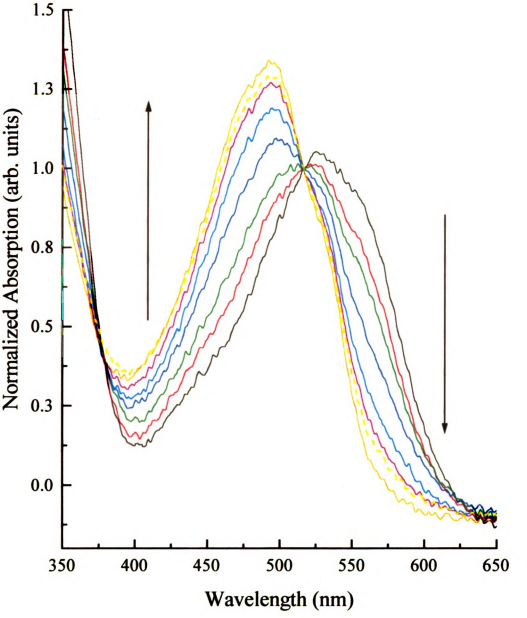

Figure 5.4. Linear absorption spectra between 350 nm and 650 nm for aqueous glucose solutions containing 10^{-5} M carminic acid. Spectra are normalized to isobestic point at 515 nm. The dashed tracing represents a saturated glucose solution. Arrows indicate the direction of peak shifts observed with increasing glucose concentrations.

similarities. As the glucose concentration increases, a blue shift of the absorption spectrum is observed, with a decrease in absorbance at 540 nm and a corresponding increase in absorbance at 490 nm. The absorption spectra observed for carminic acid in glucose and those in buffers are, however, not identical. This is not surprising given the fact that the buffer solutions have a high ionic strength (μ = 0.50) compared to that of aqueous glucose solutions ($\mu \sim 0$). Despite this difference, the absorption bands of carminic acid in glucose solutions indicate the pH of the environment in close spatial proximity to the chromophore. It is assumed that the aqueous buffers we use are homogeneous, and for these solutions the pH dependence of the carminic acid absorption response thus reflects the bulk pH of the aqueous buffer solutions. The bulk pH of aqueous glucose solutions as a function of glucose concentration are also known (Table 5.1). The pH of the glucose solutions measured using carminic acid is compared to the pH of these solutions using a bulk pH electrode. For carminic acid, the pH dependence of the absorption spectra measured using buffers (*i.e.* $A_{490}/A_{540} \propto$ pH) can be translated to the expected glucose concentration dependence by means of the relationship between bulk pH and glucose concentration (Table 5.1). The glucose concentration dependence of the carminic acid absorption response is inferred from the buffer solution absorbance data and the data in Table 5.1. Comparison of these composite data to the direct carminic acid absorption band dependence on glucose concentration yield the same result (Figure 5.5). Thus the bulk pH of glucose solutions is the same as that sensed by the carminic acid absorption spectra. This is an expected result because the time constant of the steady state absorption measurements is at least milliseconds over the relevant

Table 5.1. pH of aqueous glucose solutions at 25 °C.

% Glucose	pH
0	5.70 ± 0.01
5	6.78 ± 0.03
10	6.61 ± 0.01
15	6.15 ± 0.03
20	6.02 ± 0.01
25	5.68 ± 0.01
30	5.43 ± 0.01
35	5.33 ± 0.02
40	5.16 ± 0.01
45	5.01 ± 0.01
50	4.91 ± 0.01
55	4.73 ± 0.01
57	4.61 ± 0.01
60	4.46 ± 0.01

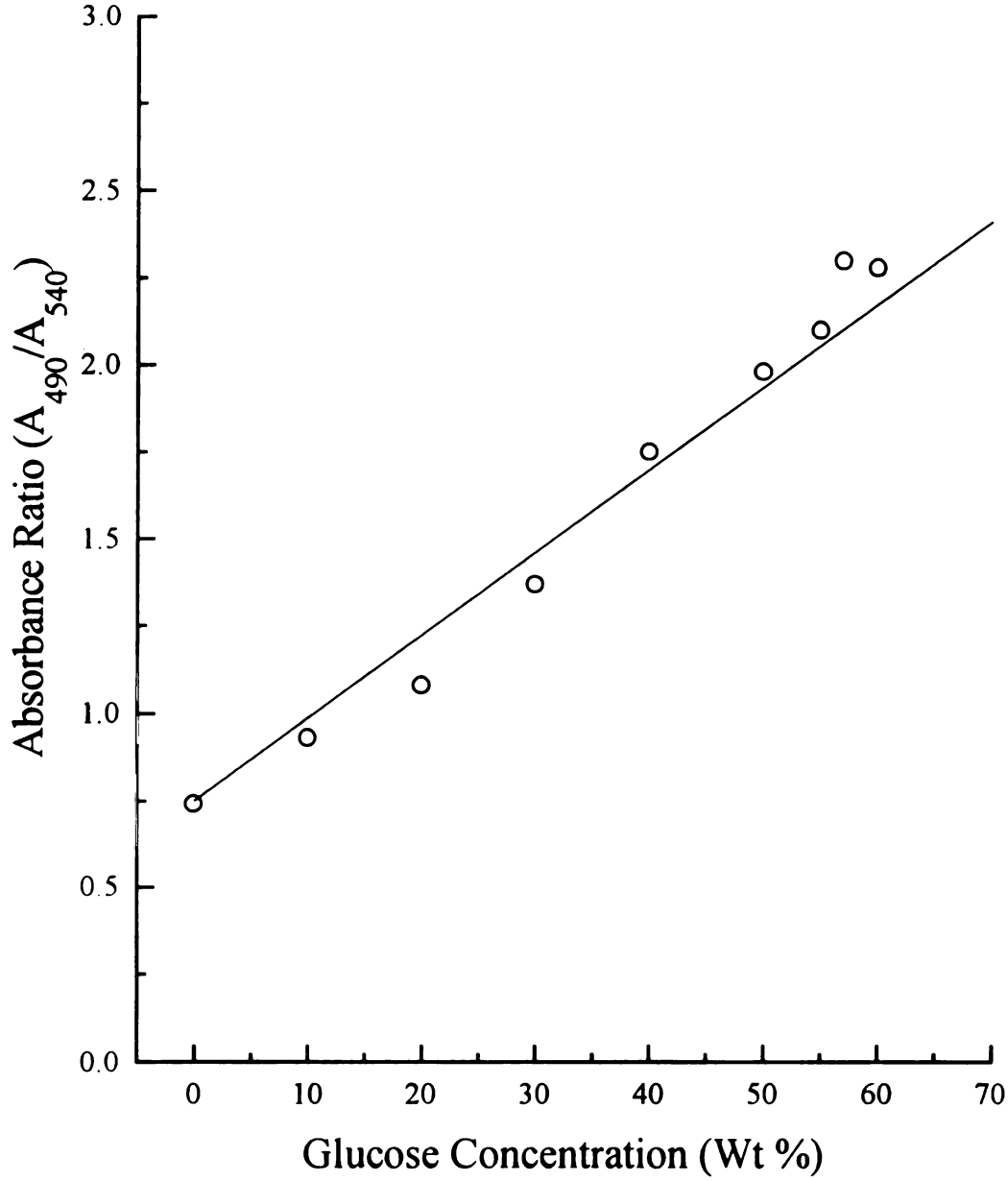

Figure 5.5. pH versus glucose concentration measured by absorbance ratio (A_{490}/A_{540}) of 5 ppm carminic acid in glucose (O) and by pH electrode (regression of calibration curve (Table 5.1) is the straight line). The points represent the absorption band intensity ratio taken from carminic acid absorption in glucose (Figure 5.4) vs. glucose concentration, and the line represents the absorption band intensity ratio taken from carminic acid absoption in buffers (Figure 5.2) vs. buffer pH that has been scaled to glucose concentration.

spectral region, whereas diffusion processes for protons in these solutions should operate over significantly less than nanoseconds.

Steady state emission spectroscopy of carminic acid. While a great deal of information can be extracted from the steady state absorption response of carminic acid, for dynamical measurements presented here, fluorescence is the property detected. It is important to consider the steady state fluorescence properties of carminic acid in order to provide a useful interpretation of the dynamical data. The steady state fluorescence spectra of carminic acid in aqueous buffer solutions between pH 2 and pH 10 are shown in Figure 5.6. These spectra were acquired using 500 nm excitation, which corresponds to excitation at the isobestic point (Figure 5.2). This emission response, in principle, contains contributions from all the carminic acid species, shifting to higher energies with increasing pH. In correspondence with the absorption data, the emission spectral shift is associated with an isoemissive point at 575 nm. At pH 2, the fluorescence maximum occurs at 590 nm, (Stokes shift ~3500 cm^{-1} for H_4CA). At pH 4, where H_3CA^- is the dominant component, the emission maximum is 560 nm, (Stokes shift of 660 cm^{-1}). At pH 8, (HCA^{3-} and H_2CA^{2-}) there is an apparent shoulder on the emission response at ~590 nm. This band intensifies at pH 10 it is thus assigned as emission from HCA^{3-}. The Stokes shift is estimated to be ~500 cm^{-1} for HCA^{3-}. The magnitude of these Stokes shifts are important because they indicate that the fully protonated form of carminic acid exhibits a large change in its permanent dipole moment on excitation, while the partially deprotonated species exhibit much smaller changes in dipole moment on excitation. The semi-empirical calculations reported earlier for carminic acid indicated no large change in dipole moment on excitation for any species (Chapter 2).[52] Such calculations are,

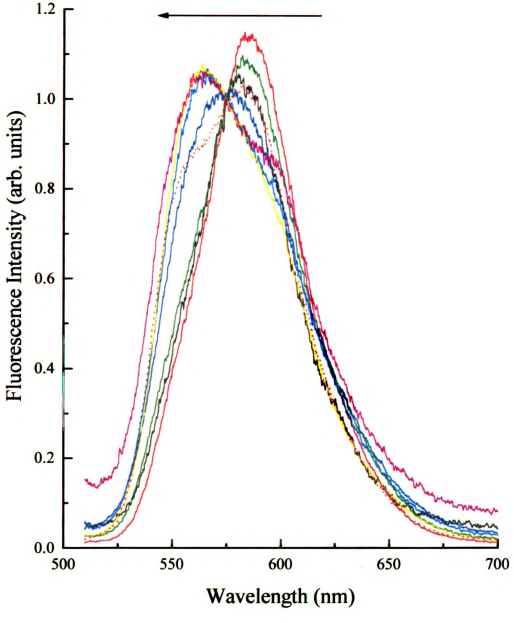

Figure 5.6. Spontaneous emission spectra for aqueous buffer solutions (pH 2 to pH 10) containing 10^{-5} M carminic acid excited at 500 nm. All buffers have a constant ionic strength of μ=0.50. Spectra were normalized to the isoemissive point at 575 nm.

however, limited by the quality of the parameterizations used and are known to account poorly for electron density distributions within charged molecules. Because of the change in dipole moment on excitation for H_4CA, a transient spectral shift may be expected,[23-29] but earlier data on carminic acid in *n*-alcohols demonstrates no such effect (Chapter 4).[54] The lifetime data reported below are not affected by fast intramolecular relaxations.[41,42]

In addition to emission from the previously reported deprotonated form of carminic acid, an additional emission feature is observed at pH $\geq$ 10. This feature, shown in Figure 5.7 and centered at 440 nm, is seen only weakly at pH 9 and is more prominent in the pH 10 buffer solution. For both of these solutions, the intensity of the 440 nm emission feature is significantly lower than that of the 590 nm band. At pH 13, however, the 440 nm band is observed to be of slightly greater intensity than the 590 nm band, indicating that the 440 nm band is associated with a carminic acid chromophore where four protons have been removed. This band is not associated with a chemical decomposition of the chromophore because the addition of excess acid to a pH 13 solution of carminic acid yields the linear response of the protonated chromophore with no additional bands. The assignment of this feature is important to the interpretation of the transient fluorescence measurements, as we discuss below. There are no previous reports on the tetraprotic nature of carminic acid, nor is the pK_a of this fourth proton equilibrium known. It is estimated *crudely* that $pK_{a4} \sim 13$, if the emission cross sections and fluorescence quantum yields for 440 nm band and the 590 nm band were the same. It is reasonable to expect that both of these suppositions are false and thus pK_{a4} may be significantly different than 13.. As with the absorption measurements, the emission

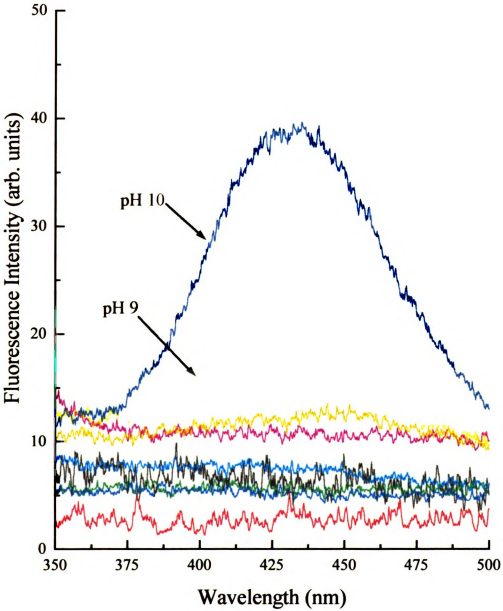

Figure 5.7. Spontaneous emission spectra for aqueous buffers solutions (pH 2 to pH 10) containing 10^{-5} M carminic acid, excited at 280 nm. All buffers have a constant ionic strength of μ=0.50.

behavior of carminic acid in aqueous glucose solutions is qualitatively similar to that seen in the buffer solutions. Figure 5.8 presents the fluorescence spectra of 10^{-5} M carminic acid in a series of aqueous glucose solutions. The band centered at 560 nm is present at low glucose concentrations, and the band at 582 nm increases with increasing glucose concentration. These data are consonant with the species assignments based on the measurements in buffered solutions, except that the fluorescence quantum yield of carminic acid varies significantly with glucose concentration, as indicated in Figure 5.8. The red shift from 564 nm to 582 nm with increasing glucose concentration indicates that pH decreases as the glucose concentration increases, in agreement with the absorption data for the same solutions.

As a comparison to the absorbance data indicating that the absorption spectra of carminic acid sense the bulk pH of the aqueous glucose solutions, the corresponding glucose concentration dependence of the carminic acid emission response has been examined. The emission intensity ratio of the 590 nm band to the 560 nm band is compared for measurements as a function of glucose concentration to the same measurements as a function of buffer solution pH, and are shown in Figure 5.9. In contrast to the absorbance results, there is not a clear correspondence between the emission peak intensity ratio curves obtained directly and those determined indirectly (*vide supra*).[56] Such data invite speculation and, while there are a variety of possible explanations for this effect, it is clear that these data do not provide the information necessary to arrive at any firm conclusions. For this reason, the dyanmical response of carminic acid has been examined.

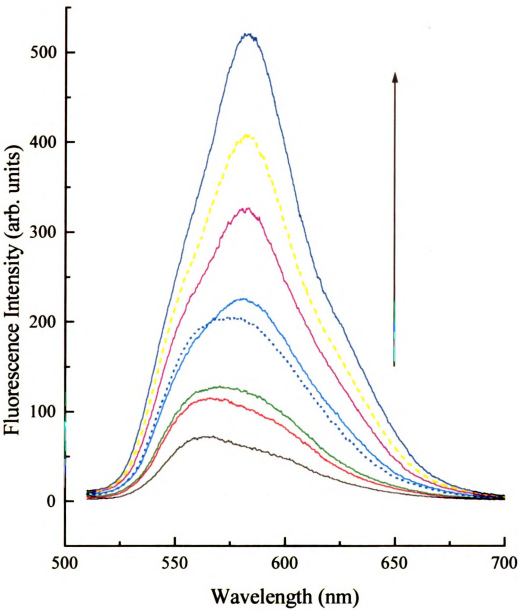

Figure 5.8. Spontaneous emission spectra between 510 nm and 700 nm for aqueous glucose solutions containing 10^{-5} M carminic acid. The dotted tracing represents a 30% glucose solution, and the dashed tracing represents a saturated glucose solution. Arrows indicate the direction of peak shifts observed with increasing glucose concentrations.

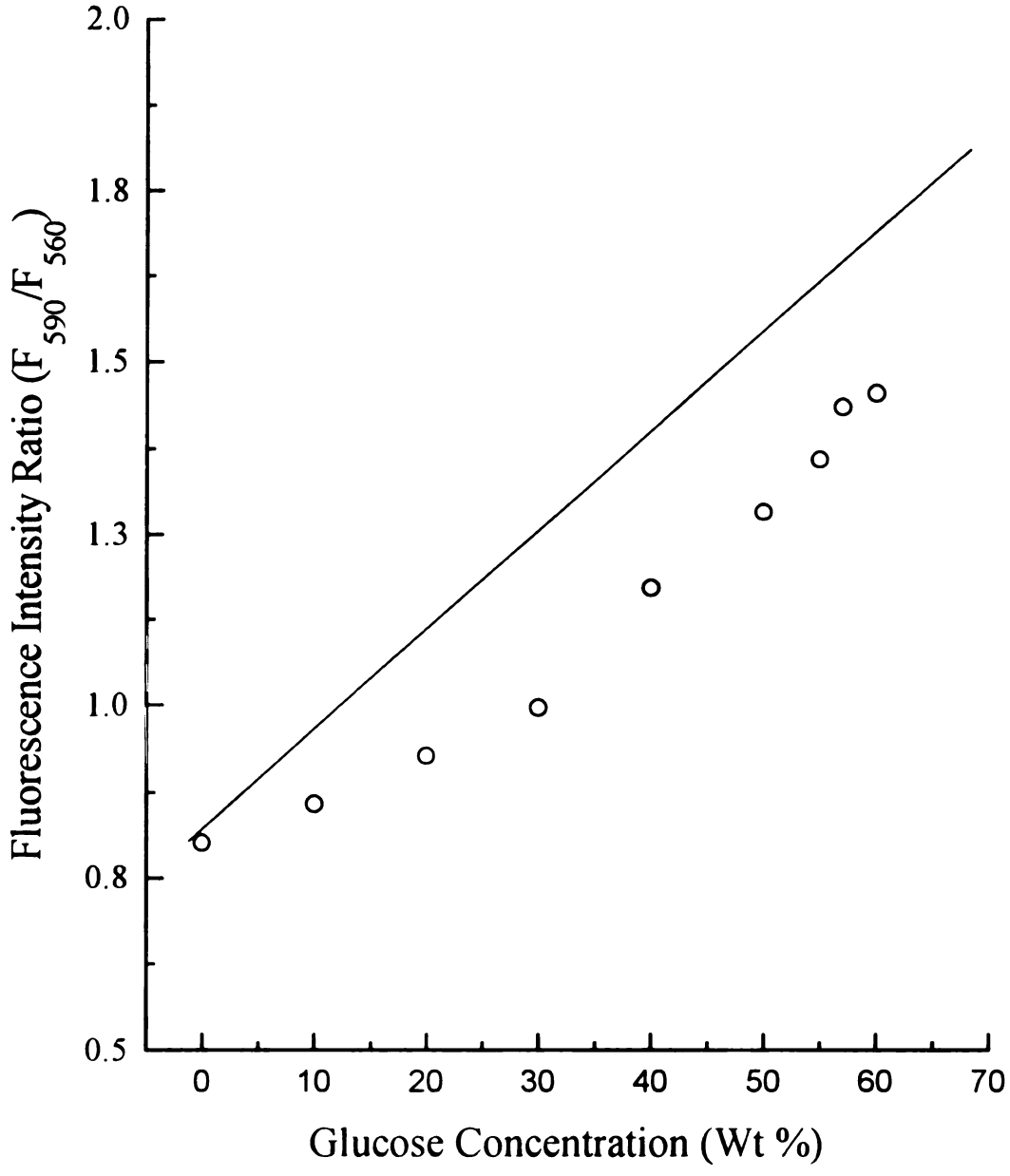

Figure 5.9. pH versus glucose concentration measured by fluorescence intensity ratio (F_{590}/F_{560}) of 5 ppm carminic acid in glucose (O) and by pH electrode (regression of calibration curve (Table 5.1) is the straight line). The points represent the fluorescence intensity ratio taken from carminic acid absorption in glucose (Figure 5.8) vs. glucose concentration, and the line represents the absorption band intensity ratio taken from carminic acid absoption in buffers (Figure 5.6) vs. buffer pH that has been scaled to glucose concentration.

The carminic acid species responsible for individual absorption and emission features are based on the α-fraction plot shown in Figure 5.1 and the experimental data for pH-buffered carminic acid solutions. These assignments are based on ground state pK_a values. When dynamical fluorescence experiments were performed using laser excitation without solution stirring a rapid (several seconds) change in emission color from orange to blue subsequent to illumination with < 1 mW of 310 nm light was noticed. This emission spectral shift corresponds to partially protonated carminic acid deprotonating to yield the fully deprotonated form CA^{4-}. This assignment is based on the experiments presented above assigning the 440 nm emission band to the fully deprotonated species. These data imply that the excited state pK_a values for carminic acid are substantially lower than their corresponding ground state values. Further, because this effect was seen for excitation at 310 nm and not for excitation at 500 nm (necessarily the case for energetic reasons), it is the pK_a values of carminic acid in the S_2 electronic state that determine this effect. However, once formed, the S_1 state of the fully deprotonated form must also possess low pK_a values based on the emission lifetime of the 440 nm band (*vide infra*). This effect is useful because it allows monitoring of the dynamical response of both highly charged (CA^{4-}) and neutral or singly charged species in aqueous glucose solutions. Data from these different forms of the probe molecule provide some insight into the polarity of the medium carminic acid senses in these solutions.

Fluorescence lifetimes of carminic acid in aqueous glucose solutions. The steady state absorption and emission responses of carminic acid as a function of glucose concentration do not provide direct information on any changes in the organization of

the medium surrounding the chromophore. In order to obtain a more complete microscopic picture of this self-assembling system, the dependence of the fluorescence lifetime for protonated and deprotonated forms of carminic acid as a function of glucose concentration have been investigated and shown in Figure 5.10. It is found that, in correspondence with earlier work on carminic acid in the *n*-alcohols (Chapter 4),[54] there are two identifiable lifetimes. In that work, the emission response of carminic acid was used to determine that the double exponential fluorescence decay profiles were not due to intramolecular relaxation dynamics, but were instead the result of two different conformers of carminic acid being present in solution. These two species, possessing different glycosyl group orientations, did not exchange population on the time scale of the fluorescence lifetime because of a large, sterically mediated barrier to isomerization. It is believed that the two lifetime components observed in aqueous glucose solutions have the same origin as those observed for the alcohols. In the earlier report, a single exponential decay functionality was measured for carminic acid in water. The reason for this apparent difference is that the emission response of carminic acid in water is concentration dependent. The earlier report showed data for 30 μM carminic acid in water and here this work reports on 10 μM carminic acid. The concentration-dependence of carminic acid emission dynamics is not a consideration for the glucose solutions because of enhanced solubility of carminic acid in these solutions. The glucose concentration dependence of the fluorescence lifetimes are also fundamentally different for the two species. This is potentially useful in the sense that it provides some insight into the nature of the environment of the chromophore. For the protonated form (Figure 5.10a), the fluorescence lifetime(s) increase with glucose solution concentration.

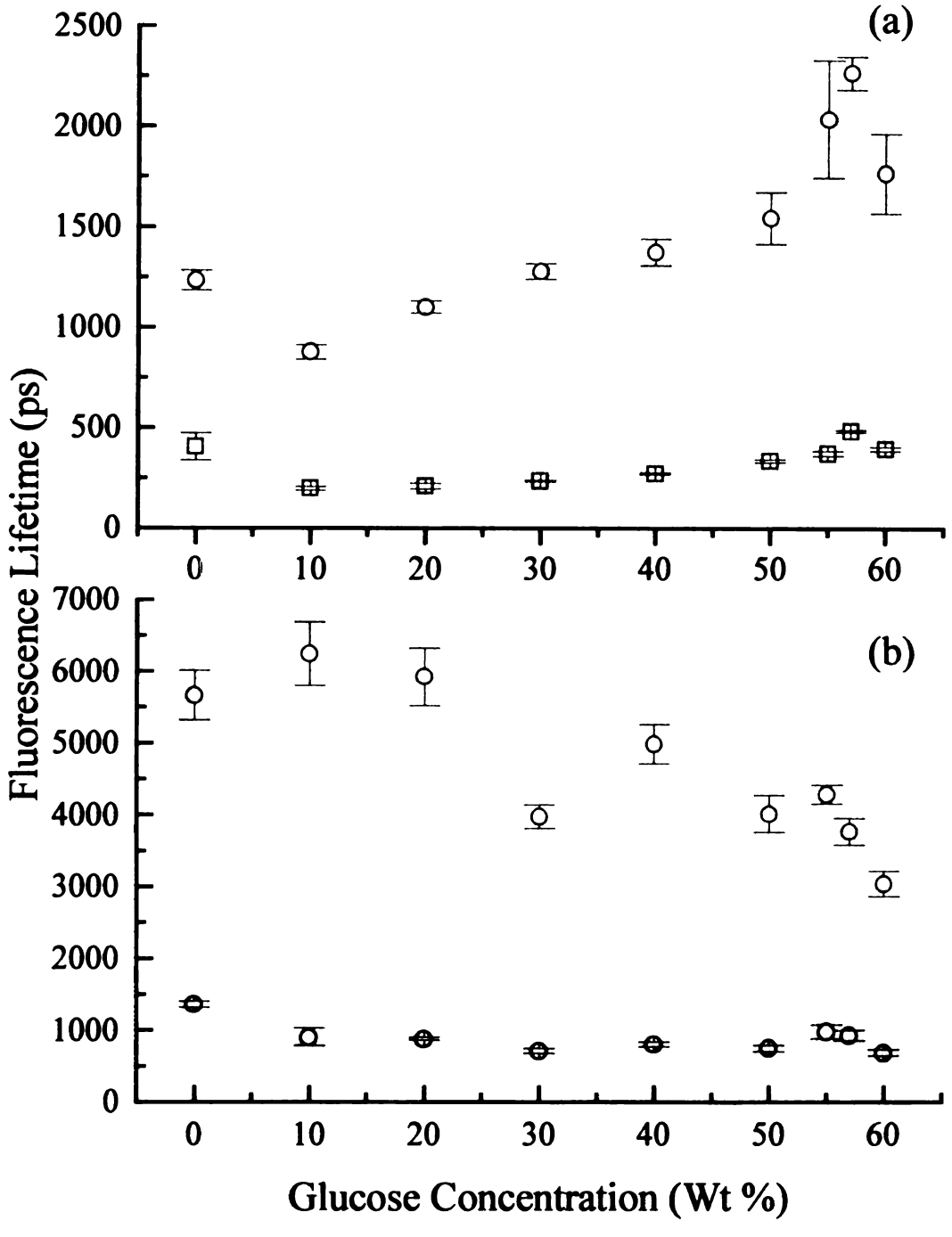

Figure 5.10. Fluorescence lifetimes measured for aqueous glucose solutions containing 10^{-5} M carminic acid. Tracing (a) is for emission at 450 nm (CA^{4-}) and tracing (b) is for emission at 575 nm (H_4CA/H_3CA^-).

Typically, such a trend is interpreted in terms of the viscosity of the medium surrounding the chromophore. As the viscosity of the solution is increased, structural freedom of the chromophore to execute large amplitude molecular motion is decreased, and thus nonradiative decay channels become less accessible. For the deprotonated form of the chromophore (Figure 5.10b), however, there is an opposite trend in the data. The lifetime(s) of CA^{4-} decrease with increasing glucose concentration. It is possible that the ionic chromophore interacts more strongly with glucose than with water, although this is doubtful. More likely is that the dielectric response of the aqueous glucose solutions stabilizes CA^{4-} more efficiently than that of pure water. Regardless of the exact reason, however, these data indicate that the population relaxation dynamics of at least two carminic acid species are mediated to a measurable extent by their immediate environments.

A second feature of the lifetime data is that the two different forms examined (H_4CA/H_3CA^- and CA^{4-}) exhibit significantly different lifetimes. This is not a surprising result because the radiative rate constant for an electronic transition depends sensitively on the structure and extent of protonation of the chromophore. These data provide direct evidence that the emission cross sections for the two transitions (440 nm band of CA^{4-} and 575 nm band of H_4CA/H_3CA^-) are not the same because, if they were, the lifetime of the 440 nm band would be somewhat shorter than that of the 575 nm band(s), based on the ν^3 dependence of the spontaneous emission rate constant.[57] It is observed experimentally that the lifetime of CA^{4-} is ~ 4 - 5 times longer than that of H_4CA. Thus the estimate of the fourth pK_a for carminic acid (~ 13) is likely somewhat high.

Rotational diffusion dynamics of carminic acid in aqueous glucose solutions. The fluorescence lifetime data for carminic acid in aqueous glucose solutions demonstrate clearly that the 440 nm band is associated with a different specie than the 575 nm band, based on the absolute difference in fluorescence lifetimes, their different dependence on glucose concentration, and that simultaneous emission from two different electronic states would be a highly unusual effect. These data, while leading, do not provide direct insight into the local environment of carminic acid. In order to learn more about the interactions between carminic acid, glucose and water, the rotational diffusion behavior of both the protonated and deprotonated forms of this probe molecule have been studied.

Previous investigation of the reorientation dynamics of carminic acid in *n*-alcohols indicated that both stable conformers of this molecule reorient as the same (prolate) ellipsoid shape and volume, and that because of the pendant glycosyl moiety, there is a significant excluded volume effect for this probe molecule (Chapter 4).[54] A larger lesson from that work, however, was that for the protonated form of carminic acid, as the environment assumes more organic character, the effective interactions between the solute and its immediate surroundings experience a decrease in the strength of frictional interactions. Thus, carminic acid is a sensitive probe of local polarity.

The rotational diffusion behavior of many systems has been interpreted within the framework of the modified Debye-Stokes-Einstein (DSE) equation,[9, 10, 15-19, 58-65]

$$\tau_{OR} = \frac{\eta V f}{kTS} \qquad [5.1]$$

where η is the solvent bulk viscosity, f is a term to account for frictional interactions between the solvent and the solute, V is the volume of the solute molecule[66] and S is a shape factor used to account for the non-spherical shape of the solute.[67] For carminic acid, reorienting as a prolate rotor, (S = 0.727) the hydrodynamic volume, including the "void" volume eclipsed by the glycosyl moiety, is 1237 Å^3. In the stick limit, f = 1 and in the slip limit, f = 0.294.[68,69] The experimental data are related to the modified DSE model through the signal intensities and induced orientational anisotropy function, R(t),

$$R(t) = \frac{I_{\parallel}(t) - I_{\perp}(t)}{I_{\parallel}(t) + 2I_{\perp}(t)} \qquad [5.2]$$

where the quantities I(t) are the time resolved emission intensities taken at polarizations parallel and perpendicular to the exciting electric field polarization. The decay of R(t) is given approximately by

$$R(t) = R(0)\exp(-t/\tau_{OR}) \qquad [5.3]$$

As mentioned above, emission from the 440 nm band of carminic acid is used to characterize the lifetime and dynamics of the deprotonated form and emission from the 590 nm band characterizes the protonated and partially protonated forms H_4CA and H_3CA^-. Detection at 575 nm does not allow separation of the response of these two carminic acid species. Figures 5.11 and 5.12 and Tables 5.2 and 5.3 show the reorientation dynamics of different species of carminic acid as a function of glucose concentration. The data in Figure 5.11 are for the deprotonated form, CA^{4-}, monitored at 440 nm. The stick and slip limit lines, calculated using Equation 5.1 are shown in the Figure for comparison. For CA^{4-} reorientation is observed that is described reasonably

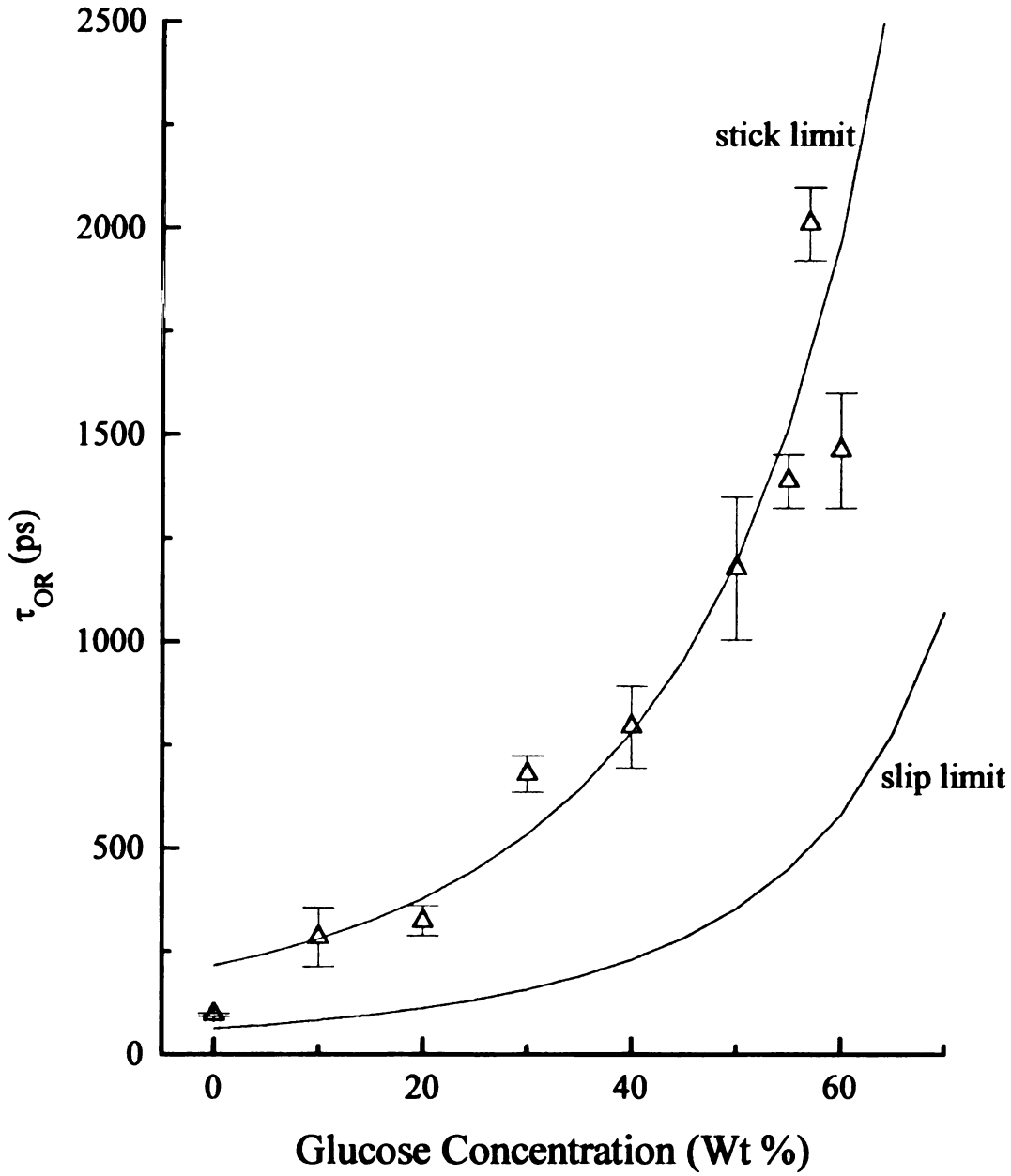

Figure 5.11. Reorientation times determined for the CA^{4-} species of 10^{-5} M carminic acid in aqueous glucose solutions.

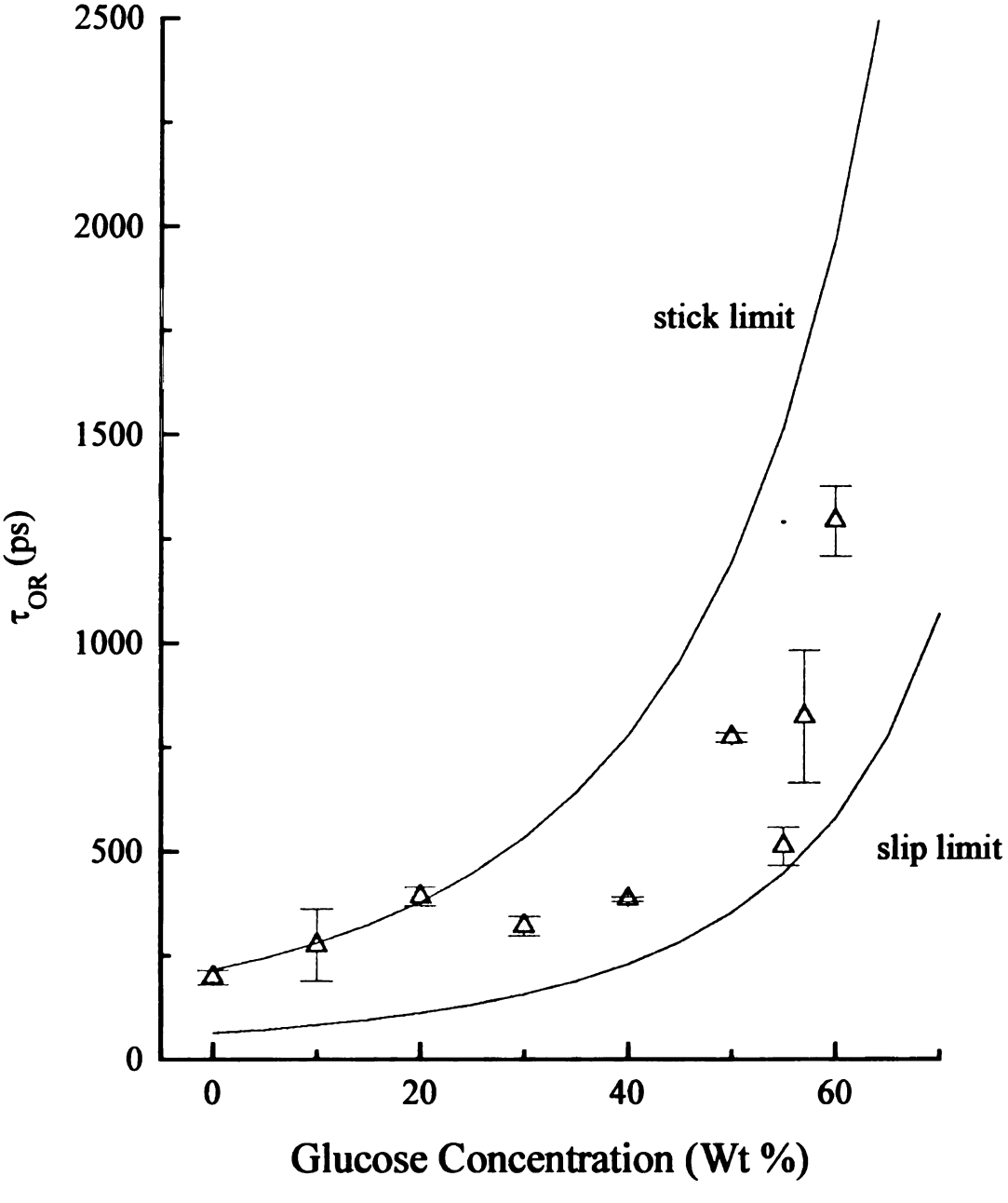

Figure 5.12. Reorientation times determined for the H_4CA/H_3CA^- species of 10^{-5} M carminic acid in aqueous glucose solutions.

Table 5.2. Solution viscosities, fluorescence lifetimes, anisotropies, and reorientation times for the 575 nm emission band of carminic acid in aqueous glucose solutions at 25 °C.

% Glucose	η, cP [a]	τ_{fl} (1) (ps)	τ_{fl} (2) (ps)	R(0)	τ_{OR} (ps)
0	0.88	405 ± 68	1232 ± 50	0.15 ± 0.02	196 ± 17
10	1.15	196 ± 10	877 ± 37	0.11 ± 0.02	275 ± 87
20	1.55	208 ± 14	1101 ± 30	0.11 ± 0.01	391 ± 23
30	2.18	234 ± 5	1280 ± 40	0.10 ± 0.01	320 ± 23
40	3.19	272 ± 4	1376 ± 67	0.07 ± 0.01	385 ± 6
50	4.89	335 ± 7	1547 ± 130	0.06 ± 0.01	773 ± 11
55	6.22	373 ± 11	2041 ± 294	0.06 ± 0.01	511 ± 46
57	6.88	485 ± 7	2272 ± 84	0.03 ± 0.01	823 ± 159
60	8.08	395 ± 12	1770 ± 198	0.05 ± 0.01	1293 ± 84

Table 5.3. Solution viscosities, fluorescence lifetimes, anisotropies, and reorientation times for the 440 nm emission band of carminic acid in aqueous glucose solutions 25 °C.

% Glucose	η, cP [a]	τ_{fl} (1) (ps)	τ_{fl} (2) (ps)	R(0)	τ_{OR} (ps)
0	0.88	1358 ± 44	5663 ± 342	0.27 ± 0.01	96 ± 3
10	1.15	901 ± 122	6242 ± 439	0.19 ± 0.03	284 ± 72
20	1.55	877 ± 21	5924 ± 400	0.21 ± 0.01	323 ± 36
30	2.18	708 ± 34	3975 ± 165	0.22 ± 0.01	679 ± 44
40	3.19	800 ± 32	4986 ± 276	0.21 ± 0.01	792 ± 99
50	4.89	745 ± 42	4014 ± 258	0.20 ± 0.01	1177 ± 174
55	6.22	972 ± 100	4290 ± 131	0.23 ± 0.01	1388 ± 64
57	6.88	922 ± 70	3766 ± 186	0.19 ± 0.01	2012 ± 90
60	8.08	683 ± 41	3040 ± 177	0.13 ± 0.01	1463 ± 139

[a] From Corson, G. E., *Critical Data Tables*, Corn Industries Research Foundation, 1957.

well by the sticking boundary condition for all glucose concentrations. This behavior is expected because charged species interact strongly with polar local environments. At 57% glucose concentration, the measured time τ_{OR} is significantly slower than at either 55% or 60% glucose. This behavior is reproducible and is an indication of significant local organization in aqueous glucose solutions near the saturation point. A discussion of this point is found below. The reorientation of protonated forms of carminic acid (H_4CA, H_3CA^-) (Figure 5.12) depends on glucose concentration in a different way than CA^{4-}. First, the 440 nm band is specific to CA^{4-} and thus all reorientation times reported in Figure 5.11 are for the same chemical species, regardless of glucose concentration. For data taken at 575 nm, however, one expects a contribution from both H_4CA and H_3CA^-. The amount that each form contributes to the observed τ_{OR} is determined by the pH of the solution. For high glucose concentrations, the pH of the solution is sufficiently low to ensure that the dominant form is H_4CA. At low glucose concentrations, it is expected that the dominant contribution will be from H_3CA^-. An estimate of these contributions can be made from the linear response data as a function of glucose concentration (Figure 5.8). It is recognized that this effect will be minimized to some extent by the fact that detection occurs at the isoemissive point, but because of a finite detection bandwidth (10 nm), a glucose concentration-dependence to the ratio $[H_4CA]/[H_3CA^-]$ is expected. For solutions up to 20% glucose, stick limit behavior is observed, consistent with the measurement of predominantly H_3CA^-. For higher glucose concentrations, measured τ_{OR} values are intermediate between stick and slip boundary conditions,[68,69] with an anomalously fast reorientation time seen for 55% glucose concentration. These data, as for the CA^{4-} data, are indicative of local organization.

Before the information content of these data is considered in detail, it is important to ensure that the reported reorientation times can be compared to one another directly. Blanchard and Wirth showed that, for an oblate rotor, variations in the angle between the excited and probed transition dipole moments gave rise to corresponding changes in the measured decay time constant of the induced orientational anisotropy function.[70] In that work, variations in the measured τ_{OR} times did not correspond to changes in the rotational diffusion coefficient. This work shows that for carminic acid the zero-time anisotropy does indeed vary as a function of glucose concentration, and therefore consideration of the effect this concentration-dependent variation of R(0) may have on the τ_{OR} data must be made. The Chuang and Eisenthal equations provide a description of the experimental R(t) function from which these effects can be evaluated.[71] Two possible ellipsoids of rotation to describe the reorientation dynamics of a molecule in solution are considered. The model treats a planar molecule with the *x*-axis corresponding to the long in-plane axis, the *y*-axis is the short in-plane axis and the *z*-axis is normal to the molecular plane. The excited transition moment coincides with the molecular *x*-axis and the emitting transition moment makes an angle θ with respect to the *x*-axis in the *x*-*y* (molecular) plane. For a prolate rotor, the Cartesian components of the rotational diffusion constant are given by the condition $D_x > D_y = D_z$ and for an oblate rotor, $D_z > D_x = D_y$. The complete Chuang and Eisenthal expression for R(t) is, in general, given by up to five exponential decay components.[71] For the conditions of this model, however, the forms of R(t) expected for the different rotor types are

$$R(t) = R_1^0(\theta)\exp\left(-\left(2D_x + 4D_z\right)t\right) + R_2^0(\theta)\exp\left(-6D_x t\right) \qquad \text{oblate rotor} \qquad [5.4]$$

$$R(t) = R^0(\theta)\exp(-6D_z t) \qquad \text{prolate rotor} \qquad [5.5]$$

where $R^0_i(\theta)$ is the zero time anisotropy for the i^{th} component of the decay. An obvious difference between these two functionalities is that the oblate rotor will, in principle, exhibit two exponential decays and the prolate rotor will decay as a single exponential. Experimentally, the finite signal to noise ratio seen in the data preclude the resolution of a second exponential decay component. For an oblate rotor, both $R^0_1(\theta)$ and $R^0_2(\theta)$ will vary with θ, changing the fractional contribution of each decay term to the measured R(t) function. Because R(t) is treated as a single exponential decay function during data processing, one would expect to see a transition dipole moment angle-dependence in the experimental τ_{OR} data, and this has been previously observed experimentally for cresyl violet in methanol.[70] For a prolate rotor, however, there is only one decay component, and the time constant for this decay is determined by the component of the rotational diffusion constant perpendicular to the plane in which the transition moments reside. Thus for a prolate rotor, the measured time constant τ_{OR} is independent of the angle between the excited and detected transition moments, and for an oblate rotor τ_{OR} depends significantly on the angle between the moments. For both of these rotor shapes, R(0) = 0 for $\theta = 54.7°$. Because it has been determined that carminic acid behaves as a prolate rotor and not an oblate rotor,[54] the τ_{OR} data reported in Figures 5.11 and 5.12 are not affected by glucose concentration-dependent variations in R(0), and the values are directly comparable to one another.

It is important to compare the reorientation behavior of H_4CA/H_3CA^- to that of CA^{4-}. For glucose concentrations below ~ 20%, the reorientation dynamics of the two

species are virtually indistinguishable. This similarity between data sets can be understood in the context of measuring two charged species (H_3CA^- and CA^{4-}). For higher glucose concentrations, however, there is a significant deviation in the reorientation behavior measured with two emission bands, with the H_4CA/H_3CA^- system interacting less strongly with its surroundings than CA^{4-}. While these results can be understood largely within the framework of polar interactions between the probe molecule and its local environment, the region of critical interest is near the saturation concentration of glucose. Specifically, the reorientation dynamics of H_4CA exhibit an anomalously fast time constant for 55% aqueous glucose solution while for CA^{4-} there is an anomalously slow reorientation seen in 57% aqueous glucose solution. These glucose concentrations are significantly and measurably different, and the temperature at which these experiments were performed are constant to within $\pm$ 0.05 K, indicating that the two different carminic acid species sense different components of the glucose pre-crystallization environment. The different signs of the anomalous responses also indicate the differences in the environments that the two species detect. Because the glucose concentrations at which anomalous behavior is seen are different for the two species, a direct comparison of the structural information contained in these data is not possible. We are left to discuss these data in the context of their deviations from reorientation times for the same species in slightly different glucose concentrations. It is noted, however, that for both data sets there appears an anomalous data point near the glucose saturation point, followed by a return (above saturation) to information consistent with the trend(s) predicted by the sub-saturated glucose solutions. Thus there appears to be local organization of glucose and water near the saturation point. For H_4CA,

reorientation appears to be unexpectedly fast, correlated with a longer fluorescence lifetime. The reorientation of H_4CA in 55% aqueous glucose solution is described well in the slip limit, indicating weak interactions with its surroundings. The fluorescence lifetime of H_4CA is also longest near this glucose concentration, indicating a rigid local environment. For CA^{4-} the reorientation time is ~50% slower in 57% glucose than it is for either 55% or 60% solutions. This finding indicates strong (possibly ionic) interactions with the local environment. For CA^{4-} the fluorescence lifetime data do not correlate with the reorientation information as they do for H_4CA. The slight differences in R(0) seen for the reorientation measurements near the saturation point also suggest strong interactions between the glucose matrix and the carminic acid chromophore, but there is little structural detail available from this information. Thus the central conclusion from these data is that there is evidence for local organization near the carminic acid chromophore in saturated aqueous glucose solutions. The reorientation data for H_4CA indicate that the local environment formed at 55% glucose concentration does not couple strongly to neutral species. For CA^{4-}, the environment formed at 57% glucose concentration apparently couples strongly to the nucleophilic chromophore.

Despite differences in the details of the reorientation behavior for the different protonated forms of carminic acid, examining these data in a broader context provides significant insight into pre-crystallizing systems. It has been demonstrated that carminic acid incorporates into glucose crystals and therefore the location of the probe molecule is comparatively well understood in these experiments. Despite this localization, reorientation times are observed that are consistent with DSE predictions for the probe molecule alone, absent any of the additive volume effects one might predict with the

formation of carminic acid-glucose aggregates. There are two possible explanations for this behavior. The first explanation is that the dominant motion sensed is chromophore rotation about the bond to its pendant glycosyl moiety. Previous calculated and experimental data,[52,54] as well as the fluorescence lifetime data presented here rule this possibility out. The second explanation for these data is that the lifetime(s) of the pre-crystalline aggregates forming near saturation are significantly less than the reorientation time constant of carminic acid. This explanation accounts for the data presented here. The significance of this finding is that crystallization cannot be thought of simply in the static limit, where there are, in principle, identifiable aggregates that exist prior to the formation of a macroscopic crystal. Rather, these aggregates must exist as transient species with lifetimes significantly less than one nanosecond. These data imply that crystallization, in many instances, will be dominated by kinetic processes and not thermodynamics. Amongst the possible contributions to the kinetics mediating aggregate formation is the presence of protons and/or charge. This possibility is considered in Chapter 6.

Previous work on understanding crystallization from supersaturated solutions suggests that some number of water molecules are coordinated to glucose and that there are additional, non-coordinated water molecules associated with the glucose.[72] From stoichiometric considerations, the glucose solutions should become "water poor" at ~ 30% (w/w) glucose concentration. In other words, at this glucose concentration, there is no longer a ~10:1 stoichiometric excess of water required to solvate the glucose fully. Evidence for a transformation in the reorientation behavior of the H_4CA/H_3CA^- system is seen between 20% and 30% glucose (Figure 5.12) but not for CA^{4-} (Figure 5.11). The

likely reason for glucose concentration-dependent change in boundary condition seen for the H_4CA/H_3CA^- system is that there is a change in the ratio of H_4CA to H_3CA^- in this concentration range, and thus the dominant specie detected in these measurements changes as a function of concentration. The negative slope of the pH vs. glucose concentration calibration suggests that, at higher glucose concentrations, there should be a greater proportion of H_4CA, where the expected polar interactions with the surrounding medium will be weaker than for the ionic H_3CA^- moiety. It is also possible that there is a significant change in the environment experienced by the carminic acid chromophore associated with the change in the stoichiometry of the glucose/water system, but further experiments will be required to validate or disprove this hypothesis.

5.4. Conclusions

The elementary stages of solution phase self-assembly encountered in crystallization using a molecular "lock-and-key" approach to ensure that the probe molecule is located in an environment that is relevant to the organizing system have been investigated. The probe molecule, carminic acid, is a tetraprotic acid with a complex linear optical response. The data presented serve to assign many of the spectral features seen for this molecule. With this understanding of the probe molecule, its dynamical response has been studied. The reorientation and fluorescence lifetime measurements demonstrate the presence of local organization near the saturation concentration of glucose and, while many of the details of this local environment remain to be understood fully, it is clear that the charge of the chromophore affects the surrounding medium significantly. Crystallization cannot, in general, be treated merely as a change between two static conditions, and transient intermolecular interactions must be accounted for to understand macroscopic self-assembly from solution.

5.5. Literature Cited

1. Aicart, E.; Tardagos, G.; Costas, M. *J. Sol. Chem.*, **1989**, *18*, 369.

2. Snyder, R. G.; Aljibury, A. L.; Strauss, H. L. *J. Chem. Phys.*, **1984**, *81*, 5352.

3. Ohtaki, H. *J. Sol. Chem.*, **1992**, *21*, 39.

4. Marcus, Y. *J. Sol. Chem.*, **1992**, *21*, 1217.

5. Stengle, T. R.; Hosseini, S. M.; Williamson, K. L. *J. Sol. Chem.*, **1986**, *15*, 777.

6. Snyder, R. G. *J. Chem. Phys.*, **1967**, *47*, 1316.

7. Snyder, R. G.; Schachtschneider, J. H. *Spectrochimica Acta*, **1963**, *19*, 85.

8. Battacharyya, S. N.; Patterson, D. *J. Sol. Chem.*, **1980**, *9*, 753.

9. Porter, G.; Sadkowski, P. J.; Tredwell, C. J. *Chem. Phys. Lett.*, **1977**, *49*, 416.

10. Spears, K. G.; Cramer, L. E. *Chem. Phys.*, **1978**, *30*, 1.

11. Blanchard, G. J. *J. Phys. Chem.*, **1988**, *92*, 6303.

12. Philips, L. A.; Webb, S. P.; Clark, J. H. *J. Chem. Phys.*, **1985**, *83*, 5810.

13. Blanchard, G. J.; Wirth, M. J. *J. Phys. Chem.*, **1986**, *90*, 2521.

14. Jiang, Y.; Blanchard, G. J. *J. Phys. Chem.*, **1994**, *98*, 6436.

15. Millar, D. P.; Shah, R.; Zewail, A. H. *Chem. Phys. Lett.*, **1979**, *66*, 435.

16. Waldeck, D. H.; Cross, A. J.; Jr.; McDonald, D. B.; Fleming, G. R. *J. Chem. Phys.*, **1981**, *74*, 3381.

17. von Jena, A.; Lessing, H. E. *Chem. Phys. Lett.*, **1981**, *78*, 187.

18. Spears, K. G.; Steinmetz, K. M. *J. Phys. Chem.*, **1985**, *89*, 3623.

19. Templeton, E. F. G.; Quitevis, E. L.; Kenney-Wallace, G. A. *J. Phys. Chem.*, **1985**, *89*, 3238.

20. Mokhtari, A.; Chesnoy, J.; Laubereau, A. *Chem. Phys. Lett.*, **1989**, *155*, 593.

21. Wagener, A.; Richert, R. *Chem. Phys. Lett.*, **1991**, *176*, 329.

22. Declemy, A.; Rulliere, C.; Kottis, Ph. *Chem. Phys. Lett.*, **1987**, *133*, 448.

23. Castner, E. W.; Maroncelli, M.; Fleming, G. R. *J. Chem. Phys.*, **1987**, *86*, 1090.

24. Nagarajan, V.; Brearly, A. M.; Kang, T. J.; Barbara, P. F. *J. Chem. Phys.*, **1987**, *86*, 3183.

25. Maroncelli, M.; Fleming, G. R. *J. Chem. Phys.*, **1987**, ***86***, 6221.

26. Simon, J. D. *Acc. Chem. Res.*, **1988**, *21*, 128.

27. Barbara, P. F.; Jarzeba, W. *Adv. Photochem.*, **1990**, *15*, 1.

28. Maroncelli, M.; Fee, R. S.; Chapman, C. F.; Fleming, G. R. *J. Phys. Chem.*, **1991**, *95*, 1012.

29. Jarzeba, W.; Walker, G. C.; Johnson, A. E.; Barbara, P. F. *Chem. Phys.*, **1991**, *152*, 57.

30. Elsaesser, T.; Kaiser, W. *Annu. Rev. Phys. Chem.*, **1991**, *42*, 83.

31. Lingle, R.; Jr.; Xu, X.; Yu, S. C.; Zhu, H.; Hopkins, J. B. *J. Chem. Phys.*, **1990**, *93*, 5667.

32. Anfinrud, P. A.; Han, C.; Lian, T.; Hochstrasser, R. M. *J. Phys. Chem.*, **1990**, *94*, 1180.

33. Heilweil, E. J.; Casassa, M. P.; Cavanagh, R. R.; Stephenson, J. C. *Ann. Rev. Phys. Chem.*, **1989**, *40*, 143.

34. Heilweil, E. J.; Cavanagh, R. R.; Stephenson, J. C. *Chem. Phys. Lett.*, **1987**, *134*, 181.

35. Heilweil, E. J.; Cavanagh, R. R.; Stephenson, J. C. *J. Chem. Phys.*, **1989**, *89*, 230.

36. Heilweil, E. J.; Casassa, M. P.; Cavanagh, R. R.; Stephenson, J. C. *J. Chem. Phys.*, **1986**, *85*, 5004.

37. Hambir, S. A.; Jiang, Y.; Blanchard, G. J. *J. Chem. Phys.*, **1993**, *98*, 6075.

38. Jiang, Y.; Blanchard, G. J. *J. Phys. Chem.*, **1994**, *98*, 9411.

39. Jiang, Y.; Blanchard, G. J. *J. Phys. Chem.*, **1994**, *98*, 9417.

40. Jiang, Y.; Blanchard, G. J. *J. Phys. Chem.*, **1995**, *99*, 7904.

41. Blanchard, G. J. *J. Chem. Phys.*, **1991**, *95*, 6317.

42. Jiang, Y.; McCarthy, P. K.; Blanchard, G. J. *Chem. Phys.*, **1994**, *183*, 249.

43. Blanchard, G. J. *Anal. Chem.*, **1989**, *61*, 2394.

44. Beddard, G. S.; Doust, T.; Hudales, J. *Nature*, **1981**, *294*, 145.

45. Christensen, R. L.; Drake, R. C.; Phillips, D. *J. Phys. Chem.*, **1986**, *90*, 5960.

46. Gudgin-Templeton, E. F.; Kenney-Wallace, G. A. *J. Phys. Chem.*, **1986**, *90*, 2896.

47. Chakraborty, R.; Berglund, K. A. *J. Cryst. Growth*, **1992**, *125*, 81.

48. Pan, B.; Chakraborty, R.; Berglund, K. A. *J. Cryst. Growth*, **1993**, *130*, 587.

49. Chakraborty, R.; Berglund, K. A. *AIChE Symp. Series*, **1991**, *284*, 113.

50. Dutt, G. B.; Doriswamy, S. *J. Chem. Phys.*, **1992**, *96*, 2475.

51. Weissbuch, I.; Addadi, L.; Lahav, M.; Leiserowitz, L. *Science*, **1991**, *253*, 637.

52. Rasimas, J. P.; Blanchard, G. J. *J. Phys. Chem.*, **1994**, *98*, 12949.

53. Schwing-Weil, M. J.; Weschler, S. *Analusis*, **1986**, *14*, 290.

54. Rasimas, J. P.; Blanchard, G. J. *J. Phys. Chem.*, **1995**, *99*, 11333.

55. Skoog, D. A.; West, D. M. Fundamentals of Analytical Chemistry, Holt, Rinehart, and Winston, New York, 1976, p. 233.

56. Richards, R.; Torgerson, B. A.; Berglund, K. A. *ACS Conference Proceedings, August 27-31, 1995*, American Chemical Society, Washington, D. C., 1995, p. 178.

57. Herzberg, G. Molecular Spectra and Molecular Structure, vol. 3, Krieger Publishing, Malabar, FL, 1966.

58. Debye, P. Polar Molecules, Chemical Catalog Co.: New York, 1929, p. 84.

59. Justus, B. L.; Cox, A. J.; Butz, K. W.; Scott, G. W. *Chem. Phys.*, **1988**, *119*, 125.

60. Blanchard, G. J. *J. Phys. Chem.*, **1989**, *93*, 4315.

61. Quitevis, E. L.; Horng, M-L. *J. Phys. Chem.*, **1990**, *94*, 5684.

62. Dutt, G. B.; Doriswamy, S.; Periasamy, N.; Venkataraman, B. *J. Chem. Phys.*, **1990**, *93*, 8498.

63. Blanchard, G. J. *J. Phys. Chem.*, **1991**, *95*, 5293.

64. Alavi, D. S.; Waldeck, D. H. *J. Phys. Chem.*, **1991**, *95*, 4848.

65. Vauthey, E. *Chem. Phys. Lett.*, **1993**, *216*, 530.

66. Edward, J. T. *J. Chem. Educ.*, **1970**, *B47*, 261.

67. Perrin, F. *J. Phys. Radium*, **1934**, *5*, 497.

68. Hu, C-M.; Zwanzig, R. *J. Chem. Phys.*, **1974**, *60*, 4354.

69. Youngren, G. K.; Acrivos, A. *J. Chem. Phys.*, **1975**, *63*, 3846.

70. Blanchard, G. J.; Wirth, M. J. *J. Chem. Phys.*, **1985**, *82*, 39.

71. Chuang, T. J.; Eisenthal, K. B. *J. Chem. Phys.*, **1972**, *57*, 5094.

72. Hills, B. P. *Mol. Phys.*, **1991**, *72*, 1099.

Chapter 6

Measuring Self-Assembly in Solution: Incorporation and Dynamics of a "Tailor-Made Impurity" in Pre-Crystalline Glucose Aggregates

Summary

The onset of crystallization from solution has been studied using a neutral or non-ionic fluorescent probe molecule that incorporates selectively into pre-crystalline glucose aggregates that form in supersaturated aqueous glucose solutions. Incorporation of the fluorophore into the aggregates is achieved by virtue of the fluorophore pendant glycosyl moiety, and comparison of the rotational diffusion data for this molecule to that for the non-glycosylated, native probe molecule demonstrates solution phase localization. This experimental approach, in conjunction with semi-empirical calculations to understand the electronic response of the fluorescent probe, provides insight into the formation and size of pre-crystalline glucose aggregates. These data indicate that the aggregates effectively isolate the fluorophore from the solution over a range of glucose concentrations spanning the saturation point, and that the lifetime of these aggregates is on the order of a nanosecond for aggregates that include the glycosylated probe molecule. The subtle but important differences between these results and those reported previously for carminic acid in aqueous glucose solutions, point to the significant role of labile protons and/or ionic charge in mediating the formation and dynamics of pre-crystalline glucose aggregates.

6.1. Introduction

Crystallization is one of the oldest and most selective means of achieving chemical separation. The utility of crystallization for this application ranges from recrystallization in the educational laboratory to the mass production and purification of industrial and pharmaceutical chemicals. A common limitation to all of these applications of crystallization is the ability to detect an incipient crystallization event, save for the application of some macroscopic, external perturbation to the system. It is ultimately the goal of this work to understand the molecular-level details of crystallization using remote observation to determine when and if a crystallization event will occur. In order to achieve this goal, "tailor-made impurities" are used in a model system, aqueous β-D-glucose, in order to understand the molecular aspects of crystalline self-assembly from supersaturated solution. To gain the requisite information from such experiments, it has been found necessary to understand the optical response of the "tailor-made impurity" in detail because the photophysical properties of the impurity affect the information content of the recovered emission signal. In addition, the chemical properties of the probe molecule affect the formation of the pre-crystalline aggregates of glucose significantly.

There are a variety of experimental measurements that may prove useful in determining the molecular processes responsible for nucleation and growth of crystals from solution.[1-22] In this work, time resolved and steady state emission spectroscopies have been used because of their combined high detectability and sensitivity to

intermolecular interactions on a several nanometer length scale.[23-30] This approach is feasible, of course, because of the identity of the probe molecule, glycosyl resorufin (GR). The steady state emission behavior of the resorufin chromophore is well understood and is sensitive to local proton concentration. In addition to steady state measurements, dynamical responses such as molecular reorientation are useful in sensing local organization.[31-41] The interpretation of rotational diffusion measurements is couched in a well developed theoretical framework and thus one can infer information on the local organization of comparatively complex aqueous glucose solutions from such measurements.

The specific identity of the probe molecule can have a significant effect on the experimental results, as is indicated by comparing the results presented here to those reported earlier for the probe molecule carminic acid (Chapter 5).[42,43] The shapes of carminic acid and GR are qualitatively similar and the primary difference between the two probe molecules is that carminic acid possesses four labile protons while GR possesses none. Based on experimental data that demonstrate the dynamics of the two probe molecules are significantly different, especially the dependence of each on glucose concentration, it is important to consider the role of protons in mediating the formation of pre-crystalline aggregates. This work reports on the reorientation dynamics of both glycosylated and non-glycosylated resorufin in a series of aqueous glucose solutions spanning the glucose saturation concentration. This work provides clear evidence for selective incorporation of the glycosylated probe, and strong but non-specific interaction between the non-glycosylated probe and glucose in solution. Given the relative

concentrations of the probe and glucose species near saturation and the prominence of the effects we observe, it is believed that this glycosylated probe is acting as a site for the initiation of aggregate self-assembly.

6.2. Experimental

Chemicals: Sodium resorufin was obtained from Aldrich (99+% purity), and glycosyl-resorufin (GR) was obtained from Molecular Probes, Inc. (99+% purity). The structures of the resorufin and GR are shown in Figure 6.1. The purity of each was confirmed by TLC, and both probes were used without further purification. Anhydrous β-D-glucose was obtained from Fluka and used as received. All solutions were prepared using triple-distilled, deionized water. Solutions used for steady state spectroscopy measurements were prepared at a concentration of 2.5×10^{-5} M (60 ppm w/v resorufin, 94 ppm w/v GR). Solutions for time resolved experiments were prepared at a concentration of 10 ppm (4.24×10^{-6} M resorufin, 2.67×10^{-6} M GR). These concentrations were found to be sufficiently low that no dye aggregation or other cooperative effects could be detected. Glucose solutions were prepared by weighing appropriate amounts of glucose and water, followed by heating to 70°C to ensure complete dissolution. For all transient emission measurements, the sample cuvette (Suprasil) was placed in a heat sink (brass block) whose temperature was maintained at 298.0 ± 0.05 K using a temperature controlled circulator (Neslab Endocal). Samples were stirred using a Teflon® coated stirbar and magnetic stirrer to eliminate absorption-induced thermal gradients.

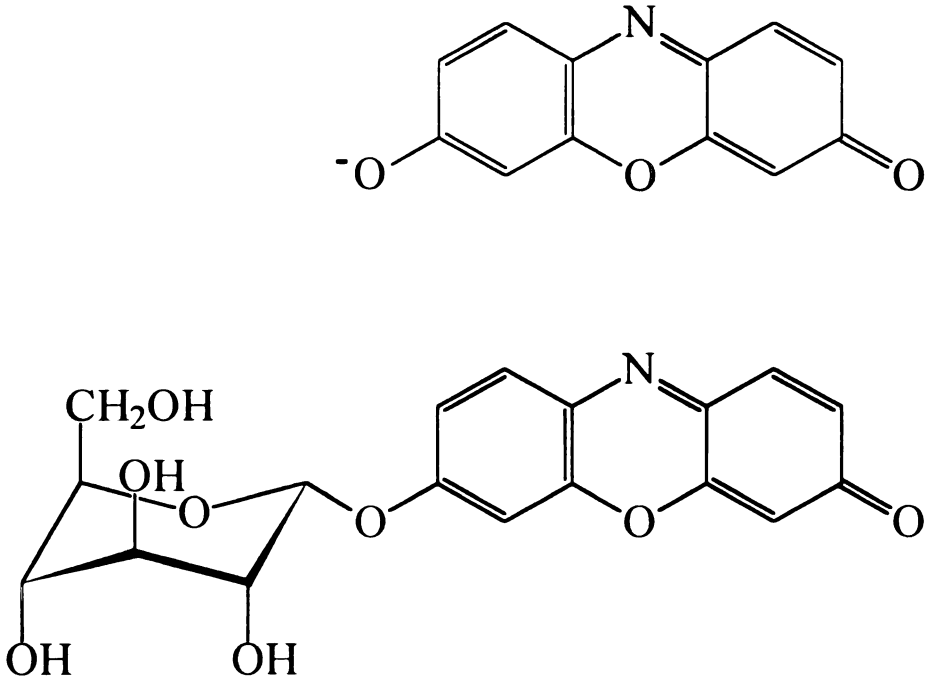

Figure 6.1. The structures of the probe molecules used in these experiments. Structure (a) is resorufin (R^-) and structure (b) is glycosyl-resorufin (GR). The anionic site on structure (a) can be protonated at low pH, yielding the chromophore RH.

Time Correlated Single Photon Counting (TCSPC) Spectrometer: The spectrometer used for the lifetime and reorientation measurements has been described in detail before (Chapter 3, Figure 3.3), and here only a brief recap of its salient features are provided here. The light pulses used to excite the sample are generated with cavity-dumped, synchronously pumped dye lasers (Coherent 702-2) excited by either the second harmonic or third harmonic of the output of a mode-locked CW Nd:YAG laser (Quantronix 416 for SHG and Coherent Antares 76-S for THG). The resorufin anion (R^-) containing samples were excited at 580 nm (Rhodamine 6G, Kodak) pumped by the second harmonic of the Nd:YAG laser output. Protonated resorufin (RH) and glycosyl resorufin (GR) were excited at 470 nm using light pulses from a dye laser (Stilbene 420 dye, Exciton) pumped by the third harmonic of the Nd:YAG laser output. The dye lasers were cavity dumped at a repetition rate of 4 MHz for all measurements. Emission was collected at 600 nm for R^- pumped at 580 nm. Emission was collected at 550 nm for RH and GR pumped at 470 nm. For all measurements, a 10 nm (FWHM) detection bandwidth was used. Detection was accomplished using a two-plate MCP-PMT (Hamamatsu R2809). Fluorescence was collected at 90° with respect to the excitation source, at polarizations of 0°, 54.7°, and 90° with respect to the excitation polarization. The typical instrument response function is ~40 ps FWHM for this system and the measured fluorescence lifetimes vary from ~200 ps to ~4 ns, depending on the probe molecule and glucose concentration.

Steady state absorption and emission spectra: Absorption spectra were acquired using a Hitachi U-4000 UV-visible absorption spectrometer operating with a 2 nm

bandpass. Emission spectra were recorded on a Hitachi F-4500 fluorimeter using 5 nm excitation and emission bandpasses.

Semiempirical calculations: Semiempirical calculations were performed using the PM3 parameterization running on Hyperchem software (Release 4.0; Hypercube, Inc.) on an IBM compatible PC. The PM3 parameterization is a modification of AM1 and MNDO parameterizations[44-48] that is more accurate for polar organic molecules and transition states. The calculation strategy was to perform an initial optimization of the structures using a molecular mechanics routine (MM+),[49] followed by geometry optimization at the semi-empirical level using an SCF algorithm. Two structures of the resorufin chromophore were calculated, the deprotonated (anionic) form, (R^-) and a protonated form (RH), and glycosylated resorufin was also calculated. Semi-empirical optimization was performed until the lowest energy conformation for each molecule was attained. Electronic energy calculations were performed on the geometrically SCF-optimized molecules. For these calculations, the optimized ground state geometry was used and RHF closed-shell calculations were performed for single configuration interaction (CI) with 100 microstates. Previously, similar calculations using a large number of CI states were believed to provide a fair approximation of correlation effects in coumarins[50] and other glycosylated chromophores (Chapter 2)[51] and it is believed that this condition will hold for these calculations as well. The energy of the rotational isomerization barrier in GR for rotation of the glucose moiety about its tethering bond to the resorufin chromophore was also calculated. It is important to recall that these calculations assume the molecules are isolated and in an absolute vacuum.

6.3. Results and Discussion

As mentioned above, the primary focus of this work is on understanding the molecular interactions that ultimately give rise to crystallization. First, it is necessary to consider the linear optical responses of the probe species and how these experimental results are related to the calculated properties of the probe molecules. This information ensures that analogous states are accessed in all forms of the chromophore such that no anomalous dipolar interactions may contribute to the dynamical responses measured.[52] After gaining an understanding of these properties, the reorientation dynamics of the probe molecules as a function of solution glucose concentration are considered. Of particular importance will be comparison of the glycosylated and native resorufin probes. From these data the contribution to the reorientation dynamics that is a consequence of probe incorporation into the pre-crystalline aggregates can be determined. First the linear optical responses of the various forms of resorufin are considered.

Steady state spectroscopy of resorufin and glycosyl resorufin: In order to use R^-, RH and GR as probes of glucose crystallization, the spectroscopic behavior of each probe molecule must be characterized. The linear electronic response of each molecule provides chemical information about the form of each specie present for a given set of experimental conditions. Figure 6.2 shows the absorption (dotted tracing) and spontaneous emission (solid tracing) spectra for R^-, RH, and GR. First the linear responses of the native resorufin chromophore, (Figures. 6.2a and 6.2b) are discussed. In aqueous solution, resorufin exists solely in its dissociated (anionic) form, R^-, with an absorption maximum at 570 nm and an emission maximum at 600 nm. In acidic

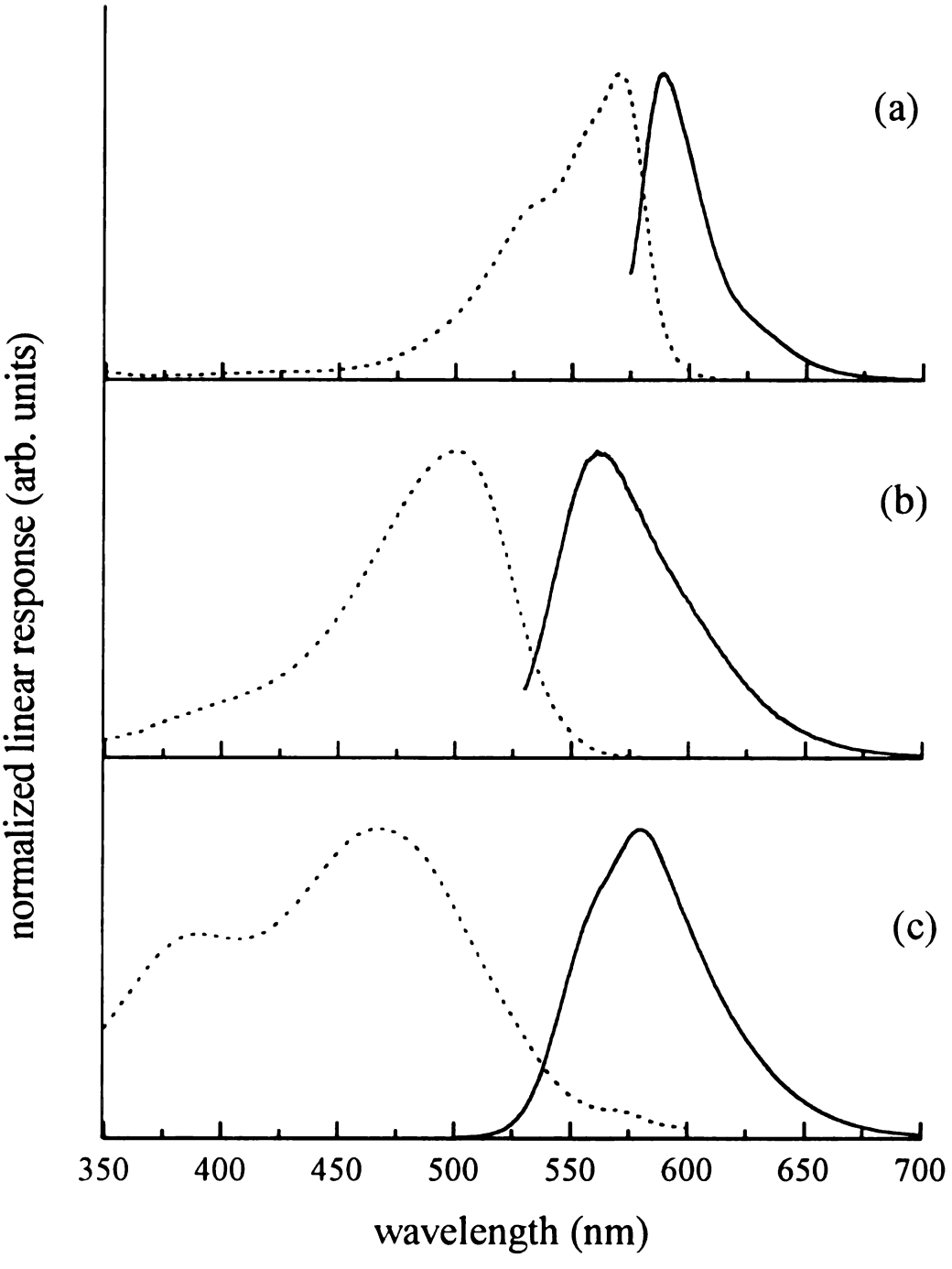

Figure 6.2. Linear absorption and emission spectra for the probe molecules used in this study. Plot (a) is for resorufin (R^-), (b) is protonated resorufin (RH), and (c) is glycosyl-resorufin (GR). The absorption spectra are represented by the dotted tracing, the emission spectra are shown with the solid tracing. Spectra were normalized for presentation purposes. A discussion of the individual spectra appears in the text.

solutions, resorufin exists in its protonated form, RH, with a broad absorption spectrum centered at 480 nm and a broad emission spectrum with a maximum at 575 nm. The RH spectrum is shown because it has been determined previously that the pH of aqueous glucose solutions decreases with increasing glucose concentration,[43] and it is expected that the resorufin probe molecule will be present in both protonated and deprotonated forms as glucose concentration increases. These spectra provide a spectroscopic road-map for the time resolved spectroscopy experiments. In addition to requiring this information in order to determine the excitation and observation wavelengths, it is important to note that the spectra of the two forms of the chromophore are sufficiently different to allow the spectroscopic selection of one over the other. Thus the role of ionic charge in determining the reorientation dynamics of the probe can be examined because there exist both R^- and RH in equilibrium for glucose solutions near saturation.

The ability to measure selectively the dynamics of the non-glycosylated probe provides information on the condition of the non-aggregating component of the glucose solutions because these species do not incorporate into glucose crystallized from solutions containing native resorufin. The linear response of glycosyl-resorufin (GR) was also examined, and absorption and fluorescence spectra for this molecule in are shown in Figure 6.2c. The absorption band is broad and featureless, with λ_{max} = 460 nm. The fluorescence band is also broad, with λ_{max} = 575 nm. These spectra are qualitatively similar to those observed for RH, in agreement with the previously discussed semi-empirical calculations (*vide infra*) and earlier work on the optical response of associated NaR (Chapter 3).[53] In addition, the effect of increasing glucose concentration on the

spectra of R^-, RH, and GR has been studied. The spectra of all species did not exhibit any significant shift or intensity variation with increasing glucose concentration, save for a decrease in the strength of R^- absorption and an increase in RH absorption with increasing glucose concentration. This shift between R^- and RH is attributed to the previous observation that increasing glucose concentration results in a decrease in solution pH.

Glucose crystals with incorporated and excluded probes: A fundamental question in the use of any probe molecule relates to the location of the probe with respect to the event of interest as it "reads" information from the solution. This work has used GR as a lock-and-key probe of glucose self-assembly (Chapter 5).[43] In order to test for the incorporation of GR into glucose, single crystals of glucose were grown in the presence of trace (10-30 ppm) amounts of probe molecule. Large, high quality crystals of glucose were able to be grown with up to 30 ppm GR. In contrast, the growth of glucose crystals was not possible in the presence of native resorufin for probe concentrations above 1 ppm, the lowest concentration used. To test for incorporation of GR into the glucose crystal, a sample crystal grown in the presence of GR was rinsed several times with cold acetone and ethanol to remove any non-incorporated probe, then dried at 40°C overnight. The washed crystal was then rinsed and dried one additional time. The rinse solution contained no detectable GR. Upon dissolution of the washed crystal, a spectroscopic profile corresponding to that of GR was recovered, demonstrating the direct GR incorporation into the glucose crystal matrix. In Figure 6.3 absorption and emission spectra obtained from the dissolution of a glucose crystal grown

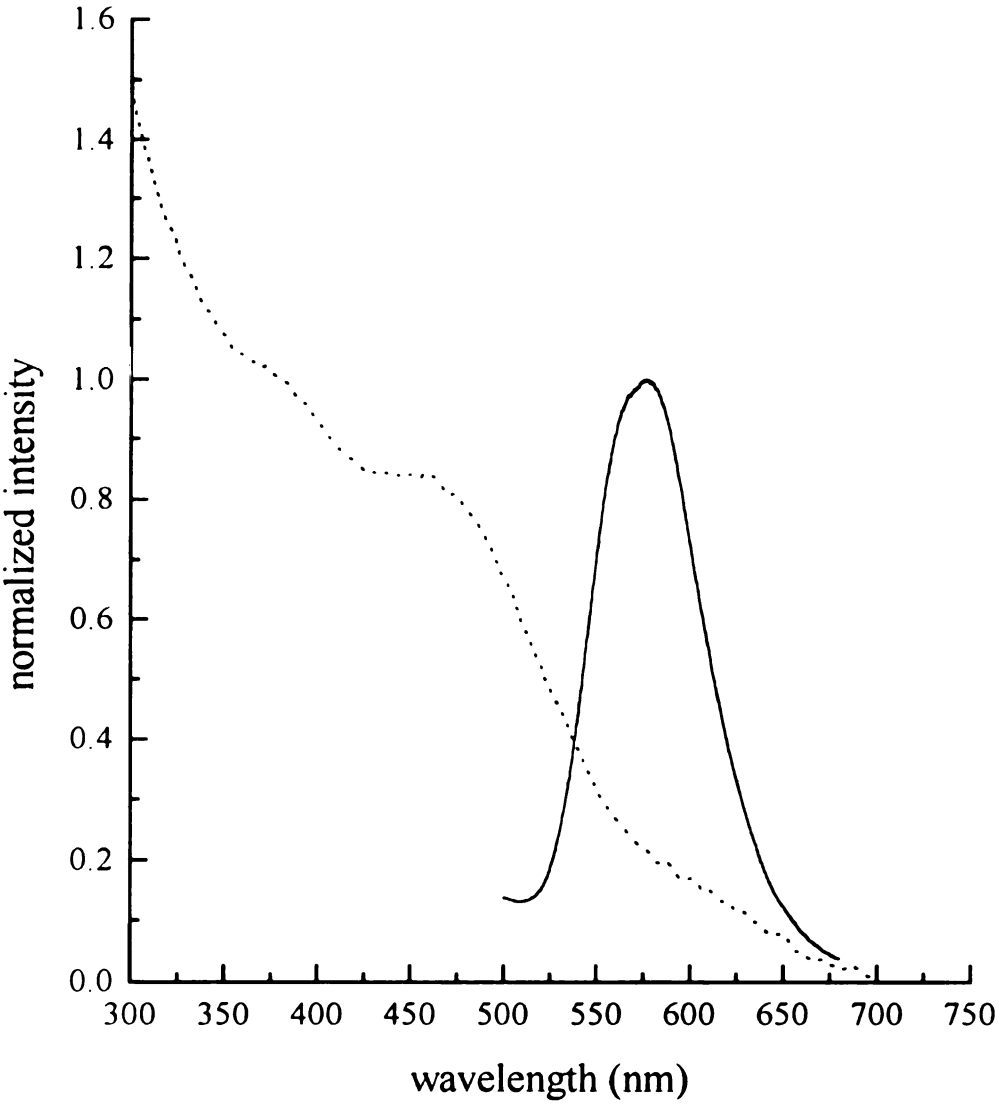

Figure 6.3. Absorption and emission spectra for glycosyl-resorufin recovered from incorporation of the "lock-and-key" probe into β-D-glucose crystals. The absorption spectrum is represented by the dotted tracing, the emission spectrum is shown by the solid tracing. Spectra are normalized for presentation purposes.

in the presence of GR are shown. The absorption band shown in Figure 6.3 exhibits a contribution from acetone absorption, a consequence of the rinsing process. The presence of the bands at 375 nm and 470 nm indicates the existence of GR. As an additional check, the steady state emission response of the dissolved crystal was acquired, and a spectrum characteristic of GR was recovered. These data confirm the direct incorporation of GR into glucose crystals, demonstrating the utility of GR for use as a "lock-and-key" probe of glucose self-assembly.

PM3 Semi-Empirical Calculations: Calculations on each of the three probes were performed to understand electronic properties and determine the isomerization barriers for rotation of the glycosyl moiety about its tethering bond to the chromophore. Table 6.1 is a summary of the calculated electronic properties for R^-, RH and GR. Figure 6.4 shows the calculated state energies for these molecules. There are several important comparisons to make from these results. The first point to note is the overall similarity of the energies for the electronic states of RH and GR. These species are treated as having essentially the same optical response. It is interesting to note that the correspondence between methylated resorufin (not shown) and GR is closer than for RH, as one would expect. The differences between the calculated energy levels for R^- and GR are now discussed. The lowest energy singlet transition in R^- is significantly lower in energy than it is for GR, in agreement with experimental absorption data (*vide supra*). The S_1 state of R^- is energetically isolated from neighboring singlet and triplet states, suggesting the dominance of a radiative relaxation pathway for this moiety. The $S_0 \leftrightarrow S_1$ transition energies of GR and RH are approximately the same, in excellent agreement

Table 6.1. Calculated properties of resorufin based probe molecules using PM3 semi-empirical parameterization. R^- = resorufin anion, RH = protonated resorufin, GR = glycosyl-resorufin.

		energy relative to S_0 (cm^{-1})							
Probe	ΔH_f (kcal/mole)	T_1	T_2	S_1	T_3	S_2	$\mu(S_0)$ (D)	$\mu(T_1)$ (D)	$\mu(S_1)$ (D)
R^-	-95.45	12363	23280	21041	26118	26439	3.12	1.75	1.63
RH	-44.13	17985	25794	27164	28364	31455	3.80	5.76	3.59
GR	-245.65	19928	29004	28109	29452	31403	5.54	6.03	3.20

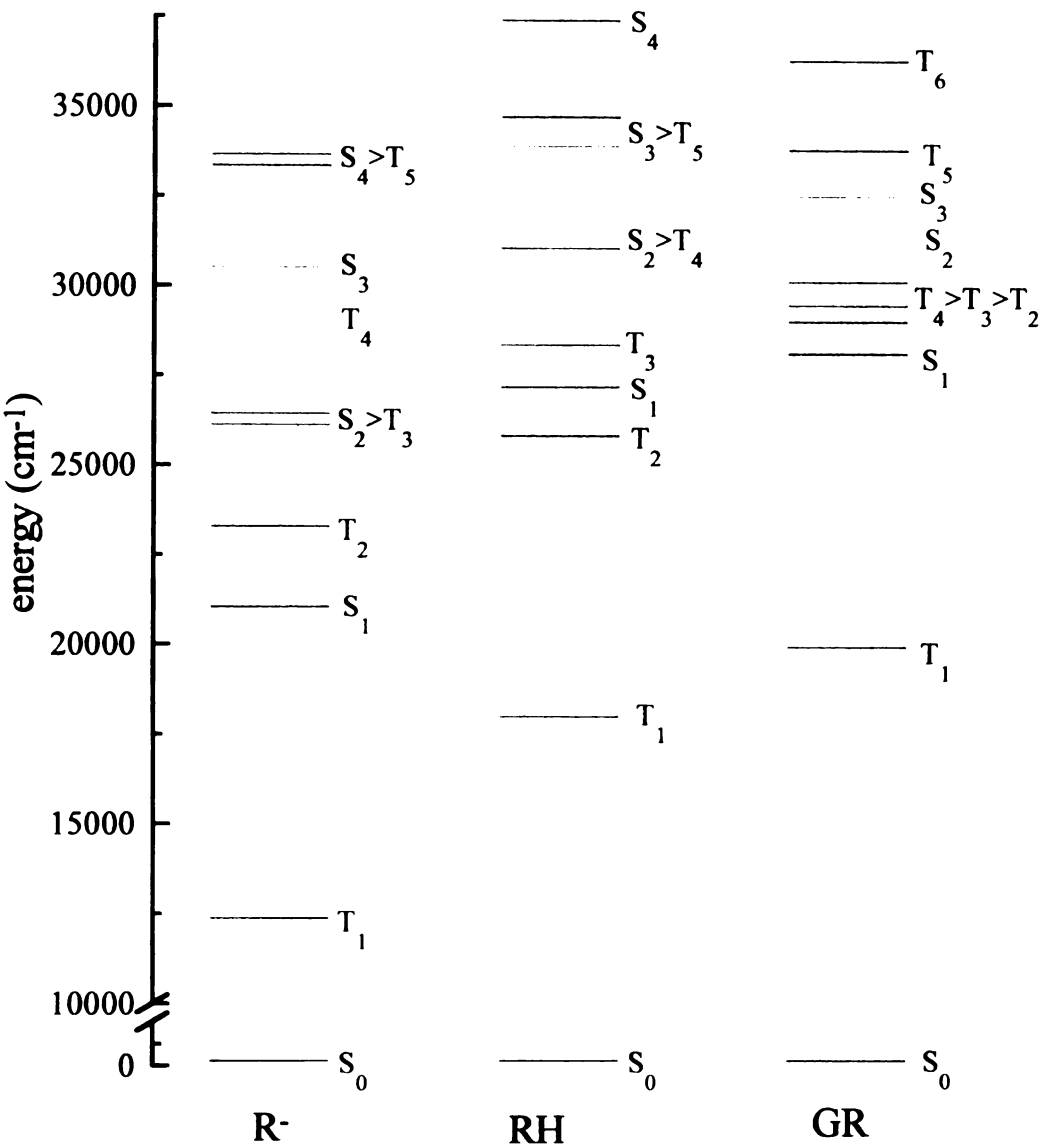

Figure 6.4. Resorufin (R^-), protonated resorufin (RH) and glycosyl-resorufin (GR) electronic state ordering determined from PM3 calculations using configuration interaction (CI).

with the experimental absorption data. There is one significant difference, however, in the calculated state energies for RH and GR. For RH there is a triplet state ~1000 cm^{-1} lower in energy than the S_1 state, with no corresponding singlet-triplet proximity for GR. This calculated result suggests that intersystem crossing may play a role in the depopulation of the RH S_1 state, but not in GR.

To this point, the transition energies of the various probe forms have been considered. It is also important to consider how the change in electron density distribution upon excitation differs among the molecules. It is important to consider this point based on the experimental observation of state dependent resorufin reorientation dynamics.[54] Figure 6.5 shows the calculated *change* in electron density (ρ_{cd}) between the S_1 and S_0 states ($\Delta\rho_{cd} = \rho_{cd}(S_1) - \rho_{cd}(S_0)$) at each atom for R^- (Figure 6.5a), RH (Figure 6.5b), and GR (Figure 6.5c). A negative sign represents an increase in electron density on excitation. In all species, the heterocyclic nitrogen gains electron density and the carbon atoms adjacent to it lose electron density. This effect is most prominent in R^- (Figure 6.5a), and agrees with previous studies of resorufin.[54] There is also an interest in the effects of glycosylation on chromophores,[51] and the calculated similarities between RH and GR suggest that the glycosyl moiety is electronically decoupled from the chromophore. The rotational isomerization barrier of GR for rotation of the glycosyl moiety about its tethering bond to the chromophore has also been calculated. Figure 6.6 illustrated the dependence of S_0, T_1 and S_1 state energies on this torsion angle. The state energies of the ground state (S_0), first triplet state (T_1), and first excited singlet state (S_1) are independent of glycosyl moiety rotation with respect to the chromophore to within

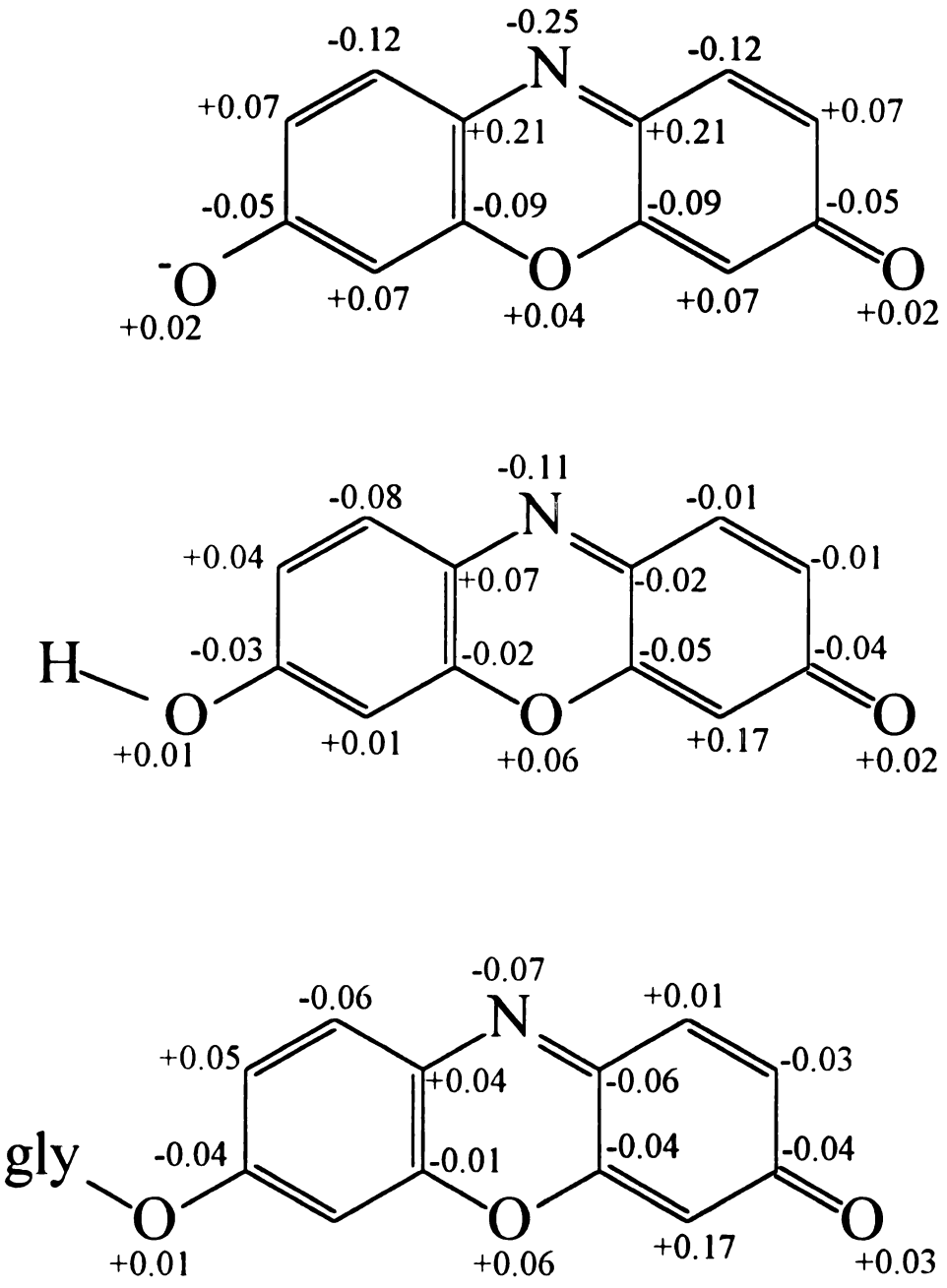

Figure 6.5. Calculated change in electron density, ($\Delta\rho_{ed}$), between the singlet excited state (S_1) and the ground state (S_0) for resorufin (R^-, a), protonated resorufin (RH, b) and glycosyl-resorufin (GR, c). A positive sign indicates a decrease in electron density upon excitation from the S_0 to S_1 electronic states. Values less than ±0.01 are not shown.

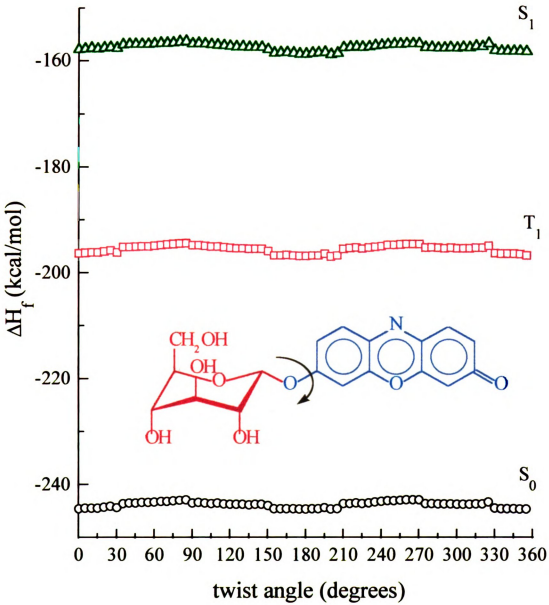

Figure 6.6. Calculated energy dependence of the glycosyl group rotation for the S_0 (O), T_1 (□), and S_1 (Δ) states of glycosyl-resorufin. The dihedral angle is the angle made by the head of the glycosyl moiety and its ether linkage with respect to the chromophore. Relative energies at a given dihedral angle were $S_1 > T_1 > S_0$.

0.5 kcal/mol, demonstrating that the rotation of the glycosyl moiety does not influence the chromophore linear response. More relevant to the experiments presented here, these calculations indicate that the electronic response of resorufin can be considered to be largely decoupled from conformational variations associated with GR incorporation into glucose aggregates.

Fluorescence lifetimes of R^-, RH and GR in aqueous glucose solutions. Table 6.2 shows the fluorescence lifetimes (τ_{FL}), rotational diffusion times (τ_{OR}) and zero-time anisotropy (R(0)) determined for R^- and RH. We present these analogous data for GR in Table 6.3. We discuss the rotational diffusion and anisotropy data in the following section. We discuss first the lifetime data for these probes. The lifetimes of all species remain essentially constant ($\tau_{fl} < 500$ ps) over the glucose concentration range studied. Furthermore, there is a 3000 ± 100 ps component observed for RH. There are several possible explanations for the appearance of an additional long decay time feature, including the formation of new, exchanging species. The protonated form of the chromophore, RH, is in equilibrium with the deprotonated form, R^-, and the lifetime of the protonated form likely depends significantly on the availability of protons in solution. Thus for high glucose concentration, we expect a longer lifetime for RH based solely on the availability of protons in its local environment.

Rotational diffusion dynamics: The fluorescence lifetime data for R^-, RH and GR in aqueous glucose solutions, while interesting, do not provide direct information on pre-crystalline aggregate formation. This is not necessarily surprising, and we have investigated the rotational diffusion dynamics of these species in glucose solutions to

Table 6.2. Fluorescence lifetimes (τ_{FL}), reorientation times (τ_{OR}), and zero-time anisotropies (R(0)) for resorufin (R^-) and protonated resorufin (RH) in aqueous glucose solutions at 25°C. A long decay time for R^- (3000 ± 100 ps) was seen in all solutions (~1 % of total intensity) and represents an average over all measurements, which was then used in fitting the fast time component. All times are in picoseconds.

Solution (wt % glucose)	R^-			RH		
	τ_{FL}	τ_{OR}	R(0)	τ_{FL}	τ_{OR}	R(0)
0%	153 ± 27	118 ± 4	0.28 ± 0.01	428 ± 41	115 ± 9	0.28 ± 0.01
25%	179 ± 43	255 ± 9	0.21 ± 0.01	418 ± 8	235 ± 17	0.14 ± 0.01
50%	194 ± 27	699 ± 37	0.22 ± 0.01	479 ± 23	303 ± 27	0.19 ± 0.01
52.5%	182 ± 22	766 ± 32	0.21 ± 0.01			
55%	156 ± 45	1002 ± 46	0.22 ± 0.01	471 ± 5	381 ± 27	0.10 ± 0.01
57.5%	174 ± 30	858 ± 24	0.19 ± 0.01			
60%	127 ± 37	874 ± 20	0.23 ± 0.01	464 ± 4	466 ± 77	0.10 ± 0.01

Table 6.3. Fluorescence lifetimes (τ_{FL}), reorientation times (τ_{OR}), and zero-time anisotropies (R(0)) for glycosyl-resorufin (GR) in aqueous glucose solutions at 25°C. All times in picoseconds.

Solution (wt % glucose)	τ_{FL}	τ_{OR}	R(0)
0%	261 ± 9	191 ± 34	0.10 ± 0.01
25%	275 ± 7	298 ± 56	0.15 ± 0.01
50%	313 ± 4	981 ± 87	0.12 ± 0.01
52.5%	319 ± 6	957 ± 67	0.15 ± 0.01
55%	308 ± 10	958 ± 71	0.12 ± 0.01
57.5%	312 ± 15	895 ± 107	0.09 ± 0.01
60%	315 ± 6	1278 ± 186	0.09 ± 0.01

provide additional insight into the local organization present in this system. Reorientation measurements sense the strength and nature of solvent-solute interactions and are related to the hydrodynamic volume of the solute. Previous studies of the reorientation dynamics of resorufin[54] have indicated that this molecule reorients as a prolate ellipsoid. A comparison of the dynamical response of the two forms of resorufin (R^- and RH) can be used as a probe of local polarity where there is no specific, structural bias toward incorporation into glucose aggregates. Comparing the dynamical responses of these probes with the reorientation dynamics of GR will provide direct insight into the formation of glucose pre-crystalline aggregates since it has been demonstrated that GR forms inclusion complexes with glucose single crystals (*vide supra*).

As has been covered in Chapters 4 and 5, the rotational diffusion behavior of many systems has been interpreted within the framework of the modified Debye-Stokes-Einstein (DSE) equation,[55-62]

$$\tau_{OR} = \frac{\eta V f}{k\ TS} \qquad [6.1]$$

where η is the solvent bulk viscosity, f is a term included to account for frictional interactions between the solvent and the solute, V is the volume of the solute molecule[63] and S is a shape factor used to account for the non-spherical shape of the solute.[64] While this model is clearly not sufficiently detailed to account for the strong and sometimes site-specific intermolecular interactions between polar solvents and solutes, it does provide a useful and surprisingly accurate frame of reference to which experimental results can be compared.

While it is recognized that the DSE model offers limited molecular insight into this problem, it is understood that comparisons to this model are useful in understanding differences in the behavior of the three probe species. With that purpose in mind, the expected reorientation behavior of each probe molecule based on the DSE model is considered. It has been determined previously that R^- reorients as a prolate rotor, (S = 0.768) with a hydrodynamic volume of 165 $Å^3$.[54,63] In the DSE stick limit, $f = 1$ and in the DSE slip limit, $f = 0.206$.[65,66] The reorientation behavior of GR has been modeled as a prolate rotor, (S=0.737) with a hydrodynamic volume of 335 $Å^3$. The hydrodynamic volume used for this molecule is greater than the sum of the constituents; the resorufin chromophore has a volume of 165 $Å^3$, and the glycosyl moiety a volume of 125 $Å^3$. It has been found before, for carminic acid, that the added volume due to rotation of the glycosyl moiety about its tethering bond to the chromophore must be considered in interpreting reorientation results, and this "excluded" volume can be approximated reasonably well using space-filling models (Chapter 5).[42] In the DSE stick limit, $f = 1$, and in the slip limit, $f = 0.280$ for a prolate ellipsoid with the aspect ratio calculated for GR, $\rho = 0.467$.[65,66] The functionality of the decay of R(t) (Chapter 4) can be complicated and it contains information on the angle between the excited and emitting transition moments as well as on the Cartesian components of the rotational diffusion constant, D. In theory, R(t) can contain up to five exponential decays, although in practice it is unusual to observe more than two decays, and the most common case is that of a single exponential decay.

$$R(t) = R(0)\exp(-t/\tau_{OR}) \qquad [6.3]$$

For all of the reorientation measurements reported here, it is observed that R(t) is described well by Equation 6.3. As shown in Tables 6.2 and 6.3, the zero-time anisotropies of R$^{\cdot}$, RH, and GR change with increasing glucose concentration. It has been shown previously that, for a prolate rotor with the transition moment along the long ellipsoidal axis, the measured time constant τ_{OR} is independent of the angle between the excited and detected transition moments, whereas for an oblate rotor, the value of τ_{OR} recovered from regression of R(t) depends sensitively on the angle between the transition moments.[43] Because it has been determined that R$^{\cdot}$, RH, and GR behave as prolate rotors and not as oblate rotors, the τ_{OR} data reported in Tables 6.2 and 6.3 and Figure 6.7 are not affected by glucose concentration-dependent variations in R(0), and the values can thus be compared to one another directly.

For the probe molecules chosen, the several potential complications to the interpretation of the reorientation data are not significant for this work, and now detail the chemical information content of the reorientation data can be focused on. For the sake of clarity the behavior of the native probe species R$^{\cdot}$ and RH will be considered separately from that of GR.

The reorientation data for R$^{\cdot}$ and RH are consistent with other reorientation measurements of polar probe molecules in polar media. Specifically, Figure 6.7a shows the glucose concentration dependence of the reorientation times for R$^{\cdot}$ and RH, along with the calculated DSE stick limit line. The viscosity of the solution does not depend linearly on glucose concentration, but this relationship is well characterized.[67] For the

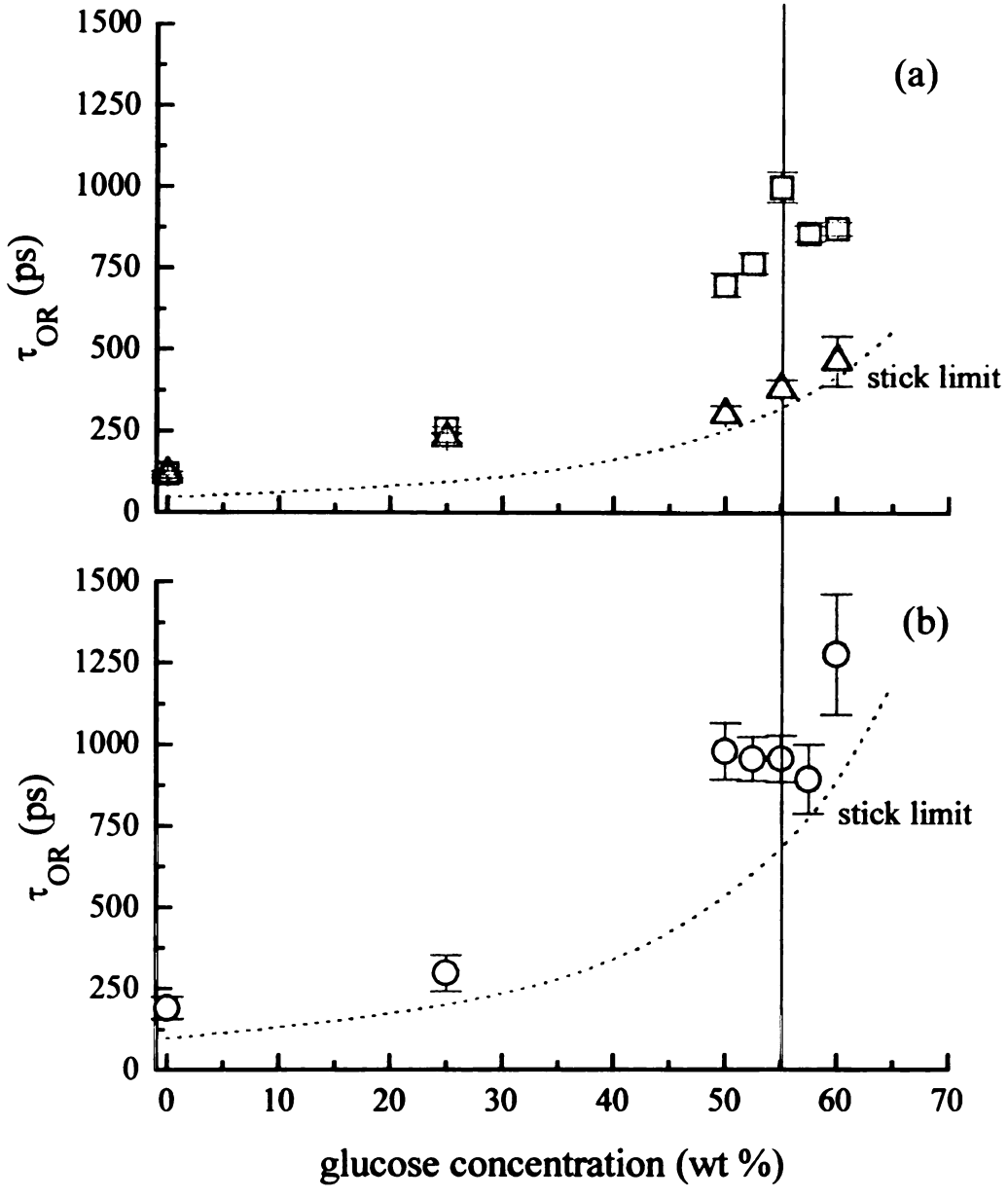

Figure 6.7. Reorientation times for resorufin (R^-, □), protonated resorufin (RH, Δ), and glycosyl-resorufin (GR, O), determined in aqueous glucose solutions. Debye-Stokes-Einstein theory stick limit lines for GR (dotted) and R-/RH (solid) are shown for comparison purposes. The vertical line represents the saturation point. A detailed discussion of these data appear in the text.

neutral RH, the experimental data follow the calculated stick limit prediction quite closely, and reveal no abrupt change in behavior near saturation (55% glucose). This result shows that RH senses the aqueous environment that is not associated with glucose aggregation. For R^-, there are two important points to note. These are that the reorientation times at all glucose concentrations measured are much longer than predicted by the DSE stick model. This result is consonant with other reports of anion reorientation, and indicate strong interactions between R^- and its local environment. While there is undoubtedly much important chemical information contained in this result, it will not be considered here. It is more relevant to focus on the form of the glucose concentration dependence of these data. It is noted that reorientation of R^- is anomalously slow at glucose saturation and, for glucose concentrations both higher and lower than 55%, τ_{OR} behaves in a systematic manner. This result is similar in form to the earlier report on the reorientation behavior of carminic acid in aqueous glucose solutions, where discontinuous reorientation behavior is observed at the saturation point (Chapter 5).[43] In that chapter, the anomalous reorientation was ascribed to local organization of the glucose/water system at saturation. The protonated form of carminic acid reoriented anomalously fast at saturation and the fully deprotonated form reoriented anomalously slow at saturation, implying the importance of charge. This result for R^-, where there is no pendant glycosyl moiety to incorporate into the aggregating glucose matrix, implicates ionic charge as a significant driving force in the association of dissimilar molecules in solution.

The reorientation data for GR in aqueous glucose solutions (Figure 6.7b) provide significant insight into the local organization that precedes larger scale self-assembly from solution. GR reorientation at low glucose concentrations is described well by the DSE model in the stick limit. The reorientation of GR at high glucose concentration, however, reveals an interesting viscosity-independence near saturation, implying the incorporation of GR in a medium that is not directly sensitive to changes in solution bulk viscosity. Further, τ_{OR} for GR approaches the stick limit more closely for glucose concentrations above saturation, indicating reorientation of the chromophore within a well defined and relatively constant local environment. The anomalous viscosity independence of these data is fully consistent with the formation of pre-crystalline aggregates in the region of saturation. This behavior suggests that the probe molecule incorporates into, *not onto*, an aggregate and thus does not sense the bulk viscosity of the system. Despite the difficulty associated with the acquisition of complementary data pointing to local organization, it is speculated that reorientation measurements on GR indicate that the probe molecule itself acts as a point of aggregation and does not simply attach to the surface of the aggregate.

Given the viscosity independence of the GR reorientation data near saturation, it is fair to consider the possibility that the effective rotor shape of the chromophore may change. Such a change could not be brought about as a direct result of modification to the local environment because the tether of the resorufin moiety to the glycoside is closest to the long axis of the fluorophore. It is possible that the aggregate as a whole may also be reorienting as either an oblate or a prolate rotor, depending on its shape. If

the aggregate were to reorient as an oblate rotor, the a double exponential decay of the anisotropy would be expected, and for all measurements only a single exponential decay is recovered. A potential complication to this interpretation of the data is that the lifetime of GR is sufficiently short that slower aggregate motion may not be resolvable. This is a question that can be resolved only through the use of a similar glycosylated probe molecule possessing a longer excited state lifetime.

The data reported here for GR near saturation differ somewhat from the data reported previously for carminic acid in the same binary system. Specifically, the GR reorientation data indicate the presence of local organization in solution that persists over a time scale of at least a nanosecond. The analogous data for carminic acid, while suggestive of local organization, indicate that the persistence time of the pre-crystalline aggregates is significantly less than a nanosecond. The only outward difference between these two probes is the presence of labile protons on carminic acid and their absence on GR. Thus either the stability of the aggregate or the incorporation of the probe into the aggregate is affected significantly by the presence of labile protons. Given that the GR data suggest the central role of the probe molecule in effecting the onset of aggregation, it is likely that the presence of protons inhibits the formation of short range structure in glucose. This is not a surprising result based on the polar nature of glucose and the importance of hydrogen bonding interactions in the formation of glucose crystals.

6.4. Conclusions

Reorientation data for the three probe molecules point to the incorporation of GR into pre-crystalline aggregates of glucose near saturation and the exclusion of RH. For R^-, the experimental data point to non-specific association, in correspondence to earlier data we reported on carminic acid. The viscosity independent nature of GR reorientation near saturation suggests that the probe is itself isolated from the bulk medium, implicating its role as a site about which aggregation proceeds.

The demonstrated experimental approach for studying local organization that occurs prior to macroscopic self-assembly illustrates the importance of aggregation phenomena leading to crystallization events. To date, attention has been directed toward using aqueous glucose solutions as a useful model system and, using different probe molecules, the effects of probe molecule identity and charge on aggregation effects have been elucidated. There is no reason that this lock-and-key approach to the examination of local organization cannot be applied to other complex ternary systems.

6.5. Literature Cited

1. Myerson, A. S.; Sorel, L. S. *AIChE J.*, **1982**, *28*, 778.

2. Chang, Y. C.; Myerson, A. S. *AIChE J.*, **1985**, *31*, 980.

3. Chang, Y. C.; Myerson, A. S. *AIChE J.*, **1986**, *32*, 1567.

4. Chang, Y. C.; Myerson, A. S. *AIChE J.*, **1986**, *32*, 1747.

5. Myerson, A. S.; Chang, Y. C. Industrial Crystallization '84, Jancic, S. J.; DeJong, E. J. eds.: Elsevier, Amsterdam, **1984,** 27.

6. Larson, M. A.; Garside, J. *Chem. Eng. Sci.*, **1986**, *41*, 1285.

7. Larson, M. A.; Garside, J. *J. Cryst. Growth*, **1986**, *76*, 88.

8. Franks, F. in Hydrogen Bonded Solvent Systems, Covington, A. K., Jones, P. (eds.), Taylor and Francis, London, **1968**, 31-47.

9. Franks, F.; Ravenhill, J. R.; Reid, D. S. *J. Solution Chem.*, **1972**, *1*, 3.

10. Franks, F.; Pedley, M.; Reid, D. S. *J. Chem. Soc. Faraday Trans. I*, **1976**, *72*, 359.

11. Franks, F. *Pure and Appl. Chem.*, **1987**, *59*, 1189.

12. Giermanska, J.; Szostak, M. M. *J. Raman Spectroscopy*, **1991**, *22*, 107.

13. Suggett, A.; Clark, A. H. *J. Solution Chem.*, **1976**, *5*, 1.

14. Suggett, A.; Ablett, S.; Lillford, P. J. *J. Solution Chem.*, **1976**, *5*, 17.

15. Suggett, A. *J. Solution Chem.*, **1976**, *5*, 33.

16. Harvey, J. M.; Symons, M. C. R. *J. Solution Chem.*, **1978**, *7*, 571.

17. Barone, G.; Castronuovo, P. Del Vecchio; Elia, V. *J. Solution Chem.*, **1990**, *19*, 41.

18. Mathlouthi, M.; Luu, C.; Meffrov-Biget, M.; Luu, D. V. *Carbohydrate Res.*, **1980**, *81*, 213.

19. Mathlouthi, M. *Carbohydrate Res.*, **1981**, *91*, 113.

20. Chakraborty, R.; Berglund, K. A. *AIChE Symp. Ser. No. 284*, **1991**, 113.

21. Chu, Y. D.; Shiau, L. D.; Berglund, K. A. *J. Crystal Growth*, **1989**, *97*, 689.

22. Cerreta, M. K.; Berglund, K. A. *J. Crystal Growth*, **1990**, *102*, 869.

23. Aicart, E.; Tardagos, G.; Costas, M. *J. Sol. Chem.*, **1989**, *18*, 369.

24. Snyder, R. G.; Aljibury, A. L.; Strauss, H. L. *J. Chem. Phys.*, **1984**, *81*, 5352.

25. Snyder, R. G.; Schachtschneider, J. H. *Spectrochimica Acta*, **1963**, *19*, 85.

26. Marcus, Y. *J. Sol. Chem.*, **1992**, *21*, 1217.

27. Ohtaki, H. *J. Sol. Chem.*, **1992**, *21*, 39.

28. Snyder, R. G. *J. Chem. Phys.*, **1967**, *47*, 1316.

29. Battacharyya, S. N.; Patterson, D. *J. Sol. Chem.*, **1980**, *9*, 753.

30. Stengle, T. R.; Hosseini, S. M.; Williamson, K. L. *J. Sol. Chem.*, **1986**, *15*, 777.

31. Porter, G.; Sadkowski, P. J.; Tredwell, C. J. *Chem. Phys. Lett.*, **1977**, *49*, 416.

32. Templeton, E. F. G.; Quitevis, E. L.; Kenney-Wallace, G. A. *J. Phys. Chem.*, **1985**, *89*, 3238.

33. Blanchard, G. J.; Wirth, M. J. *J. Phys. Chem.*, **1986**, *90*, 2521.

34. Spears, K. G.; Cramer, L. E. *Chem. Phys.*, **1978**, *30*, 1.

35. Blanchard, G. J. *J. Phys. Chem.*, **1988**, *92*, 6303.

36. Philips, L. A.; Webb, S. P.; Clark, J. H. *J. Chem. Phys.*, **1985**, *83*, 5810.

37. von Jena, A.; Lessing, H. E. *Chem. Phys. Lett.*, **1981**, *78*, 187.

38. Jiang, Y.; Blanchard, G. J. *J. Phys. Chem.*, **1994**, *98*, 6436.

39. Waldeck, D. H.; Cross, A. J.; Jr.; McDonald, D. B.; Fleming, G. R. *J. Chem. Phys.*, **1981**, *74*, 3381.

40. Spears, K. G.; Steinmetz, K. M. *J. Phys. Chem.*, **1985**, *89*, 3623.

41. Millar, D. P.; Shah, R.; Zewail, A. H. *Chem. Phys. Lett.*, **1979**, *66*, 435.

42. Rasimas, J. P.; Blanchard, G. J. *J. Phys. Chem.*, **1995**, *99*, 11333.

43. Rasimas, J. P.; Berglund, K. A.; Blanchard, G. J. *J. Phys. Chem*, **1996**, *100*, 7220.

44. Dewar, M. J. S.; Zoebisch, E. G.; Healy, E. F.; Stewart, J. J. P. *J. Am. Chem. Soc.*, **1985**, *107*, 3902.

45. Dewar, M. J. S.; Dieter, K. M. *J. Am. Chem. Soc.*, **1986**, *108*, 8075.

46. Stewart, J. J. P. *J. Comput.-Aided Mol. Des.*, **1990**, *4*, 1.

47. Dewar, M. J. S.; Thiel, W. *J. Am. Chem. Soc.*, **1977**, *99*, 4899.

48. Dewar, M. J. S.; Thiel, W. *J. Am. Chem. Soc.*, **1977**, *99*, 4907.

49. Allinger, N. L. *J. Am. Chem. Soc.*, **1977**, *99*, 8127.

50. McCarthy, P. K.; Blanchard, G. J. *J. Phys. Chem.*, **1993**, *97*, 12205.

51. Rasimas, J. P.; Blanchard, G. J. *J. Phys. Chem.* **1994**, *98*, 12949.

52. Jiang, Y.; McCarthy, P. K.; Blanchard, G. J.; *Chem. Phys.*, **1994**, *183*, 249.

53. Rasimas, J. P.; Blanchard, G. J. *J. Phys. Chem.*, **1996**, *100*, XXXX

54. Blanchard, G. J.; Cihal, C. A. *J. Phys. Chem.* **1988**, *92*, 5950.

55. Debye, P. Polar Molecules, Chemical Catalog Co.: New York, 1929, p. 84.

56. Justus, B. L.; Cox, A. J.; Butz, K. W.; Scott, G. W. *Chem. Phys.*, **1988**, *119*, 125.

57. Blanchard, G. J. *J. Phys. Chem.*, **1989**, *93*, 4315.

58. Quitevis, E. L.; Horng, M-L. *J. Phys. Chem.*, **1990**, *94*, 5684.

59. Dutt, G. B.; Doriswamy, S.; Periasamy, N.; Venkataraman, B. *J. Chem. Phys.*, **1990**, *93*, 8498.

60. Blanchard, G. J. *J. Phys. Chem.*, **1991**, *95*, 5293.

61. Alavi, D. S.; Waldeck, D. H. *J. Phys. Chem.*, **1991**, *95*, 4848.

62. Vauthey, E. *Chem. Phys. Lett.*, **1993**, *216*, 530.

63. Edward, J. T. *J. Chem. Educ.*, **1970**, *B47*, 261.

64. Perrin, F. *J. Phys. Radium*, **1934**, *5*, 497.

65. Hu, C-M.; Zwanzig, R. *J. Chem. Phys.*, **1974**, *60*, 4354.

66. Youngren, G. K.; Acrivos, A. *J. Chem. Phys.*, **1975**, *63*, 3846.

67. Corson, G. E. *Critical Data Tables*, Corn Industries Research Foundation, **1957**.

Chapter 7

Conclusions and Future Work

7.1. Conclusions

This dissertation has shown the validity of using "tailor-made" molecules as selective probes of solution microstructure. Specifically, Carminic acid and glycosyl-resorufin were used to study the aqueous β-D-glucose system. These probe molecules were shown to incorporate into crystalline β-D-glucose without dramatically affecting the crystal structure. This indicated, in the static limit, that these molecules are able to act as "lock-and-key" probes of the glucose system. Time resolved dynamical data for Carminic acid show that this molecule holds promise as a probe of saturation, as discontinuous behavior was observed at the point of saturation. Similar data for glycosyl-resorufin demonstrate that pre-crystalline aggregates have long (>1 ns) persistence times. This finding also suggests that these aggregates may lead to the formation of nucleation sites. This point, however, has not been proven unambiguously due to the short fluorescence lifetime and reorientation time of glycosyl-resorufin. A comparison of the dynamics data for glycosyl-resorufin and Carminic acid provides insight into the formation of pre-crystalline aggregates. The short aggregate lifetimes observed using the Carminic acid probe suggest that the availability of protons is important in stabilizing these aggregates. This finding is supported by the long aggregate lifetimes observed using glycosyl-resorufin as a "lock-and-key" probe. These studies

also demonstrate that there is significant transient molecular-scale organization and local inhomogeneity in aqueous glucose systems.

The data discussed in this dissertation provide useful criteria for selecting a "tailor made" probe molecule for use in studying solution phase self-assembly. The probe molecule should be chemically neutral if the goal to observe aggregate formation. If the parameter to be interrogated is local polarity, then a probe with ionic character is suitable. However, in either case, the spectroscopic behavior of the probe must be examined in a simple system before meaningful interpretations of complex ternary systems can be made.

7.2. Future Work

While this dissertation has shown the usefulness of the "lock-and-key" approach to studying self-assembly in aqueous glucose solutions, there is no reason that this methodology cannot be applied to other complex systems. Identification of appropriate "tailor-made impurity" chromophores whose fluorescence lifetimes are sufficiently long to allow examination of long-time (>1 ns) aggregate formation and motion would provide additional information into the kinetic contribution of aggregation.

A system which is amenable to examination using long lifetime "tailor-made impurity" molecules in a "lock-and-key" scheme is aqueous carboxylic acids. One example of this type of system currently being investigated, is aqueous maleic acid.[1] The pre-crystalline behavior of this carboxylic acid can be interrogated using the "lock-and-key" probes pyrene-butyric acid and kermesic acid. The relevant structures for this system are shown in Figure 7.1. The fluorescence lifetime and rotational diffusion

behavior of this pyrene butyric acid are well understood.[2-5] The fluorescence lifetime is long (~100 ns), therefore this probe will allow examination of pre-crystalline aggregation and aggregate lifetime and rotational motion. This molecule will also provide a measurement of microscopic polarity. Kermesic acid is identical to the Carminic acid chromophore, and this dissertation has developed a detailed understanding of the pH dependence of its optical response. This "tailor-made impurity" probe molecule can be used to interrogate the local pH of crystallizing and pre-crystallizing maleic acid.

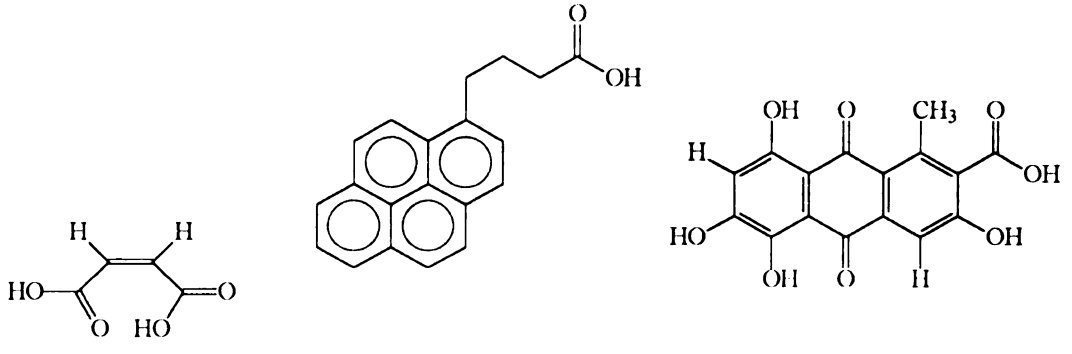

maleic acid pyrene butyric acid kermesic acid

Figure 7.1. The structures of maleic acid, pyrene butyric acid and kermesic acid.

By using the "lock-and-key" methodology studied in this dissertation, these future studies will be useful in determining the local environment of the probe molecule and in sensing local structure, local inhomogeneity, and macroscopic solution phase self-assembly. These additional investigations will advance the understanding of pre-crystalline behavior in these simple systems, and provide additional insights into the requisite events for molecular crystallization to occur.

7.3. Literature Cited

1. Tulock, J. J.; Berglund, K. A.; Blanchard, G. J. *private communication.*

2. Pan, B.; Chakraborty, R.; Berglund, K. A. *J. Cryst. Growth*, **1993**, *130*, 587.

3. Chakraborty, R.; Berglund, K. A. *AIChE Sym. Ser.*, **1991**, *87*, 114.

4. Pan, B.; Berglund, K. A. *J. Cryst. Growth, in press.*

5. Karpovich, D. S.; Blanchard, G. J. *J. Phys. Chem.*, **1995**, *99*, 3951.